



**COLLAPSE OF 3d (4f) ORBITALS
IN 2p (3d) EXCITED CONFIGURATIONS AND
ITS EFFECT ON THE X-RAY AND
ELECTRON SPECTRA**

REIN RUUS

**COLLAPSE OF 3d (4f) ORBITALS
IN 2p (3d) EXCITED CONFIGURATIONS AND
ITS EFFECT ON THE X-RAY AND
ELECTRON SPECTRA**

REIN RUUS



TARTU UNIVERSITY
PRESS

This study was carried out at the Institute of Physics, Tartu University, Tartu, Estonia

Dissertation was admitted on June 28, 1999 in partial fulfilment of the requirements for the degree of Doctor of Philosophy (solid state physics), and allowed for defence by the Council of Department of Physics, University of Tartu

Supervisor: Prof. Mart Elango, Institute of Physics, University of Tartu, Estonia

Opponents: Prof. Nikolai Kristoffel, University of Tartu, Estonia
Prof. Helena Aksela, University of Oulu, Finland

Defence: October 6, 1999, at Tartu University, Tartu, Estonia

The publication of this dissertation is granted by the University of Tartu

CONTENTS

LIST OF ORIGINAL PAPERS	6
1. INTRODUCTION	9
2. X-RAY ABSORPTION AND DECAY PROCESSES	13
2.1. X-ray absorption	13
2.2. Decay of the resonantly excited states	14
3. CALCULATIONS	18
3.1. Calculation of the wavefunctions	18
3.1.1. Calculation of the bound wavefunctions	18
3.1.2. Calculation of the continuum wavefunctions	19
3.2. Calculation of the transition probabilities	20
3.3. Calculation of the Auger transition probabilities	21
4. EXPERIMENTAL TECHNIQUE	24
5. COLLAPSE OF THE 3d WAVEFUNCTION IN THE ISOELECTRONIC SEQUENCE OF ARGON-LIKE IONS	26
5.1. Effect of collapse of the 3d orbital on atomic properties	26
5.2. Collapse of the 3d orbital and 2p absorption spectra	28
5.3. Crystal field splitting of the 3d electrons	29
5.4. Resonant electron spectra of RbCl. Case of uncollapsed 4s orbital and effect of the 3d-electron collapse on the spectator decay spectrum	32
5.5. Resonant electron spectra of KCl. Case of collapsed 3d orbital.	34
5.6. Shake probabilities.....	36
6. COLLAPSE OF THE 4f WAVEFUNCTION IN THE ISOELECTRONIC SEQUENCE OF XENON-LIKE IONS	38
6.1. Collapse of the 4f orbital and 3d absorption spectra.....	38
6.2. Resonant electron spectra of CsI. Case of uncollapsed 4f orbital ..	40
6.3. Resonant electron spectra of BaF ₂ . Case of collapsed 4f orbital and effect of the 4f electron collapse on the spectator decay spectrum	42
6.4. Branching ratios of 4d photolines	44
THE MAIN ARGUMENTS PROPOSED	48
CONCLUSIONS	49
SUMMARY IN ESTONIAN	52
ACKNOWLEDGMENTS	55
REFERENCES	56
PUBLICATIONS	59

LIST OF ORIGINAL PAPERS

This thesis is based on the following papers, which will be referred to in the text by their Roman numerals:

- I. A. A. Maiste, R. E. Ruus, S. A. Kuchas, R. I. Karaziya, and M. A. Elango, Collapse of 4f-electron in the configuration $3d^9 4f$ in xenonlike ions, *Zh. Eksp. Teor. Fiz.* **78**, (1980), pp. 941–951 [*Sov. Phys. JETP* **51**, (1980), pp. 474–479] (in Russian).
- II. A. A. Maiste, R. E. Ruus, and M. A. Elango, 3d electron collapse in the $2p^5 3d$ configuration of argon-like ions, *Zh. Eksp. Teor. Fiz.* **79**, (1980), pp. 1671–1677 [*Sov. Phys. JETP* **52**, (1980) pp. 844–847] (in Russian).
- III. R. V. Vedrinskii, L. A. Bugajev, I. I. Gegusin, V. L. Kraizman, A. A. Novakovich, S. A. Prosandeev, R. E. Ruus, A. A. Maiste and M. A. Elango, X-ray absorption near edge structure (XANES) for KCl, *Solid St. Comm.* **44**, (1982), pp. 1401–1407.
- IV. R. E. Ruus, Collapse of the 3d orbital in configurations with a 2p vacancy and its effect on the $2p^6$ - $2p^5 nd, ns$ transitions, *Opt. Spektrosk.* **59**, (1985), pp. 745–750 [*Opt. Spectrosc.* **59**, (1985) pp. 450–453] (in Russian).
- V. M. Elango, A. Ausmees, A. Kikas, E. Nõmmiste, R. Ruus, A. Saar, J. F. van Acker, J. N. Andersen, R. Nyholm and I. Martinson, Auto-ionization phenomena involving the $2p^5 3d$ configuration of argon-like ions in ionic solids, *Phys. Rev. B*, **47**, (1993), pp. 11736–11748.
- VI. R. Ruus, A. Kikas, M. Elango, A. Maiste, E. Nõmmiste, A. Saar, Auger decay processes of resonantly excited $3d^1 4f$ configuration of xenon-like ions in ionic solids, *J. Electron Spectrosc. Relat. Phenom.* **68**, (1994), 277–286.
- VII. M. Elango, R. Ruus, A. Kikas, A. Saar, A. Ausmees, and I. Martinson, Interplay of atomic and solid-state effects in inner-shell-resonant photoelectron spectra, *Phys. Rev. B*, **53**, (1996), R5978–R5981.
- VIII. R. Ruus, A. Kikas, A. Saar, A. Ausmees, E. Nõmmiste, J. Aarik, A. Aidla, T. Uustare, and I. Martinson, Ti 2p and O 1s X-ray absorption of TiO_2 polymorphs, *Solid State Commun.* **104**, (1997), 199–203.

Most of the papers have several authors, and I will therefore point out my own contribution to the various papers.

Paper I. I took part in the experimental work and in the preparation of the manuscript and also performed a substantial part of the calculations.

Paper II. I took part in the experimental work, but not in the preparation of the manuscript.

Paper III. I took part in the experimental work, performed the crystal field calculations and prepared corresponding part of the manuscript.

Papers V and VII. I performed the calculations and prepared the theoretical part of the manuscript.

Paper VI. I took part in the experimental work, performed the calculations and prepared the manuscripts.

Paper VIII. I took part in the experimental work and prepared the manuscript.

The following list of papers are not included in this thesis. They may be useful as they also deal with these problems, and will be referred to in the text.

1. M. Elango, A. Maiste and R. Ruus, Continuum and discrete states in the 3d photoabsorption spectra of Xe-like ions, *Physics Letters* **72A**, (1979), pp. 16–18.
2. R. E. Ruus, A. A. Maiste and Yu. A. Maksimov, Atomic and solid-state effects in the $L_{2,3}$ absorption spectra of calcium in some compounds, *Izv. Akad. Nauk SSSR Ser. Fiz.*, **46**, (1982), pp. 789–792 [*Bull. Acad. Sci. USSR, Phys. Ser.* **46**, (1982) pp. 155–158] (in Russian).
3. A. Kikas, A. Ausmees, M. Elango, E. Nõmmiste, R. Ruus, Auger decay of $K^+ L_{23}$ excitations in potassium halides, *Physica Scripta*, **T41**, (1992), pp. 237–240.
4. R. Ruus, A. Kikas, A. Maiste, E. Nõmmiste, A. Saar, M. Elango, J. F. van Acker, J. N. Andersen, R. Nyholm, M. Qvarford and I. Martinson, $M_{45}N_{45}N_{45}$ Auger decay spectra of the resonantly excited $3d^9 4f$ configuration of Xe-like ions in solids, *Phys. Rev. B*, **49**, (1994), 14836–14844.
5. A. Kikas, A. Ausmees, M. Elango, E. Nõmmiste, R. Ruus, A. Saar, Auto-ionization phenomena involving the $2p^5 3d$ configuration of argon-like ions in ionic solids, *J. Electron Spectrosc. Relat. Phenom.* **68**, (1994), 287–296.
6. T. Fondén, A. Kikas, R. Ruus, A. Saar, and M. Elango, Appearance of crystal-field splitting in 2p-resonant electron spectra of K^+ ions in ionic solids, *J. Electron Spectrosc. Relat. Phenom.* **76**, (1995), 589–594.

7. M. Elango, A. Kikas, A. Maiste, R. Ruus, A. Saar, NEXAFS of ionic solids as seen through resonantly excited electron spectra, *Physica B*, **208&209**, (1995), 47–48.
8. A. Maiste, A. Kikas, R. Ruus, A. Saar, and M. Elango, 3d-resonant photo-ja Auger emission of Ce in CeO₂, *J. Electron Spectrosc. Relat. Phenom.* **76**, (1995), 583–587.
9. F. M. F. de Groot, R. Ruus, and M. Elango, A charge transfer multiplet analysis of the resonant 2p3p3p Auger spectra of CaF₂, *Phys. Rev. B* **51**, (1995), 14062–14068.
10. R. Ruus, A. Saar, J. Aarik, A. Aidla, T. Uustare, and A. Kikas, Resonant Auger spectra of TiO₂ at Ti 2p and O 1s absorption edges, *J. Electron Spectrosc. Relat. Phenom.* **93**, (1998), 193–199.

1. INTRODUCTION

This thesis is rather unusual at least because of the papers, on which thesis is based, was done during the last two decades. Core spectroscopies, as near-edge x-ray absorption fine structure (NEXAFS), x-ray photoelectron spectroscopy (XPS), Auger electron spectroscopy (AES) have been very rapidly developed during the last decades and have improved considerably the knowledge of electronic structure of solids. The new techniques which have become available have made it possible to look at old problems from new angles and so reader can see progress in the theoretical understanding problems under study.

In large, we can divide papers, on which thesis is based, into two groups. The first group contains papers I–IV, which was published in 1980–1985. The main objects of the study in these papers were the electron excitations of ionic solids created by inner-shell excitation of two sequences, the argon-like (K^+ , Ca^{2+} , Sc^{3+} 2p excitations) and xenon-like (Γ , Cs^+ , Ba^{2+} , La^{3+} 3d excitations) sequences of ions. In the papers of this group it is demonstrated by using X-ray absorption spectroscopy (XAS) and electron excited X-ray emission spectroscopy (XES) that core hole drastically affect the electron densities of compounds. We found of strong atomic-like peaks in XAS spectra and explained the quasiatomic character of XAS spectra of argon- and xenon-like series by a collapse (an abrupt spatial contraction of the radial wave function) of 3d and 4f wavefunction, respectively. Collapse of excited electron wavefunction makes it impossible to explain the observed spectra by using the conventional interpretations based on energy band theory. The experimental work was done mainly on conventional X-ray sources. Some experimental work has been done by using synchrotron radiation from the VEPP-2M storage ring at Institute of Nuclear Physics, Novosibirsk.

The development of studies at the qualitative new level became possible at early 1990-ies when the spectroscopy of synchrotron radiation and electron spectroscopy reached the level, needed for a detailed study of the decay products of selectively created electron excitations (resonant excitations) of solids. So in the second group of papers, which contains papers V–VIII published in 1993–1997 we report on the resonant-photon-excited Auger and photoelectron spectra of the argonlike and xenonlike ions in ionic solids excited, respectively, in the vicinity of 2p and 3d absorption edges of these ions. The electron spectra have been studied to obtain detailed new data on the dynamics of X-ray excitations (including atom-like core excitons) in these solids and on the nature of their decay products. The observation of resonantly excited electron spectra has led us to a number of very interesting results and provides new insights about the electronic structure and excitation dynamics in argon-like and xenon-like sequences of ions in solids. The experiments have been carried out using synchrotron radiation at MAX-lab, Lund University, Sweden.

The interpretation of the complex observed phenomena couldn't unambiguously be made only on experimental ground. The interpretation of these experimental results is impossible without essential theoretical calculations. As if the first results indicated a dominating role of atomic effects in the collapsed electron excitations of ionic crystals, a calculation model based on the Hartree-Fock method was used. The solid-state effects on the wave functions were accounted using so called Watson sphere which reduces the effect of ions surrounding the considered ion (atom) to corrections of spherical symmetry. The intensities of electron transitions (photoexcitation cross sections, Auger transition rates) were calculated in the approximation of the intermediate coupling scheme. For the calculations the effective FORTRAN codes was developed and used.

This work is devoted to an experimental and theoretical study of collapse of 3d and 4f wavefunctions. The phenomenon of sudden compression of the radial wave function of an electron in neutral atoms or in an isoelectronic sequence, which was named electron collapse, was predicted by Fermi in 1928¹. He used the Thomas-Fermi (TF) statistical model of the atom to predict a collapse of orbitals to explain the formation of the rare-earth series of elements.

Goeppert Mayer² showed that the collapse of f electrons arises because of specific features of the effective potential for f electrons. In the central field model the atomic wave functions are determined by the atomic Coulombic attraction potential $V(r)$ and the centrifugal repulsion term $l(l+1)/2r^2$; the sum of both gives the effective potential $V_{eff}(r)=V(r)+l(l+1)/2r^2$ (atomic units are used throughout this thesis). For $l \geq 2$ electrons it consists of two wells separated by a potential barrier. The outer well is dominated by the long-range Coulombic potential and behaves asymptotically as $-1/r$ for neutral atoms. It is broad and shallow and can support an infinite Rydberg series of nl bound states. The inner well, on the other hand, is much narrower and deepens with increasing nuclear charge Z . For example, the first bound state of the inner well appears near $Z=58$, leading to the transfer of the f wave function from the outer to the inner well, to the collapse of the 4f wave functions (for reviews see Connerade³ and Karazija⁴).

Since the beginning of the 1970s, in connection with the extensive studies of excited configurations of atoms and ions, the potential barrier effects attract considerable attention and made it possible to explain a number of interesting effects in atomic spectra and in the physics of atomic collisions⁵.

The localization of the electron in the field of effective potential is highly sensitive to a change in the charge of the nucleus or of the states of the other electrons. Whereas in a certain configuration of the atom the wave function of the excited electron is localized predominantly in the region of the outer potential well, for the same configuration of the next atom in the Periodic Table, or even for another multielectron state of the atom, it can be localized already in the region of the internal well. This localization leads to a radical change even by several orders of magnitude for the values of the different characteristics of

the excited electron and manifests itself in the spectra by a nonmonotonic change of the type of coupling and of the energy positions of the lines, as well as by a redistribution of the intensity in the spectrum⁶. Griffin, Andrew and Cowan⁷ argued that configuration interaction is very important in determining orbital collapse.

The electron collapse is more clearly pronounced the larger the orbital quantum number of the electron. One can therefore expect a strong influence of the effect of the collapse of a nf electron in the configuration nd^9nf on the structure of the corresponding XAS, XES and decay spectra. In a number of papers⁸ the collapse of the $4f$ electron in the configuration $4d^94f$ (which occurs near $Z=55$) and its influence on the $4d$ absorption spectra were considered. The intensity of the spectrum should become redistributed among the channels $4d \rightarrow 4f$ and $4d \rightarrow \epsilon f$. In the indicated spectra, however, owing to the strong multielectron effects, a broad maximum predominates and masks the collapse effect. An interesting result of the experimental investigations is the establishment of the fact that the form of the $4d$ absorption spectra of elements that follow xenon in the Periodic Table is mainly of atomic origin, and the spectra of the vapors, metals, and solid-state compounds are very similar. In these systems the effective Coulomb interaction between the core hole and the excited electron is sufficiently strong to promote atomic-like localization. It is then appropriate to specify the initial and final states of the transition by atomic quantum numbers, and the observed spectral structure is associated with atomic multiplets rather than a peak in the density of states associated with the energy bands in the solids.

The detailed studies of the $4d$ excitations demonstrated the importance of electron correlation. For example, the large repulsive electrostatic interaction shifts the $Ba\ 4d^{10}\ ^1S_0 \rightarrow 4d^9\ ^1P_1$, oscillator strength into the continuum giving rise to the giant resonance above the ionisation threshold. In comparison to this, due to the smaller overlap of the $3d$ and $4f$ wavefunctions the Coulomb and exchange interactions are considerably reduced in case of the $3d$ excitations. Therefore in the $3d$ spectra the collapse of the $4f$ wavefunctions is expected to show up clearly along the series Xe to Ba .

Until 1980'th, the $4f$ and $3d$ orbital collapse phenomenon has been extensively investigated in both atoms and solids. In large part, these studies have concentrated on the transition $4d \rightarrow 4f$ in the pre-rare-earth metal and on the transition $3p \rightarrow 3d$ pre-transition metal atoms, respectively. There were no investigations on $4f$ and $3d$ orbital collapse in excited $3d$ and $2p$ configurations, neither theoretically nor experimentally. The main purpose of the present work is to investigate the $4f$ and $3d$ orbital collapse phenomenon in the case of $3d$ and $2p$ excitations in the Xe and Ar isoelectronic sequences, respectively. By studying the isoelectronic sequence, where these ions have the same electronic configuration, we can gain important insight into the collapse phenomenon from the systematic trends of these levels and other spectral properties.

In this thesis I laid emphasis on the theoretical analyses of our experimental resonant Auger spectra which have shed new light on the core-excited electronic states. For example, exposing the important role of localization of the 4f-electron wavefunction and the electron correlation. The observed trends of behaviour of 4f-features of photoexcited electron emission spectra in prelanthanide elements are useful to understand the corresponding features in the case of early rare-earth elements.

2. X-RAY ABSORPTION AND DECAY PROCESSES

2.1. X-ray absorption

If an x-ray photon absorbed in a solid, a core electron is excited to an empty state below the ionization threshold (x-ray excitons) or above threshold. The x-ray absorption spectrum can be divided into near edge and extended fine structure. The x-ray absorption near-edge structure (XANES) is extended in the first 30–40 eV past the absorption edge, while the extended x-ray absorption fine structure (EXAFS) covers the photon energy range from about 40 eV to about 1000 eV past the edge. It is now well established that EXAFS is a consequence of the modification of the photoelectron final state due to scattering by the surrounding atoms⁹. EXAFS spectroscopy has become a useful technique for investigating the local environment of specific atomic species in complex chemical system.

The interpretation of XANES spectra is more complicated than EXAFS spectra. So the observation of core excitons is a long-standing theoretical problem. The formal theory of solid state excitons concentrates on the tightly bound limit of the Frenkel exciton and on the loosely bound limit of the Wannier exciton¹⁰. The Frenkel exciton is usually approximated by molecular cluster methods or even atomic excitations and the translational invariance of the lattice is neglected¹¹. On the other hand, the Wannier exciton limit is treated using the effective mass formulation. Note that from a solid-state viewpoint, the bound to bound transitions to the collapsed final states are the atomiclike Frenkel excitons. The appearance of the core excitons and its type is dependent on the core hole-excited electron interaction, on the type of chemical bond, and on the widths of the bandgap. Indeed, Parrat¹² have proposed first, in the late 1950s, that some of the absorption peaks in the XANES spectra of alkali halides are due to the x-ray excitonic states produced by electron-hole Coulomb interaction. Nevertheless, in the case XANES of insulators there have been arguments on whether the observed peaks are within the forbidden gap (core excitons) or in the continuum because of the ambiguity in the position of absorption threshold. Note that in contrast to metals, which have a sharp density-of-states (DOS) cutoff at Fermi edge, the valence-band photoelectron spectra of insulators do not have a sharp edge on side nearer the vacuum level. Consequently the photoemission curves for these compounds do not terminate abruptly at low photon energies and therefore it is difficult to obtain an exact value for the photoelectric threshold¹³.

Nonexcitonic part of the XANES spectra is formed by the transitions to the unoccupied states above threshold. The procedures employed so far to calculate this part of the XANES spectra within an independent-electron picture have been based on one of two approaches: scattering formalism¹⁴ (short range) or band structure calculations¹⁵ (long range). Because of a core-excited atom of

nuclear charge Z is virtually identical to an impurity of charge $Z+1$, the final state wave function must correspond to an eigenstate of the system in the presence of the core hole. Nevertheless, the X-ray absorption is a complex many-particle process due to the change in potential when the core hole is created. So in correlated electronic systems like valence fluctuating compounds where the ground or/and absorption final states are described by a mixing of atomiclike configurations, the XANES spectra at threshold show a splitting of localized atomiclike resonances due to multielectron configurations.

2.2. Decay of the resonantly excited states

The advances in synchrotron radiation have provided a power tool to study the properties of resonantly excited states through their decay dynamics. When the energy of monochromatic x-rays is tuned through the threshold for ionization of an atomic inner shell, discrete excitonic states can be excited and decay emitting Auger electron. Note the very low fluorescence yields for soft x-rays. Typically only 0.1% of the core hole states of low Z elements decay by x-ray emission while the large majority decays through nonradiative processes (Auger and Coster Kronig). This process of resonant photon absorption accompanied by electron emission forms a resonant Auger Raman scattering. Nowadays, resonant Auger Raman scattering theory based on a unified theory of inelastic x-ray scattering which has been developed by Åberg *et al.*¹⁶ in terms of time-independent resonant scattering theory. This unified theory treated Auger electron emission including resonant Auger Raman scattering as resonances in the double-photoionization cross section and x-ray fluorescence as a resonance in inelastic x-ray scattering¹⁷. This general theory incorporates the evolution from the Raman scattering region below the threshold to post-collision region above the threshold and also asymptotically the two-step model of excitation and decay. The decay spectra in the Raman scattering region show the characteristics of the Auger resonance Raman effect: the resonance Auger peak positions move linearly with the photon energy, and the lifetime broadening does not contribute to the widths of the resonance Auger peaks. Nevertheless, linear dispersion of the resonant decay lines is valid for a single excited line. In the presence of vibrational degrees of freedom and closeness of many crystal field and vibrational sublevels make the energy dispersion of the center of gravity of the emission band a complicated function of the exciting photon energy¹⁸. When the excitation energy is varied over the threshold core-hole deexcitation or auto-ionization should continuously develop into the post-collision interaction (PCI) modified Auger spectrum and then into the Auger spectrum itself. In the case of the PCI, the Coulomb repulsion between a slow photoelectron receding from the atom and a fast Auger electron emitted in the decay leads to an energy loss of the photoelectron and a corresponding energy gain of the Auger electron. As a result, the effect displays as a shift and a

distortion of the shape of Auger electron lines in the spectrum. For example, it has been observed that in Xe the shift of the Auger peak due to the PCI is about 0.3 eV at the ionization threshold of the core level¹⁹. Nevertheless, I think that more important than PCI induced energy shift or broadening of the lineshapes for resonant decay spectra is that both semiclassical²⁰ and relativistic quantum theories²¹ of PCI predict the possibility of recapture of the photoelectron. The existence of the PCI induced recapture can be produce above the threshold these spectral features which are characteristic for the decay of the core excitons and leads to the vanishing of a clear difference in the decay spectra excited above and below the threshold. Recent model calculations²² show that the possibility of recapture of the photoelectron depends strongly on the inherent core level width and extend quite far above threshold.

Although a one step model of the photoemission process described above is more general and exact, the conventional two step model involving excitation and subsequent Auger decay in most of the cases works well. The two step model, in which Auger electron emission is considered to be independent from the x-ray absorption process and excitation and deexcitation steps are treated as consecutive and incoherent events has the virtue of simplicity and some pedagogic value. In a first step, a core electron is excited to an unoccupied orbital (free or localized), creating a core hole. The core hole states will mainly deexcite by Auger type processes. The normal decay of the core ionized state leaves two vacancies in the core or valence region. For the core excited (excitonic) states the decay takes place in the presence of an additional excited electron. If this electron is not directly involved in the decay the process is denoted spectator decay. If, on the other hand, the additional electron takes part in the Auger decay the process is referred to as a participator transition, and the final state is a similar one hole state as created in direct photoemission and the participator lines are degenerate with normal photoemission lines. These two processes may interfere cause the asymmetric, Fano line shapes in the electron spectra²³. The participator transition is identical with the autoionization phenomenon appearing commonly in outer shell ionizations. Recently the multi-atom resonant photoemission (MARPE) was discovered^{24,25} in MnO as the resonant enhancement of the O 1s photoelectron emission when the exciting photon energy was tuned across the Mn 2p resonances. In principle, this phenomenon can be ascribed to inter-atomic "participator" Auger transition, where the resonantly excited state decays through the direct recombination between the excited electron and core hole, leading to emission of an electron from one of the inner orbital of the neighbouring atoms.

For the MARPE, there is a most surprising the magnitude of this effect (as high as 100%) because one cannot exclude the possibility that these observations are artifacts of the experimental method. For a better understanding of this phenomenon detailed theoretical analyses as well as additional experimental information are required.

The resonance Auger spectator spectra show the shifts towards higher kinetic energy relative to the normal Auger spectra since a localized spectator electron will screen the final two hole states. In addition to the two dominant resonant Auger processes, the shake processes of the spectator electron related to the electronic screening of the core hole can be substantially modify the resonance Auger spectator spectra. Some important processes are shown pictorially in Fig. 1. Auger transition energies and probabilities are computed using the perturbation Wentzel (nonrelativistic theory) or Moller (relativistic theory) formulas²⁶.

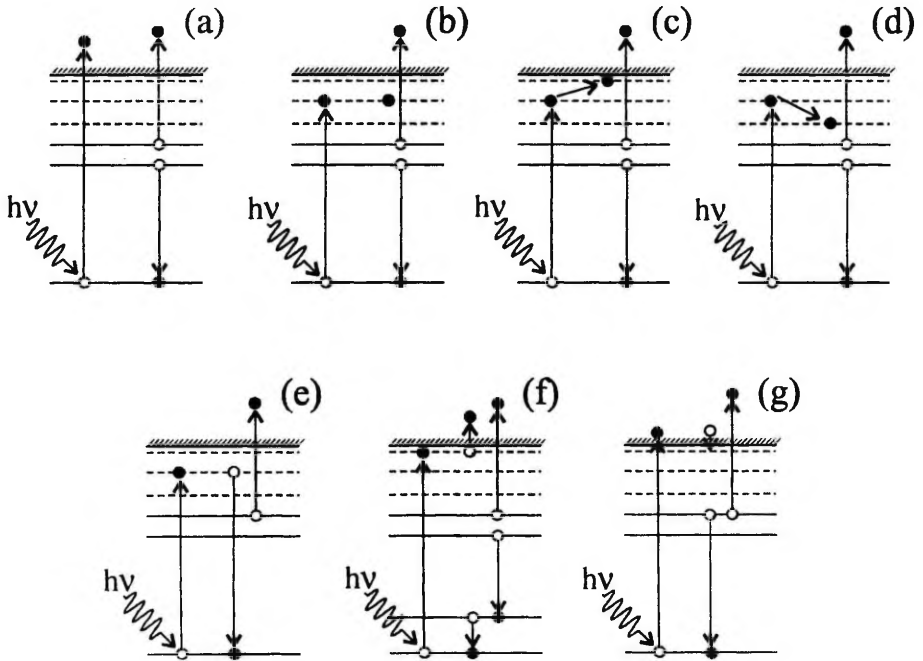


Fig. 1. Pictorial presentation of some important decay processes: a) normal and b) spectator Auger transitions, c) shake-up and d) shake-down modified spectator Auger transitions, e) participator Auger transition, f) Coster-Kronig and a subsequent normal Auger decay, g) PCI induced recapture.

The influence of the crystal environment on the Auger spectra depends crucially on the localization of the holes in Auger final ionic state. If the holes are well-localized i.e. are core holes, the solid state spectra is, in large, quite atomic-like. One of the most nowadays popular schemes for resonant photoemission calculations in solids is based on the configuration-interaction-type charge transfer model. The electronic structure can be described in terms of few

parameters, namely, the ligand-to-metal charge-transfer energy Δ , the on-site (d-d or f-f) Coulomb repulsion energy U , and the metal-ligand transfer integrals T . These parameters display systematic trends with atomic number and formal valence state (see e.g. ²⁷).

In contrast, if the Auger final ionic hole(s) falls to the valence band the solid state effect is very strong. The core-valence-valence (CVV) Auger spectral profiles considered two limiting cases. In first case the two valence holes may be found on different atomic sites due to hopping interactions. Then the interaction between holes is weak and the Auger process can be described by the self-convolution of the occupied part of the valence band DOS. In second case the strong correlation effects may localize the holes at the same atomic site. In this case the Cini-Sawatzky theory²⁸ explain the Auger profile of CVV transitions in terms of the relationship between correlation energy and the single-electron bandwidth.

3. CALCULATIONS

3.1. Calculation of the wavefunctions

3.1.1. Calculation of the bound wavefunctions

The necessary calculations for the various atomic configurations of the ions was performed using a selfconsistent-field procedure within the nonrelativistic single-electron Hartree-Fock-Pauli (HFP) approximation. This approximation uses the radial wave functions of the zero-order Hartree-Fock (HF) Hamiltonian and for the total energies takes into account the relativistic effects as corrections of the order α^2 (α is the fine structure constant)²⁹. The wavefunction calculations were carried out using the code,³⁰ which have been worked out in the Institute of Physics of the Lithuanian Academy of Sciences (Vilnius). To obtain the electronic wave functions for the ions in the crystals the original HFP code was modified. Mostly, in the calculations of the solid state spectra I have used the HFP approximation in conjunction with the Watson sphere model³¹. Note that the crystal field model, which is based on an Heitler-London picture and also described deformation of the wave functions of free ions in crystals, had already been proposed by Petrashen *et al.*³² before the work by Watson. The theoretical investigation of the properties of defects in ionic crystals as well as the perfect crystal systems by using wave functions generated by Petrashen model show good agreement with experimental data (for review, see monograph by Kristoffel³³ and references therein). In our calculations we used the Watson model because this is more simple and crystal structure independent. In this model the influence of the solid matrix on the electrons of an ion is simulated by superimposing on the potential of the free ion an additional potential due to a hollow sphere with charge $-Q=(Z-N)e$ and an appropriately chosen depth V_c or radius R of this potential well. Thus, the Hamiltonian in the crystal in this model is given by

$$H_{cr} = H_0 + \sum_{i=1}^N V(r) \quad (1)$$

where H_0 is the Hamiltonian for a free ion with nuclear charge Ze and N is number of electrons and

$$V(r) = \begin{cases} V_c = Qe/R & \text{for } r \leq R \\ Qe/r & \text{for } r > R \end{cases} \quad (2)$$

As an example, Fig. 2 demonstrates the effect of the choice of depth of the Watson sphere (V_c) on the radius of the calculated excited 3d and 4f radial wavefunction. As one can see in right panel of Fig. 2, the V_c dependence of the radius the 3d orbital can roughly be divided into three parts: first one ($-V_c=0-7$ eV),

where radius of the collapsed 3d wavefunction show almost no changes, the second one ($-V_c = 7-12$ eV), which show the linear increase of the radius with V_c and the third one, ($-V_c > 12$ eV), where 3d wavefunction is uncollapsed and show again only little changes. In left panel of Fig. 2 is displayed the analogous curve for 4f wavefunction in the case of the $3d^{-1}4f$ configuration of Cs^+ . The main difference in this case is the absence of the second part, i.e. the radial part of the 4f wavefunction crucially depends on the value of the Watson correction; if $-V_c$ becomes greater than 5.2 eV the mean 4f radius abruptly increases from 1.5 to 17 a.u. Unfortunately, the choice of the parameters of the Watson sphere for a particular compound are substantially optional. Nevertheless, for the ionic crystals the physically justified parameters associated with the Watson sphere are the total charge Q , which equals to the ionicity of the ion, and the V_c , which is equal to the Madelung potential in the ion site, i.e. the potential (V_c) at the ionic site coincides with the Coulombic crystal potential at that site. Generally, the influence of the Watson sphere on the wavefunction reduces to the compression of the orbitals for the anions and to delocalization ones for the cations (nephelauxetic effect).

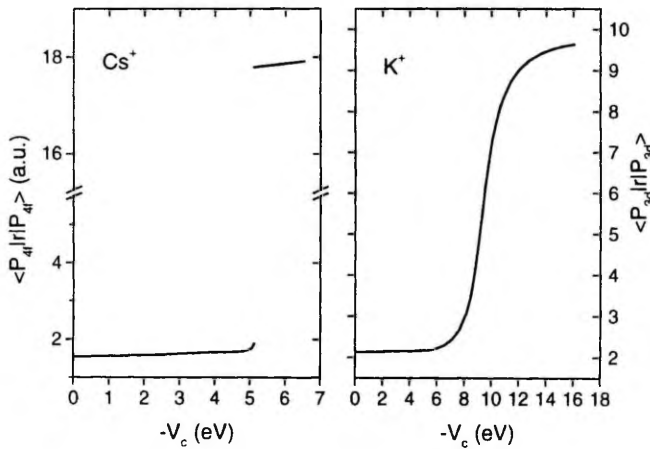


Fig. 2. The depth of the Watson sphere (V_c) dependence of the radius of the calculated excited 3d (K^+ , in right panel) and 4f (Cs^+ , in left panel) radial wavefunction.

3.1.2. Calculation of the continuum wavefunctions

For the calculation of Auger rates, one needs the simultaneous knowledge of the bound and the continuum wavefunctions. The continuum wavefunctions were generated by solving the Hartree-Fock equations corresponding to the Auger final state. A Schmidt orthogonalization to the bound wavefunctions was used. The numerical calculation of a continuum wavefunction depends critically on the normalization of the wavefunction. Since continuum wavefunction oscillate

in the larger radial distances, the usual logarithmic grid mesh which was used for calculation of the atomic bound states, is not practical in a computational procedure. In calculating continuum orbitals the whole radial region was divided into two parts, i.e., the inner region, where the logarithmic grid and the outer region, where the linear grid was used and where calculation is performed without the exchange interaction between the bound and continuum electrons. The radial function $P_{\epsilon l}(r)$ has the asymptotic form:

$$P_{\epsilon l}(r) \xrightarrow{r \rightarrow \infty} 2^{1/4} \pi^{-1/2} \epsilon^{-1/4} \sin \left(\sqrt{2\epsilon} r - \frac{Z-N}{\sqrt{2\epsilon}} \ln(2\sqrt{2\epsilon} r) - \frac{l\pi}{2} + \delta_l \right) \quad (3)$$

where ϵ and l are energy and orbital momentum of the continuum electron, respectively, N is number of electrons and δ is a phase factor. Normalization constant was found by matching $P_{\epsilon l}(r)$ with a specific comparison function at the asymptotic region. Calculated continuum wavefunctions are then used to determine the Auger rates.

3.2. Calculation of the transition probabilities

The oscillator strength $f_{n \rightarrow m}$ for electric multipole transitions from state n to state m was calculated by using the following formula:

$$f_{n \rightarrow m} = \frac{(2k+1)(k+1)\alpha^{2(k-1)}}{k[(2k+1)!!]^2 g_n} (E_m - E_n)^{2k-1} \left| \sum_{ij} a_{mj} a_{ni} D_{ij} S_{ij} \right|^2 \quad (4)$$

where a_{ni} and a_{mj} are expansion coefficients of intermediate coupling (indices n and m) over the functions of LS coupling (i and j indices).

$$D_{ij} = \left\langle \gamma_i L_i S_i \left| R^{(k)} \right| \gamma_j L_j S_j \right\rangle \quad (5)$$

is the transition matrix element in LS coupling

$$S_{ij} = \prod_q \left\langle n_{iq} l_{iq} \left| n_{jq} l_{jq} \right. \right\rangle \quad (6)$$

is the overlap factor and $g_n = 2J_n + 1$ statistical weight of n 'th level

The multipole radiation field operator $R^{(k)}$ of order k ($k=1$ for dipole transitions) is³⁴

$$R^{(k)} = Q^{(k)} + G \sqrt{k/(k+1)} \left(\frac{1}{E_m - E_n} Q'^{(k)} - Q^{(k)} \right) \quad (7)$$

where G is the gauge parameter: $G=0$ for the Coulomb gauge and $G=[(k+1)/k]^{1/2}$ for the Babushkin gauge. In the nonrelativistic limit $G=0$ gives

the length form of matrix elements whilst $G=[(k+1)/k]^{1/2}$ gives the velocity form and

$$Q^{(k)} = -r^k C^{(k)} \quad (8)$$

$$Q'^{(k)} = -r^{k-1} \left\{ C^{(k)} \frac{\delta}{\delta r} + \frac{i}{r} \sqrt{k/(k+1)} [C^{(k)} \times L^{(1)}]^{(k)} \right\} \quad (9)$$

Relativistic corrections to the transition operator were found to be small and in calculations published in the papers these corrections had been neglected.

$\sigma_{n \rightarrow m}$ is the excitation cross section

$$\sigma_{n \rightarrow m} = 2\pi^2 \alpha f_{n \rightarrow m} = 109.794 f_{n \rightarrow m} \text{ (Mb} \cdot \text{eV)} \quad (10)$$

Equation (4) differs from the standard one by the presence of the overlap coefficient S_{ij} (formula 6) using which, in the first approximation, the relaxation of the core can be taken into account. Use of the velocity formula is associated with the fact that it is preferred when calculating transitions from deep levels. The calculation indicated that the oscillator strengths, calculated according to the velocity and length formulas, in the case of transitions to uncollapsed states, differ by <15%, and for the case of collapsed states practically coincide.

3.3. Calculation of the Auger transition probabilities

In the calculations the resonant Auger spectrum we treat the inner-shell excitation and its Auger decay as a two-step process. In terms of a two-step approach in which the decay is treated independently from the primary excitation the resonant Auger emission intensity can be given as

$$I(E, h\nu) \propto \sum_{if} \sigma_i W_{if} \quad (11)$$

Here E is the Auger energy and $h\nu$ is the photon energy i refer to the intermediate state and f to the final state. σ_i is the photoexcitation cross section (from the ground state to the state i) using the formula (10). In the calculations of the normal Auger spectra has been assumed that the intermediate levels i are uniformly populated with a statistical weight of $\sigma_i \propto 2J_i + 1$ (J_i is the total quantum number for the state i). W_{if} is the Auger transition rate from the intermediate state i to the final ionic state f with continuum wave functions $|el\rangle$ normalized to represent one ejected electron per unit time is

$$W_{if} = \sum_i \left| \sum_{\mu} \sum_{\mu'} C_{i\mu} C_{f\mu'} \langle \gamma L' S' J' e l j J | \sum_{\alpha < \beta} 1/r_{\alpha\beta} | \gamma L S J \rangle \right|^2 \quad (12)$$

where L, S, J (or L', S', J') are the orbital, spin, and total quantum numbers of the intermediate (or final ionic) state of the ion (γ and γ' includes whatever other quantum numbers are required). $C_{i\mu}$ and $C_{f\mu'}$ are mixing coefficients for the states i and f in the intermediate coupling scheme. In intermediate coupling the spin-orbit interaction is treated as a perturbation which couples different states $|SLJ\rangle$ with the same J , constructed as zero-order wave functions in LS coupling. The total angular momenta J' and j of the final ionic states and the continuum electron, respectively, are recoupled in the final state of the system. The transition matrix elements in Eq. (12) can be evaluated by using the Jj-LS unitary transformation. Then

$$\begin{aligned} \langle \gamma L' S' J' \epsilon j J | \sum_{\alpha < \beta} 1/r_{\alpha\beta} | \gamma L S J \rangle &= [L, S, j, J']^{1/2} \begin{Bmatrix} L' & l & L \\ S' & \frac{1}{2} & S \\ J' & j & J \end{Bmatrix} \times \\ &\times \langle \gamma L' S' \epsilon l L S | \sum_{\alpha < \beta} 1/r_{\alpha\beta} | \gamma L S \rangle \end{aligned} \quad (13)$$

In the configuration interaction approach we used the wave functions for each state written as a linear combination of basis wave functions, each of which represents a particular single-configuration state in the LS coupling scheme. For the determination of the Auger decay of the $2p^5 3d$ excited state only the most important final configurations $3s^2 3p^4 3d$, $3s^2 3p^4 4s$, and $3s 3p^6$ are included in the configuration interaction calculations. In the case of the collapsed $4f$ orbital, the interaction of $4d^{-2} 4f$ and $4p^{-1}$ configurations is expected to be very strong. We treat these configurations together and calculate transitions $3d^{-1} 4f \rightarrow 4p^{-1} + 4d^{-2} 4f$ in a configuration-superposition approximation.

Following I depict in Fig. 3 scheme of calculation of the Auger intensities and list of program codes used for the calculation.

1. Program F computes the bound wavefunctions in the HFP approximation.
2. Program T computes the angular coefficients for electrostatic and spin-orbit interactions.
3. Programs TT, TT1, TT2, TT3 compute different types of the configuration interaction matrix elements:
 - TT computes $\left[l_1^{N_1} l_2^{N_2} l_3^{N_3} \alpha L S \parallel H^e \parallel l_1^{N_1} l_2^{N_2-1} l_3^{N_3+1} \alpha' L S \right]$
 - TT1 computes $\left[l_1^{N_1} l_2^{N_2} l_3^{N_3} \alpha L S \parallel H^e \parallel l_1^{N_1-1} l_2^{N_2-1} l_3^{N_3+2} \alpha' L S \right]$
 - TT2 computes $\left[l_1^{N_1} l_2^{N_2} l_3^{N_3} \alpha L S \parallel H^e \parallel l_1^{N_1} l_2^{N_2-2} l_3^{N_3+2} \alpha' L S \right]$
 - TT3 computes $\left[l_1^{N_1} l_2^{N_2} l_3^{N_3} l_4^{N_4} \alpha L S \parallel H^e \parallel l_1^{N_1-1} l_2^{N_2-1} l_3^{N_3+1} l_4^{N_4+1} \alpha' L S \right]$

where H^e is the electrostatic operator

$$H^e = \sum_{j>i=1}^N \sum_k \frac{r_{<}^k}{r_{>}^{k+1}} (C_i^{(k)} \cdot C_j^{(k)})$$

4. Program TAA computes excitation energies and cross-sections, configuration interaction is accounted for by using superposition of different configurations.
5. Program FF computes continuum wave functions optimized in the field of the frozen Auger final ionic state and Auger radial matrix elements.
6. Program TAU computes Auger energies and intensities.

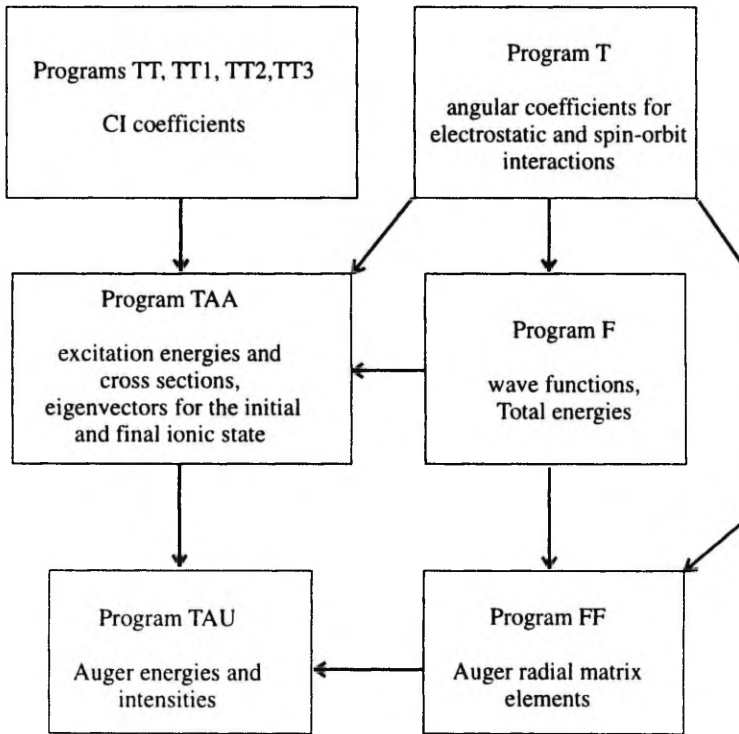


Fig. 3. Scheme of calculation of the Auger transitions.

Several restrictions apply to possible calculations. Although the calculation of the angular part Auger transitions (in code TAU) is quite general, the input data organization limits the use of this program only for calculations single-ionized or excited closed shell ions/atoms. The transition probabilities package, code TAA, is more general and limits the orbital quantum numbers l , L and number of different configurations to a maximum value of 10 and number of unfilled subshells is restricted to be at most three.

4. EXPERIMENTAL TECHNIQUE

The experimental part of the studies presented in this thesis may be divided into two parts.

In first one performed in 1980–1985, experimental work based on conventional x-ray absorption and emission techniques. The measurements were performed with an RSM-500 x-ray monochromator spectrometer, with a glass diffraction grating (600 lines/mm, curvature radius 6 m) equipped with a x-ray tube with a tungsten anode operated at 5 kV and 90 mA. The higher orders of the bremsstrahlung emission were suppressed by a focusing mirror. The x-rays were recorded with an argon-methane flow proportional counter equipped with a nitrocellulose window. Thin films of the investigated substances, whose thickness was measured with the aid of a quartz oscillator accurate to ~20%, were evaporated on the nitrocellulose films in vacuum in the measuring chamber of the spectrometer. In some cases instead of the absorption spectra we measured the photoelectric quantum-yield (electron emission) spectra $\alpha(h\nu)$, using the bremsstrahlung of the tungsten target cathode. The validity of such a substitution in study of the structure of the $\mu(h\nu)$ spectrum is well known and widely used when direct measurement of absorption is impossible or inexpedient³⁵. Some spectra were measured by using instead of a x-ray tube the synchrotron radiation from the VEPP-2M storage ring. In the measurement of the x-ray emission spectra, the samples were attached in the form of thin sheets to copper plates serving as the target cathode of the x-ray tube, and were covered with thin aluminum sheets which provided for some deceleration of the exciting electrons (in order to reduce reabsorption) and for protection from radiolysis in the more powerful operating regimes of the tube.

Second part of the experimental work has been carried out at beam line 22 MAX-lab (in Lund, Sweden). This beam line equipped with a modified SX-700 monochromator (360 l/mm and 1220 l/mm gratings) with plane-elliptical focusing mirror giving reasonable photon flux in the 20–1000 eV. The experimental end station consists of separate analyzer and preparation chambers accessible via a long-travel manipulator. The analyzer chamber is equipped with a hemispherical SCIENTA electron energy analyzer (SES-200).

Yield spectra, which are compatible to the absorption, were recorded by constant final state (CFS) mode, the final energy being set to monitor the low energy background of inelastically scattered electrons (total yield), or, the final kinetic energy being set equal to some intense Auger transition energies. Some spectra was taken in constant initial state (CIS) mode where the photon energy and detector-energy window are swept synchronously in order to count the electrons being emitted from only one initial state.

The samples has been usually deposited by evaporation in a vacuum of about 10^{-7} Torr at room temperature on a stainless-steel substrate with evaporation rates about some Å per sec. Then, the samples were *in situ* transferred into the

analysis chamber with base pressure of about 10^{-10} Torr. In order to prevent the charging-up effect of the sample, the thickness of the samples was about 100 Å. The only exception being the TiO₂ films which were grown *ex situ* on (111)-oriented silicon substrates using the low-pressure flow-type atomic layer deposition reactor³⁶. The thickness of the TiO₂ films was about 40 nm which structure was checked by high-energy electron diffraction measurements.

5. COLLAPSE OF THE 3d WAVEFUNCTION IN THE ISOELECTRONIC SEQUENCE OF ARGON-LIKE IONS

5.1. Effect of collapse of the 3d orbital on atomic properties.

In the paper IV the 3d electron collapse at the 2p excitations in the Ar-like ions has been studied theoretically. Note at first that in a series of papers, e.g.³⁷, in which the collapse of the 3d electron in configurations with a 3p vacancy and its effect on $3p^6 \rightarrow 3p^5 3d$ transitions have been studied in detail, a strong dependence of the 3d orbital on the term has been discovered. For example in the K^+ ion, the 3d orbital of the singlet 1P term is localized in the external potential well (uncollapsed), and the triplet 3P and 3D terms in the internal well (collapsed). However, calculations of the excited configurations with a 2p vacancy show substantial differences.

In Table I are presented the calculated values for the mean radius of the nd orbitals r_{nd} , the radial integrals of the nonspherical part of electrostatic interaction $F^2(2p, nd)$ and $G^1(2p, nd)$, the constant of spin-orbit interaction of the nd shell $\eta(nd)$, and of the integrals of dipole transition $\langle 2p | r | nd \rangle$ of a series of 2p shell excited configurations in argon and argon-like ions. Examination of the data in Table I show that the collapse of the 3d electron in the isoelectronic series of argon occur beginning of the K^+ ion, and in a series of argon ions beginning of the Ar^+ ion; in this case r_{nd} varies in a step-like manner by many times, and the electrostatic and spin-orbit interaction of the 3d shell by 1 to 2 orders of magnitude.

The weak overlap of the 2p and uncollapsed nd orbitals leads to the small value of the integrals of electrostatic interaction and dipole transition between corresponding states, and the smallness of $\eta(nd)$ indicates the small probability of penetration of the uncollapsed nd electron into the inner region of the atom. The fact that in configurations with uncollapsed nd orbitals spin-orbit interaction of the 2p shell significantly exceeds $G^1(2p, nd)$ and $F^2(2p, nd)$ indicates the closeness of the coupling to the jj type. On collapse of the 3d electron, the electrostatic pd interaction converges in value with the spin-orbital interaction, and a significant deviation from a pure jj coupling occurs; the coupling acquires an intermediate character. In contrast to the calculations with a 3p vacancy where term-dependence was expected to be strong in our calculations the dependence of the 3d orbital on the term, caused by Coulomb interaction in the 2p shell, was not taken into account, since the effective potential for the 3d electron in the $2p^5 3p^N 3d$ configuration is determined primarily by the 2p vacancy.

Table I. Effect of localization of an excited nd electron on atomic properties (in a.u., η in eV).

Atom	Config.	r_{nd}	$G^1(2p,nd)$	$F^2(2p,nd)$	$\eta(nd)$	$\langle 2p r nd \rangle$
Ar	$2p^5 3d$	9.3	0.0009	0.00235	0.0001	0.023
Ar	$2p^5 4d$	18.9	0.0007	0.00152	0.0001	0.019
Ar ⁺	$2p^5 3p^5 3d$	2.7	0.0309	0.0552	0.0044	0.132
Ar ²⁺	$2p^5 3p^4 3d$	1.8	0.0675	0.11	0.0095	0.194
Ar ⁶⁺	$2p^5 3d$	1.2	0.163	0.215	0.021	0.275
K ⁺	$2p^5 3d$	2.1	0.0537	0.0844	0.0079	0.147
K ⁺	$2p^5 4d$	10.1	0.0469	0.00727	0.0008	0.043
Ca ²⁺	$2p^5 3d$	1.5	0.1	0.144	0.018	0.175
Sc ³⁺	$2p^5 3d$	1.2	0.141	0.192	0.03	0.183
Ti ⁴⁺	$2p^5 3d$	1.1	0.181	0.237	0.046	0.187

Due to strongly varying values of pd interaction on collapse, the position of the levels changes and a redistribution of the transition intensities in the multiplets occur. On transition to uncollapsed states, the ratio of the oscillator strengths $\frac{f(2p_{1/2} \rightarrow nl)}{f(2p_{2/3} \rightarrow nl)} = \frac{2}{3}$, i.e., it corresponds to an approximately statistical intensity

distribution under jj coupling. For the collapsed 3d orbital, both components of the multiplet in K^+ have approximately the same intensity. The relatively high values of the oscillator strengths for the $2p \rightarrow 4d$ transitions in K^+ are explained by the penetration of the first maximum of the 4d wave function into the internal potential well.

The intensity of the $2p \rightarrow 4s$ transitions increase only by several times and their influence on the formation of near edge structure of the $L_{2,3}$ absorption spectrum in argon-like ions is insignificant. However, the configuration interaction leads to significant changes in oscillator strengths because of the closeness in energy of the excited 4s and 3d some levels in K^+ and Ca^{2+} . In fact configuration interaction leads to a redistribution of the oscillator strengths of transitions between some states of the $2p^5 3d$ and $2p^5 4s$ configurations. Note that on collapse there is a strong dependence of 3d orbital on the potential, and a relatively small change in the wave functions strongly affects the calculated oscillator strengths.

5.2. Collapse of the 3d orbital and 2p absorption spectra

In paper II the collapse of the 3d orbital was investigated experimentally by means of a x-ray absorption technique in the $2p \rightarrow 3d$ photoabsorption region. In order to demonstrate the dynamics of 3d-electron collapse in the isoelectronic sequence of argon-like ions in Fig. 4 is presented together the $L_{2,3}$ absorption spectra of Cl^- (in KCl^{38}), Ar^{39} , K^+ (in KCl), and Ca^{2+} (in CaF_2). The dashed line indicates the ionization energy $E(L_3)$ of the L_3 subshell of the corresponding free ions. From Fig. 4 it is evident that the spectra for Cl^- and Ar are radically different from the spectra for K^+ and Ca^{2+} . These spectra are interpreted well from the point of view of 3d orbital collapse in the Ar-like isoelectronic sequence. Since these orbitals are located far from the nucleus (in the case of Cl^- and Ar), the maximum of the photoabsorption cross section is attained in the continuum region of the spectrum. As Z increases, the oscillator strength is shifted closer to the absorption threshold and increases in absolute magnitude. On going to K^+ , the role of the $2p \rightarrow 3d$ transitions sharply increases; they completely dominate in the spectrum. In the case of Ca^{2+} the intensity of the main maxima increases even more. All of the data presented show that the sharp contraction of the 3d orbitals begins on going from Ar to K^+ and is continued on going from K^+ to Ca^{2+} . Thus, the data presented in Fig. 4 show that, in the isoelectronic sequence of argon like ions, 3d-orbital collapse in the $2p^5 3d$ configuration occurs in the $\text{Ar} \rightarrow \text{K}^+ \rightarrow \text{Ca}^{2+}$ sequence.

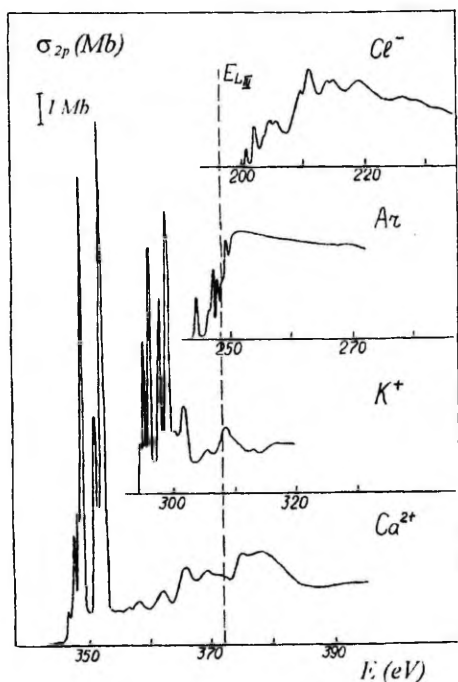


Fig. 4. Photoabsorption cross sections of the argon-like ions Cl^- in KCl , Ar, K^+ in KCl , Ca^{2+} in the $L_{2,3}$ -edge region.

According to the solid-state classification of electronic excitations, the intense maxima at the threshold of all the spectra under consideration correspond to the so-called x-ray excitons. The fact that such excitonic states are similar to the corresponding free-ion states is well understood on the basis of the 3d-orbital collapse. The $2p \rightarrow 3d$ transition occurs practically within the cation. Therefore for such transitions, the situation on the crystal is not much different from the situation in the free ion, and the effect of the environment may be considered as a perturbation (for example, within the framework of ligand field theory).

5.3. Crystal field splitting of the 3d electrons

Paper III is devoted the calculations of the XANES spectra of KCl. The main part of this paper have been focused to the cluster calculations of the spectra performed by Vedrinskii and co-workers from Rostov-on-Don (Russia), but there is presented (paper III, in the insert of Fig. 2) also the results of my calculation of the $2p \rightarrow 3d+4s$ transitions for K^+ ion in cubic crystal field. This paper III is included in the list of papers because of the first, to my knowledge, successful interpretation of $L_{2,3}$ XANES of potassium in solids by means of crystal field theory.

In contrast to 4f electrons, which are deeply embedded inside the rare earth ion and consequently are insensitive to its external environment, the 3d electrons with the larger spatial extent are strongly affected by crystal field. The response of the 3d electrons to the environment can be observed through a number of physical phenomena, i.e. crystal field splitting, line intensities in the optical spectra, paramagnetic resonance etc. In this respect the differences between 3d and 4f electrons are well illustrated by the respective values of their crystal field parameters. Typical values of the e_g-t_{2g} splitting ($10Dq$) for iron in octahedral complexes are 1.6–1.9 eV,⁴⁰ whereas the same parameter for triply ionized lanthanide ions seldom exceeds 0.2–0.3 eV.

According to the simple ionic model and the O_h point symmetry of system the orbitals relevant to the $2p \rightarrow 3d$ and $2p \rightarrow 4s$ excitations are assumed to be bases of irreducible representations, t_{1u} , a_{1g} , t_{2g} and e_g , corresponding to cation atomic orbitals 2p, 4s, 3d. Radial parts of t_{2g} and e_g orbitals are assumed to be same and to have the d-character only. The mixing of the final state configurations $2p^5 3d$ and $2p^5 4s$ has to taken into account because of the closeness of the energies that may result in the redistribution of the intensities in the spectra. Calculations was performed using the method of calculation similar to this was applied to calculations of $4p^6 \rightarrow 4p^5 5s$ and $4p^6 \rightarrow 4p^5 4d$ excitations in Rb halides⁴¹. However, the main difference between our and above mentioned one is this that in latter calculations the diagonal elements of the secular matrix was produced neglecting the relaxation effects induced by the inner hole while

in my calculations these effects was accounted. Because of the magnitudes of the Coulomb interaction between electrons, the spin-orbit interaction and the cubic field splitting was expected to be of the same order so that we have to diagonalize a nine-dimensional energy matrix, while seven states originates from $2p^5 3d$ and two from $2p^5 4s$ final configuration. As an example we present on Fig. 5 $2p^6 \rightarrow 2p^5 3d + 2p^5 4s$ transition energies and intensities in K^+ ion in O_h crystal field as a function of crystal field parameter $10Dq$.

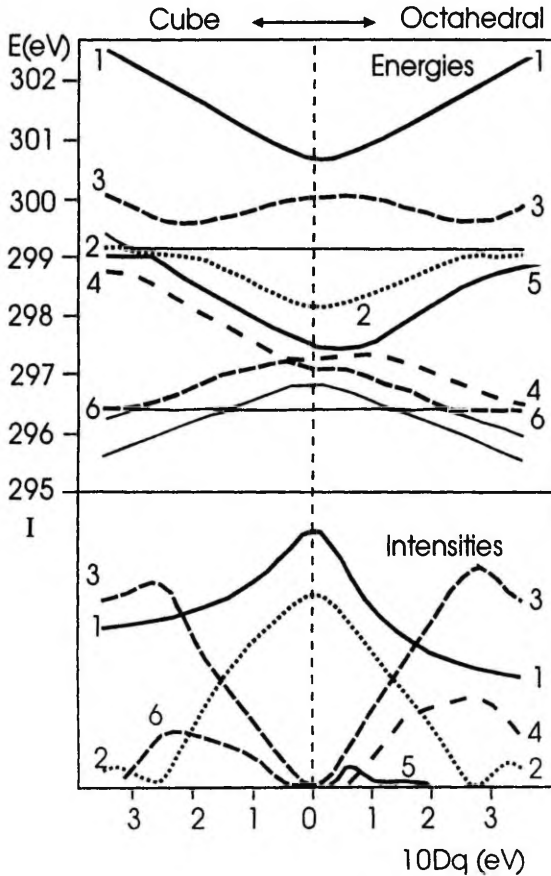


Fig. 5. $2p^6 \rightarrow 2p^5 3d + 2p^5 4s$ transition energies and intensities in K^+ ion in O_h crystal field as a function of crystal field parameter $10Dq$.

The crystal field mixes the free ion states with different total angular momentum. The intensities of the computed spectra are more dependent on the crystal field than the energies of levels. It is interesting to note that the distribution of the intensities and energy levels depends weakly on the crystal structure (cubic or octahedral). This is mainly due to the strong spin-orbit interaction in the $2p$ shell.

In Fig. 6 we show $L_{2,3}$ absorption spectra of K^+ in potassium halides and main theoretical crystal field intensities indicated as ticks in the spectra. The

crystal field parameters, $10Dq$, was calculated by using the same calculated free ion 3d orbital for all the compounds. The calculated $10Dq$ values are 1.5 eV for KF, 1.1 eV for KCl, 1 eV for KBr and 0.9 eV for KI. Theory shows that the crystal field has a slightly different effect on the L_3 edge, compared to the L_2 edge. This small difference between these edges can also be seen in the experimental spectra. Our crystal field calculations are in good agreement with the latter, more detailed theoretical investigation by de Goot *et al.*⁴² Note that Figures 5 and 6 are not published but were presented in the poster session at the 2th All-Union Conference on Quantum Chemistry of the Solid State, Riga, 1985⁴³.

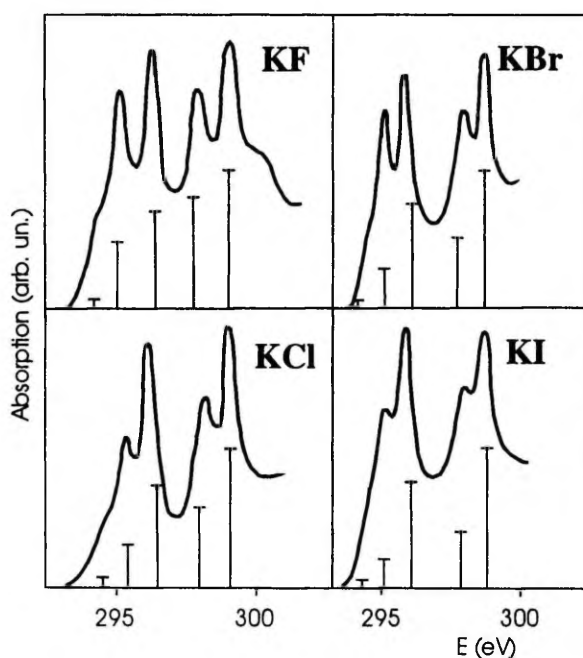


Fig. 6. The experimental $L_{2,3}$ absorption spectra (solid lines) of K^+ in potassium halides compared with crystal field calculations (ticks).

Without explicitly taking into account the 3d electron collapse phenomena it is impossible the correct interpretation $L_{2,3}$ absorption spectra in the isoelectronic of Ar-like ions. So assignment of the experimental $L_{2,3}$ absorption spectra⁴⁴ is incorrect as they overestimated role of $2p^6 \rightarrow 2p^5 4s$ transitions in spectra. Also is incorrect the crystal field calculation⁴⁵ of the $M_{4,5}$ absorption spectra of potassium halides where was not accounted the singlet-triplet term-dependent collapse of 3d wavefunction.

Very interesting from crystal field viewpoint is to study of polymorphic forms of particular compound which enables one to elucidate the influence of the "pure" crystal structure on the electronic system of a compound. TiO_2 as an insulating d^0 compound has a good candidate for such study. In paper VIII we perform experimental XANES and resonant Auger studies of TiO_2 -II, rutile and anatase. Previous experimental and theoretical studies of Ti $2p$ ⁴⁶⁻⁵⁰ and of low-

pressure TiO_2 phases show that crystal field theory provides generally an adequate interpretation of the XANES spectra. Nevertheless, the high-energy part of the Ti L_3 XANES and its structural sensitivity remains unexplained by a ligand field multiplet model⁵¹. Our measurements of various TiO_2 polymorphs demonstrate the sensitivity of x-ray absorption spectra to structural changes in the solid state. From the resonant electron spectra at the L_3 threshold of Ti it is concluded a strong delocalization of the 3d electron for the excitations where the largest differences between the Ti 2p XANES of TiO_2 polymorphs are observed. These differences in absorption spectra are attributed to increasing strength of the crystal field caused by delocalization of the excited 3d electron.

5.4. Resonant electron spectra of RbCl. Case of uncollapsed 4s orbital and effect of the 3d-electron collapse on the spectator decay spectrum

In paper VII the resonant Auger spectra of RbCl were investigated. The photoelectron spectra of metal chlorides excited at the chlorine 2p absorption edge are good examples to investigate of the decay spectra from the uncollapsed excitations. Considering the absorption final states as the empty *s*- and *d*-like conduction band states the comparison with the band structure calculations⁵² leads to the picture, according to which the first few absorption maxima reflect the core excitons at the Γ_1 and X_3 points of the Brillouin zone (see, e. g. Watanabe⁵³). We had shown in paper VII that the photoelectron and Auger spectra of RbCl exhibit strong resonance behaviour when the energy of incident photons passes through the L_{23} absorption edge of chlorine. The theoretical study of the electron spectra somewhat surprisingly show that decay spectra may be described in terms of atomlike normal $2p^5 \rightarrow 3p^4$ as well as the spectator $2p^5 4s(3d) \rightarrow 3p^4 4s(3d)$ transitions. Consequently, the absorption spectra of core excitons may be understood in terms of atomic $2p^6 \rightarrow 2p^5 4s(3d)$ transitions. In the sequence of chlorides with increasing valence bandwidth the band-like shape of the spectra continuously replaces the atomic-like resonance decay spectra.

Fig. 7 shows effect of the collapse of 3d wavefunction on the Auger $L_3 M_{23} M_{23}$ 3d spectator spectra. The calculated $2p_{3/2} 3d \rightarrow 3p^4 3d$ Auger spectrum is very sensitive to the mean radius of the 3d wavefunction of the final ionic two-hole configuration, R_{3d} . With increasing R_{3d} the spectrum obtains the normal Auger two-band structure observable in RbCl^- .

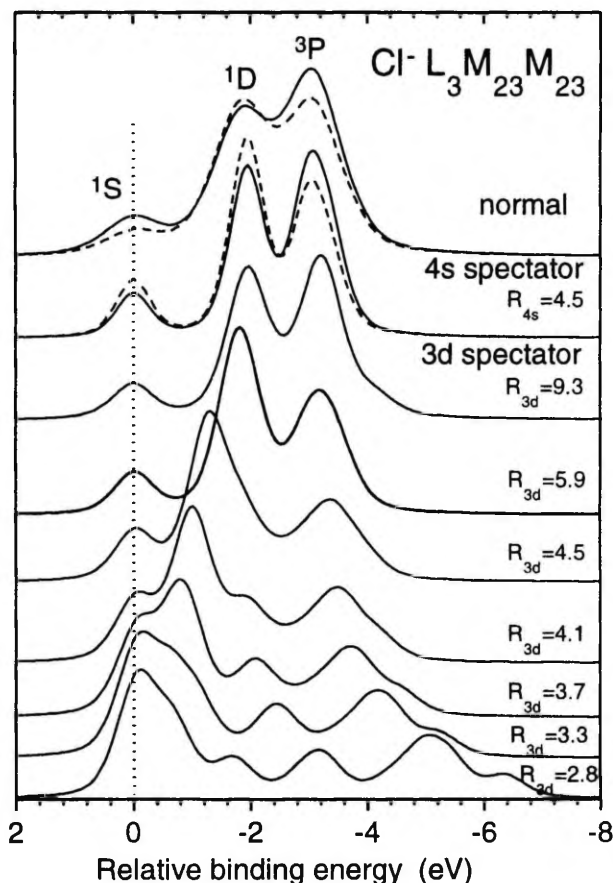


Fig. 7. Calculated $\text{Cl}^- L_3 M_{23} M_{23}$ Auger spectra for RbCl . The zero binding energy corresponds to the transition energy of the highest level of the final ionic configuration. The normal, $4s$ and $3d$ spectator spectra are broadened by the Voigt function with FWHM of 1.1, 0.7, and 0.8 eV, respectively. For the $3d$ spectator Auger spectra the depth of the Watson sphere varies from zero (the uppermost spectrum) to 16.3 eV (the bottom spectrum). The mean radius of the spectator electron R_{3d} in the final ionic configuration is indicated at each spectrum. The dashed spectra are corrected ones using the experimental data for argon atoms⁵⁴.

This comparison indicates that the interpretation of the absorption spectrum in terms of atomic-like Frenkel excitons may well compete with the traditional interpretation based on the calculated structure of the undisturbed conduction band⁵⁵. Thus, the creation and decay of excitations related to the chlorine L_{23} pre-edge region of RbCl may reasonably well be understood in terms of atomic processes within chlorine ions.

5.5. Resonant electron spectra of KCl.

Case of collapsed 3d orbital

In paper V the photo-induced in the vicinity of the L_{23} absorption edges Auger and photoelectron spectra of argonlike ions Cl^- (in NaCl), K^+ (in KCl), Ca^{2+} (in $CaCl_2$ and CaF_2), and Sc^{3+} (in Sc_2O_3) have been studied both experimentally and theoretically. Here, as an example, is presented some results of a study of 3d collapse phenomena in the case of resonant photoionization of the $2p^6$ shell of the argonlike ion K^+ in KCl.

The photoabsorption may be described here as a transition $2p^6 \rightarrow 2p^5 3d(4s)$ in the particular ion, modified by the crystal field. More detailed information about the core-excited states can be obtained by studying their subsequent decay. The electron emission spectra of KF^{56} and KBr^{57} show similar with KCl resonant emission bands when photon-excited in the K^+ 2p-threshold region. The dominant decay channel for the 2p-core hole is the $L_{23}M_{23}M_{23}$ Auger process.

When this process occurs in the presence of an extra screening electron in the K^+ 3d orbital (a so-called spectator Auger process), emission lines appear to the high kinetic energy side of the normal Auger spectrum. These high-energy spectator structures show small changes in their form if different crystal-field split lines in the absorption spectrum are excited⁵⁸.

In Fig. 8(a) is shown the calculated spectator decay $2p^{-1}3d \rightarrow 3p^{-2}3d$ spectrum at the L_3 resonant excitation. The calculated spectrum in Fig. 8(c) is a good agreement in position and relative intensity of the experimental resonant spectra in low binding energy region.

However, there is a large discrepancy between calculation and experimental spectra, because intensity in higher-binding energy part of the spectrum seems completely lacking. In order to clarify that lacking we have compare the experimental spectra excited at different crystal field splitted states of L_3 absorption spectrum (in Fig. 8 (a) and (c)). The difference of these experimental spectra is shown in Fig. 8(b). The comparison of the experimental difference spectrum with the calculated $L_3M_{23}M_{23}$ Auger structure, also presented in Fig. 8(b), suggests that it can be ascribed to a normal $L_3M_{23}M_{23}$ Auger transition. This leads to the conclusion that at resonant $2p^6 \rightarrow 2p^5 3d(4s)$ excitation the photoemission spectra of K^+ in the vicinity of the $L_{23}M_{23}M_{23}$ Auger structure contains two components, the spectator-induced structure and the normal $L_{23}M_{23}M_{23}$ Auger structure.

Evidence for the normal Auger transitions (more exactly, normal Auger decay transitions from the $2p_{3/2}^5$ level) in the resonant spectra may be easily explained for the $2p_{1/2}$ excitations because of the strong Coster-Kronig decay channels involving the K $2p_{1/2}$ and $2p_{3/2}$ levels. The existence of the strong Coster-Kronig channels we can conclude from the K 2p absorption spectrum, which shows the broadening of the structures, related to the $2p_{1/2}$ level. For the $2p_{3/2}$ (L_3) excitations this experimental feature of is highly nontrivial.

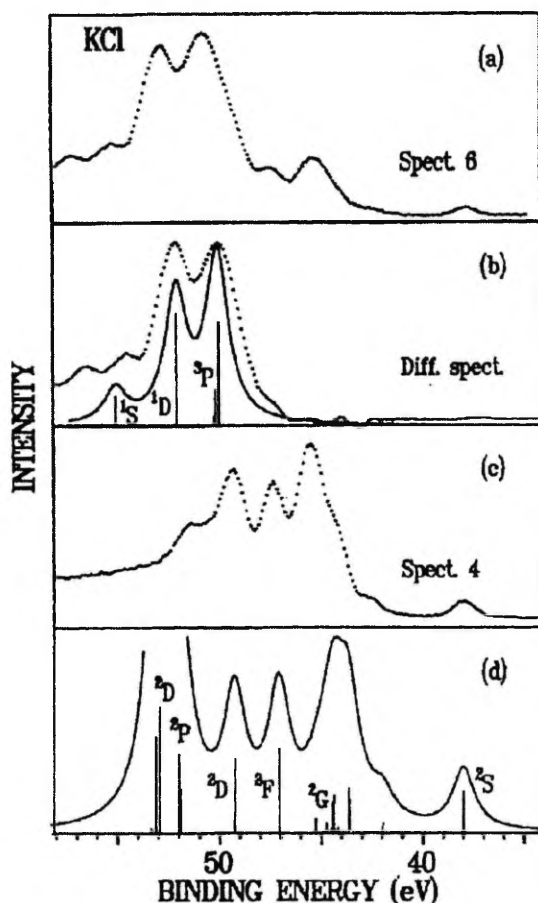


Fig. 8. Resonant $L_3M_{23}M_{23}$ Auger spectra for KCl as compared to the calculation of the $3s^23p^43d + 3s^13p^6$ final ionic states. In (a) and (c) are shown spectra excited at high (e_g) and low energy (t_{2g}) crystal field splitted states of L_3 absorption spectrum of K^+ , respectively. Their difference spectrum is shown in (b) and compared with the calculated $L_3M_{23}M_{23}$ normal Auger spectrum (solid line). Calculation of the spectator $L_{23}M_{23}M_{23}$ decay spectra to the $3s^23p^43d+3s^13p^6$ final states is shown in (d). The theoretical multiplets are broadened with a Lorentzian of 1.5 eV FWHM.

There are at least three possibilities to explain the evidence of the normal Auger decay features above the ionization limit. First, it is possible that the resonantly excited 3d state relaxes to the ionized state before the core hole decays. I propose that this cannot be the main reason because this is in contradiction with the sharpness of the absorption peaks which reflect the localization of the excited 3d wavefunction. Second, there should exist a large overlap between of the normal $L_{23}M_{23}M_{23}$ Auger and the $L_{23}M_{23}M_{23}$ spectator Auger satellite final ionic widely spread configurations. This overlap may offer a new possibility for

the double-Auger decay processes, i.e. decay from the K 2p excited state directly to the normal Auger final ionic state. The extent of this overlap affects more strongly the high-binding-energy part of the spectator Auger spectrum. Third, the shape of the Auger spectator satellite becomes similar to normal Auger one if the spectator electron wavefunction delocalizes in the final state. This is possible in shake-up-modified Auger final state. For covalent compounds, it is possible that the creation of the double-hole final state increases charge transfer from the ligand valence band states to the K 3d states for the screening of an additional core hole and, as a consequence, creation of the $3p^4 3d^2 L^{-1}$ (where L^{-1} stands for a hole in the anion valence band) final state. This core hole induced charge transfer process depends strongly on the covalency and should be more effective in the covalent compounds. The $3d^2$ wavefunction obtains the less localized character than $3d^1$ or becomes fully delocalized and the shape of the spectator decay spectra becomes similar to the normal Auger spectrum. I propose that the origin for the observed normal-Auger-like structures in resonant spectra of Sc_2O_3 may be explained by this simple schematic scenario described above. de Groot *et al.*⁶³ proposed mechanisms of hybridization-induced Coster-Kronig channels which also can give rise to normal Auger features in decay spectra. Moreover, the results of decomposition and data-fitting procedures show that shake-up processes play an important role in the resonant Auger decay in KF ⁵⁶. Of course, more exact exploring through above-mentioned scenarios needs sophisticated *ab initio* theoretical treatments.

5.6. Shake probabilities

The creation of a core hole by x-ray excitation produces a sudden change of the hamiltonian (the orbitals around the vacancy contract due to the decreased shielding of the nucleus) which may induce non-adiabatic electron jumps. These jumps are observed as satellites in photoelectron emission spectra. These satellites due to the sudden change of the Hamiltonian are called “shake” satellites (monopolic shake-up, shake-down, shake-off and dipolic+monopolic conjugated shake excitations, see e.g. ⁵⁹) and the approximation method dealing with a sudden change of the Hamiltonian is known as the sudden approximation.

In the case of Ar atoms the shake processes (mainly $3d \rightarrow 4d$ and $4s \rightarrow 5s$) were shown to play an important role in the formation of the final state^{60,61}. In paper V we looked for the dynamics of shake phenomena when collapse of the 3d wavefunction occur. We have calculated the total overlap probabilities P_{ij} to verify that no ejection or excitation of 3d and 4s electrons of the configurations $2p^5 3s^2 3p^6 3d$ (4s) takes place during the $L_{23}M_{23}M_{23}$ -like deexcitation (Table II). This overlap is given by the formula:

$$P_{nl} = \left(\int R_{nl}^i R_{nl}^f r^2 dr \right)^2$$

where R_{nl}^i and R_{nl}^f are the initial and final state radial wavefunction of nl (3d or 4s) electrons, respectively. As seen in Table II, for 3d electrons $\langle r_{nl} \rangle$ decreases sharply in the sequence from Ar to Ca^{2+} . In the case of Ar the 3d electron collapses during the Auger decay and the shake probability is large, while for K^+ and even more for Ca^{2+} it is completely collapsed in the Auger initial $2p^5 3d$ and final ionic $3p^4 3d$ configuration. During the Auger decay its mean radius changes little and the shake probability is small. This conclusion is supported by the electronic decay spectra of photoexcited 2p resonances of atomic Ar, K, and Ca^{62} where for K and Ca shake effects was found to be much smaller than for Ar.

Table II. The calculated probabilities P_{nl} for 3d and 4s electrons not to be ejected or excited during the Auger decay. $\langle r_{nl} \rangle$ is the mean radius of the nl excited orbital (in atomic units).

Initial and final configurations		Ar		K (KCl)		Ca (CaF_2)	
		$\langle r_{nl} \rangle$	P_{nl}	$\langle r_{nl} \rangle$	P_{nl}	$\langle r_{nl} \rangle$	P_{nl}
Initial	$2p^5 3s^2 3p^6 3d$	9.24	0.23	2.92	0.86	1.63	0.99
Final	$2p^6 3s^2 3p^4 3d$	2.79		1.85		1.47	
Initial	$2p^5 3s^2 3p^6 4s$	5.34	0.87				
Final	$2p^6 3s^2 3p^4 4s$	4.1					

Nevertheless, the excited collapsed wavefunctions in solids may obtain more extended character than show our calculations where solid state is approximated by the Watson sphere. So the role of the shake processes for resonant Auger decay in solids may be substantially greater than that is evident from our calculations. For example, the shake processes were found to be strong in KF^{56} . As noted by de Groot et al.⁶³ there is an analogy between the $3p^4 4d^1$ shake-up Auger final ionic states in the atomic model and $3p^4 3d^2 L^{-1}$ states in the charge-transfer model if the ligand hole states are represented as delocalized nd states ($L \equiv nd^{10}$ and $L^{-1} \equiv nd^9$). In both cases a 3d electron is exchanged for a 4(n)d electron, but the direction of transfer is opposite, which is a striking difference between the models.

6. COLLAPSE OF THE 4f WAVEFUNCTION IN THE ISOELECTRONIC SEQUENCE OF XENON-LIKE IONS

6.1. Collapse of the 4f orbital and 3d absorption spectra

In paper I the effect of the 4f orbital collapse on the 3d (M_{45}) absorption spectra of xenon-like ions Γ , Cs^+ , Ba^{2+} , and La^{3+} in various halides was investigated in the region of the 3d (M_{45}) absorption edge. The absorption spectra show two-peak structure, which is practically independent of the second component of the compound. This demonstrates that the main features of the spectra are of quasi-atomic character. They characterize the corresponding ion, which is possibly slightly perturbed by the crystal field.

For a detailed interpretation, the absorption spectra in the region of the 3d edges of the isoelectronic ions Γ (in CsI), Xe^{64} , Cs^+ (in CsI), Ba^{2+} and La^{3+} (in LaF_3) are gathered together in Fig. 9.

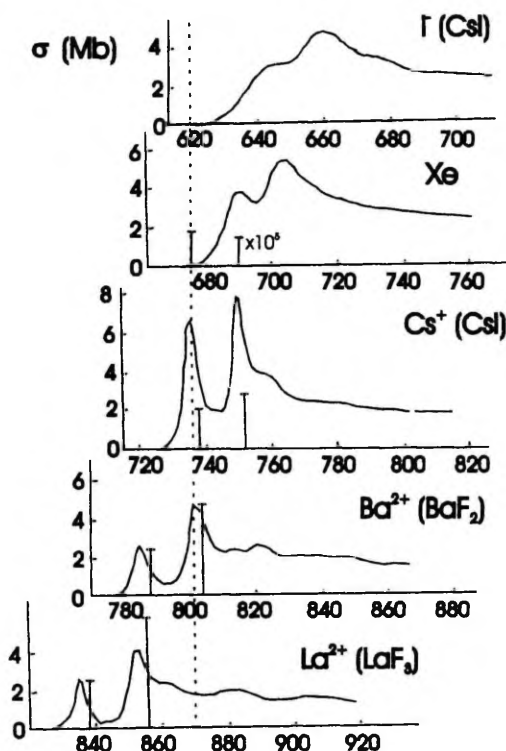


Fig. 9. Partial photoabsorption cross sections of the 3d shell of Xe-like ions. The spectra coincide in position at the ionization energies of the $3d_{5/2}$ shells of the corresponding ions. The theoretical $3d^{10} \rightarrow 3d^9 4f$ transitions are marked by vertical lines.

In general, the spectra are clearly divided into two groups. In the case of Γ and Xe, the broad smooth maxima are located beyond the ionization threshold, and with further distance from the threshold the absorption decreases, but still remains appreciable. For Cs, Ba, and La, two intense relatively narrow maxima below the ionization threshold which is due to the spin-orbit splitting of the 3d shell predominate in the spectrum, and the absorption in the region of the continuous spectrum is much weaker than in the cases of Γ and Xe.

There are good theoretical grounds for assuming that the absorption spectra of Γ and Xe are determined entirely by transitions of 3d electrons into a continuum of f symmetry, i. e., by $3d \rightarrow \epsilon f$ ^{65,66}. Since the f states are retained by the intra-atomic potential barrier in the region of the outer potential well, the transitions $3d \rightarrow \epsilon f$ become effective only at energies sufficient for the f wave to penetrate into the inner well, and this leads to a quiresonant concentration of the oscillator strengths of the transitions in the region above the ionization threshold.

For Cs, Ba, and La can be used interpretation similar for the corresponding spectra of the rare-earth atoms (see, e. g. Ref.⁶⁷). As in the latter case the oscillator strength stems primarily from $3d \rightarrow 4f$ transitions and the $3d \rightarrow \epsilon f$ channel is already much less effective⁶⁸, it must be concluded that the clearly pronounced doublets in the initial regions of the spectra of Cs, Ba, and La are due to $3d \rightarrow 4f$ transitions. Thus, a qualitative analysis of the spectra presented in Fig. 9 leads to the conclusion that a collapse of the 4f orbital in the configuration $3d^9 4f$ takes place on going from Xe to Cs^+ and Ba^{2+} .

In Fig. 10 is shown the mean radius of the 4f wavefunction calculated in the configuration-average Hartree-Fock approximation for some excited $3d^9 4f$ configurations. The radius of the 4f wavefunction changes during the collapse by about order of magnitude. In the case of a collapsed electron, the localization of the electron is highly sensitive to the change of the potential, and therefore for the case $3d^9 4f$ in Cs^+ refinement of the calculation can substantially change the results. So it is possible the delocalization of the 4f wavefunction in solid state as show our Hartree-Fock calculations where solid state environment was simulated by a Watson sphere (Fig. 2). In paper I we perform also Hartree-Fock-Slater calculations for the $3d \rightarrow \epsilon f$ ionization channel which show (in Fig. 7 of paper I) that shape of the experimental 3d absorption curve for Cs^+ as well as for Xe and Γ can be interpreted as due to the transitions to ϵf continuum. The calculations of transitions $3d \rightarrow \epsilon f$ presented in paper I are crude ones and the result is qualitative. Nevertheless, the 3d photoabsorption in xenon-like ions was considered theoretically by Goroshenko *et al.*⁶⁹ and Amusia *et al.*⁷⁰ within the framework of random phase approximation with exchange (RPAE) and their calculations showed also that in Cs^+ 3d absorption structures are due to the transitions to ϵf continuum.

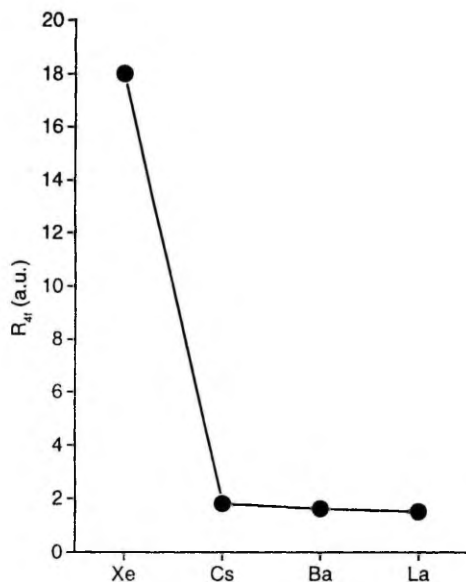


Fig. 10. Radius of 4f orbital (R_{4f}) in the configuration $3d^9 4f$ in the isoelectronic sequence of Xe-like ions

6.2. Resonant electron spectra of CsI. Case of uncollapsed 4f orbital

In paper VI the effect of the 4f orbital collapse on the electron spectra of xenon-like ions Γ , Cs^+ , Ba^{2+} , and La^{3+} in various halides was investigated around the 3d-absorption edge. The resonant spectra of Γ and Cs^+ in CsI (Fig. 11) are dominated by the “normal” photon-energy-independent $M_5 N_{45} N_{45}$ and $M_4 N_{45} N_{45}$ structures, shifted slightly (by ~ 0.5 eV for I and 1 eV for Cs) to higher energies most probably by extraatomic relaxation effects.

The situation is fully understandable in the light of the nature of the near-edge 3d excitations of I and Cs: as the 4f orbital is not collapsed the $3d^{-1} \rightarrow 4d^{-2}$ transitions dominate the resonantly excited MNN spectra. In this sense our resonant Auger data once more confirm that the M_{45} near edge absorption bands of these ions are caused by transitions to above-threshold states.

However, the resonant spectra of Cs contain two additional weaker bands pronounced most clearly on the curves B and E of Fig. 11. Their relative positions (between the $4p_{3/2}$ photoline and normal MNN bands) and the photon energy dependence closely follow the behaviour of the 4f spectator bands. The calculation of $3d^{-1} 4f \rightarrow 4d^{-2} 4f + 4p^{-1}$ spectra for Cs^+ , using a collapsed 4f orbital, fully supports this suggestion. Thus, one can conclude that the observed resonant MNN spectra of Cs contain simultaneously the $3d^{-1} \rightarrow 4d^{-2}$ and

$3d^{-1}4f \rightarrow 4d^{-2}4f$ -like structures. In other words, the M_{45} near-edge photoexcitations of Cs exhibit both continuous ($3d \rightarrow \epsilon f$) and localized ($3d \rightarrow 4f$) character.

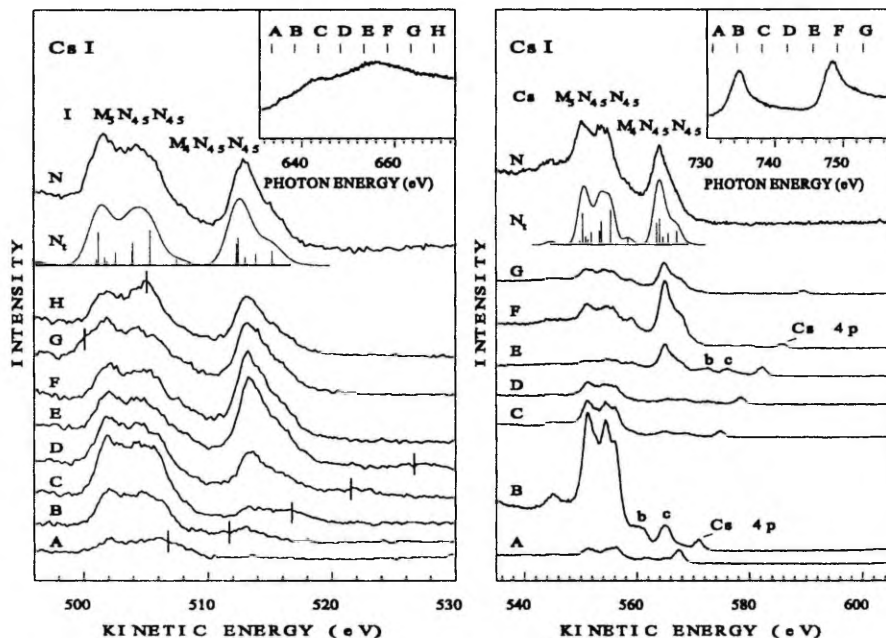


Fig. 11. *Left panel:* The resonantly excited electron spectra recorded around the 3d absorption edge (shown in the insert) of I in CsI. The capital letters at each curve corresponds to the vertical bar with the same capital letter in the insert and show the photon energy used. The normal Auger spectrum is excited by 800 eV photons, the calculated spectrum is broadened with a Gaussian of 2 eV FWHM. The positions of the Cs $4p_{3/2}$ photoline in spectra H and G, and of the I $4p_{3/2}$ photoline in spectra A to E are indicated by vertical bars.

Right panel: The resonantly excited electron spectra recorded around the 3d absorption edge (shown in the insert) of Cs in CsI. The normal Auger spectrum is excited by 850 eV photons.

This “dualistic” nature of the 3d-excitations of Cs has earlier been observed in the M_{45} X-ray emission of Cs in CsCl^{71} . Now we may add that resonant Auger electron spectroscopy seems to be a very sensitive technique to investigate such “partially localized” excitations. In our case the apparent localization of the excited-state electron may be considered as a result of the interaction of a low-energy ϵf photoelectron with a fast Auger electron leading to the recapture of the photoelectron by the ionized core and, subsequently, to the shake-down-like transitions $3d^{-1}\epsilon f \rightarrow 4d^{-2}4f$ (see also Sec. II for PCI induced recapture). A similar

explanation was used to interpret the ion yield spectra of Ar near its L_{23} thresholds⁷².

The striking difference between M_{45} absorption spectra of I and Cs in CsI could be explained by behaviour of “pre-collapsed” ϵf continuum wavefunction. So, when this wavefunction passes through shape resonance close to 3d threshold, its amplitude inside the barrier is strongly enhanced. This penetration of continuum ϵf wavefunction into inner well accompanied with a rapid increase of the spatial overlap between the initial 3d and final ϵf state, and subsequently the strong increase the absorption cross section close to threshold. To partition between these “pre-collapsed” ϵf and “common” ϵf wavefunction we introduce here the notation of “resonantly localized 4, ϵf ” state for above-mentioned “pre-collapsed” ϵf state.

6.3. Resonant electron spectra of BaF_2 .

Case of collapsed 4f orbital and effect of the 4f electron collapse on the spectator decay spectrum

As an example we consider the resonantly excited $M_{45}N_{45}N_{45}$ spectra with $Ba^{2+}(BaF_2)$ in which case the 4f orbital is collapsed both in core-excited initial ($3d^{-1}4f$) and final ionic ($4d^{-2}4f$) states. Fig. 12 shows a set of on-resonance electron spectra for Ba.

In the region of the Ba MNN Auger transitions a strong and well-developed structure appears which vanishes off-resonance and drastically differs from the normal Ba $M_{45}N_{45}N_{45}$ bands also shown in Fig. 12. This resonant structure consists of a broad band “a” and a doublet of close-lying bands “b” and “c”. The $4p_{3/2}$ photoline is followed by the strong doublet “b”–“c” and the broad low-energy band “a”.

This three-band resonant structure moves linearly with exciting photon energy as a photoemission feature and is repeated on the M_4 resonance. This band has the same width as the normal $M_5N_{45}N_{45}$ band, and nearly the same energy, which does not change with changing photon energy. Therefore, it can be attributed to the normal $M_5N_{45}N_{45}$ channel opened by the $M_4M_5N_{67}$ Coster-Kronig decay. The high-kinetic-energy shift (about 2 eV) of this band is most probably related to extraatomic relaxation.

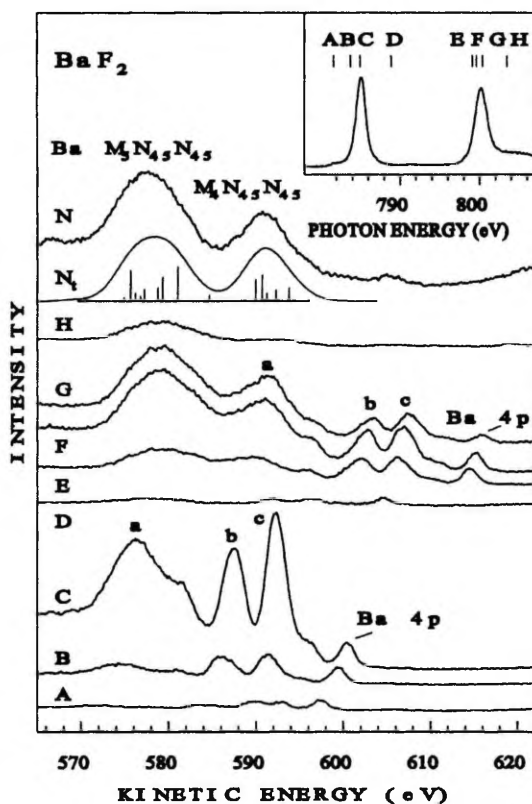


Fig. 12. The resonantly excited electron spectra recorded around the 3d absorption edge (shown in the insert) of Ba in BaF_2 . The capital letters at each curve corresponds to the vertical bar with the same capital letter in the insert and show the photon energy used. The normal Auger spectrum is excited by 880 eV photons, the calculated spectrum is broadened with a Gaussian of 5 eV FWHM.

In Fig. 13 the observed on-resonance M_{45} spectra are compared with computed $3d^{-1}4f \rightarrow 4d^{-2}4f + 4p^{-1}$ spectra. The calculations reasonably well reproduce the high-energy region of the measured spectra, but there is a clear mismatch in the low-energy region, which cannot be compensated for by the reduction of electrostatic integrals. The calculations show that band "a" lies at the energies where the $4d^{-2}$ threshold is expected to be found. In Fig. 13 these thresholds, i.e. the lowest-binding-energy states of $4d^{-2}$ ionic configuration are marked as the vertical bars on the kinetic energy scale. The $4d^{-2}4f$ states with energies above this threshold (dashed parts of theoretical curves) are thus allowed to delocalize and seem not to contribute to the spectator structure. So, our calculations show that the region of relatively narrow resonant bands "b" and "c" corresponds to the $4d^{-2}4f$ states lying below the $4d^{-2}$ limit. Only these bands could be considered as the true 4f spectator features.

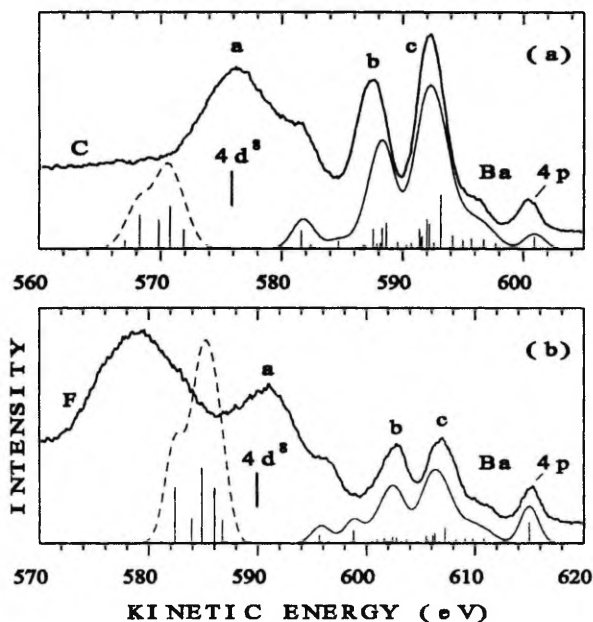


Fig. 13. Resonant $M_{45}N_{45}N_{45}$ Auger spectra (thick lines) for BaF_2 as compared to the calculation (thin lines) of the Auger transitions $3d^{-1}4f(^1D_1) \rightarrow 4d^{-2}4f + 4p^{-1}$ (a) and $3d^{-1}4f(^1P_1) \rightarrow 4d^{-2}4f + 4p^{-1}$ (b). In (a) and (b) are shown, respectively, the spectra C and F of Fig. 12. The dashed part of the computed spectra corresponds to the $4d^{-2}4f$ states with energies lying above the $4d^{-2}$ threshold (labelled by the vertical bars). The computed spectra are broadened with a Gaussian of 2-eV FWHM.

The interpretation of the broad low energy band “a” is, however, much more complicated. Our theoretical and experimental data allow to suggest that the band “a” is induced by the $3d^{-1}4f \rightarrow 4d^{-2}$ Auger shake-off-like (double Auger) transitions. These transitions produce electrons with kinetic energies slightly lower than the $3d^{-1} \rightarrow 4d^{-2}$ transitions. As seen in Fig. 12, the band “a” nearly coincides with its “normal” but, on the other hand, it has a clearly different shape than the “normal” band, which is at least by 2.5 eV broader. However, the proper solution of this problem is beyond our theoretical model.

6.4. Branching ratios of 4d photolines

Right panel of Fig. 14 presents a set of electron spectra for CsI , BaF_2 and LaF_3 in the region of the 4d photolines which are obtained with various photon energies around M_{45} absorption edges of iodine, cesium, barium and lanthanum. Each curve denoted by a capital letter indicates the intensity variation at the same capital letter in the left panel of Fig. 14, where the M_{45} absorption spectra

are displayed. Photoelectron lines of $4d_{3/2}$ and $4d_{5/2}$ core levels of Ba and La show drastic change in intensity as the photon energy is turned through the M_{45} absorption features. This effect is for Cs less expressive, but still visible. The electron spectra of LaF_3 in Fig.14 show the strong enhancement of the 4d-photoline components on the excitation energies corresponding to the M_5 and M_4 absorption peaks. This enhancement suggest that 4f electron frequently participates in the decay of $3d^9 4f$ excited state. The total intensity of 4d photoline is roughly 15.2 and 9.3 times larger on-resonance excitation at M_5 and M_4 absorption peaks, respectively, than the off-resonance excitation at M_5 and M_4 absorption peaks, respectively, than the off-resonance 4d intensity. This indicates very dramatically how weak the direct process of $4d^{10} \rightarrow 4d^9$ photoionization is compared to the indirect process of autoionization ($3d^9 4f \rightarrow 4d^9$ participator decay) through the $3d \rightarrow 4f$ resonances.

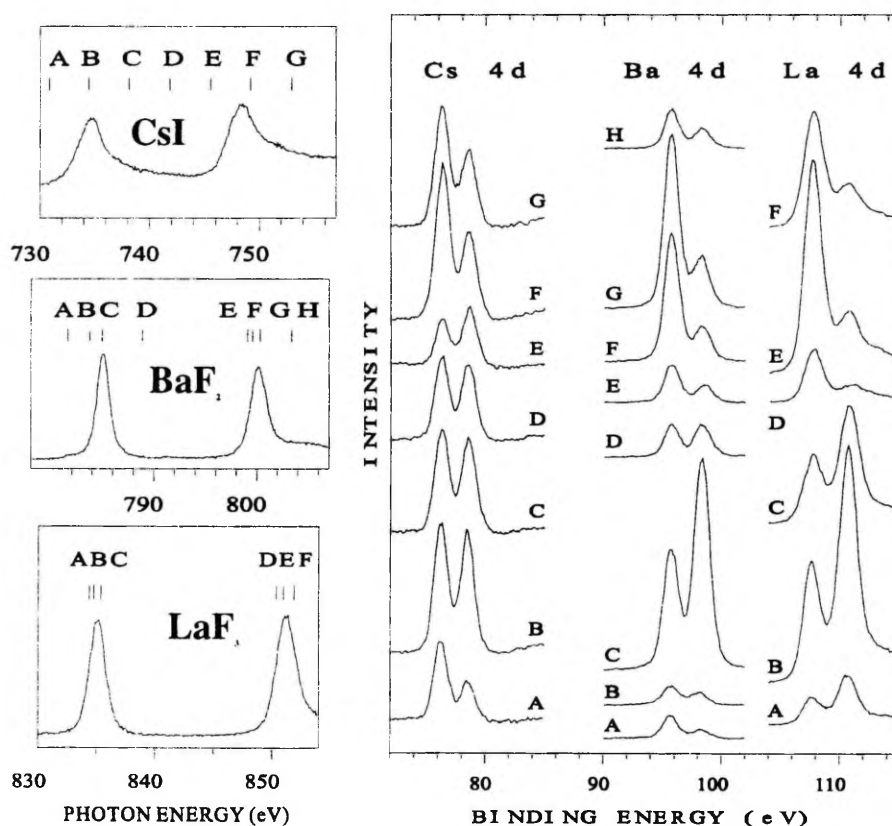


Fig. 14. Left panel: absorption spectra of Cs^+ in CsI , Ba^{2+} in BaF_2 and La^{3+} in LaF_3 in the region of the M_{45} absorption edge of cations.

Right panel: the electron spectra of Cs^+ in CsI , Ba^{2+} in BaF_2 and La^{3+} in LaF_3 in the region of the $4d_{5/2}$ and $4d_{3/2}$ photolines excited at the M_{45} absorption edge of cations. The capital letter at each spectrum correspond to the vertical bar with the same capital letter in left panel and show the photon energy used.

Nevertheless, the most striking feature of these spectra is different behaviour of the intensity distribution between $4d_{5/2}$ and $4d_{3/2}$ photolines in the region of M_5 and M_4 absorption peaks. So the intensity of the $4d_{3/2}$ photoline exceeds roughly two times intensity of the $4d_{5/2}$ photoline on M_5 resonance excitation.

On the contrary, intensity of the $4d_{3/2}$ photoline on the M_4 resonance excitation is about of four times less than intensity of $4d_{5/2}$ photoline. Note that term-dependence and anomalous change of the branching ratio of $5p_{1/2}$ to $5p_{3/2}$ photolines have been observed at the $4d \rightarrow 4f$ resonant excitation of La in LaF_3 and Ba in BaF_2 ⁷³ and attributed to the multiplet dependence of the Auger transition probabilities⁷⁴.

The electron spectra of BaF_2 in Fig. 14 show quite similar behaviour at the excitation energies around the M_{45} absorption edges. However, the enhancement of the 4d photoline in Ba is somewhat less than in La. So the total intensities of the 4d photoline are about of 6.3 and 10.3 times larger on the M_4 and M_5 resonance excitations, respectively, than intensity of the direct 4d-shell photoionization under the off-resonance conditions.

In Fig. 15 we compare the experimental M_5 and M_4 on-resonance electron spectra of La in LaF_3 and Ba in BaF_3 in the region of 4d photolines with the calculated $3d^9 4f(J=1) \rightarrow 4d^9$ Auger spectra. The computed curves satisfactorily reproduce the intensity variations of the observed spectra. The somewhat smaller strength of the $4d_{5/2}$ photoline relative to the $4d_{3/2}$ one in the observed spectra as compared to the calculated spectra is maybe mainly due to simultaneously excited direct $4d^{10} \rightarrow 4d^9$ photoemission lines as well as solid state effects. The latest are more significant for La taking into consideration the higher covalency of LaF_3 crystal. The theoretical $4d_{3/2}:4d_{5/2}$ branching ratio for Auger transitions $3d^9 4f \rightarrow 4d^9$ of La is 2.6 for M_5 resonant excitation and 0.33 for M_4 excitation and thus agree well with corresponding experimental results: 2.4 and 0.18 for M_5 and for M_4 on-resonance excitations, respectively. Therefore, our computations suggest that the change of the $4d_{3/2}:4d_{5/2}$ branching ratio in resonant photoemission originates from the term dependent Auger participator transitions $3d^9 4f \rightarrow 4d^9$. Although the computed spectra reproduce the relative intensities, i.e. branching ratio, of the 4d photoline components well, there are a considerable discrepancies in the predicted relative integrated intensities of 4d photoline excited at M_5 and M_4 resonance. The difference between calculated relative intensities and experimental data maybe ascribed to the Koster-Cronig transitions $3d_{3/2}^9 4f \rightarrow 3d_{5/2}^9$, which is not considered in our calculation.

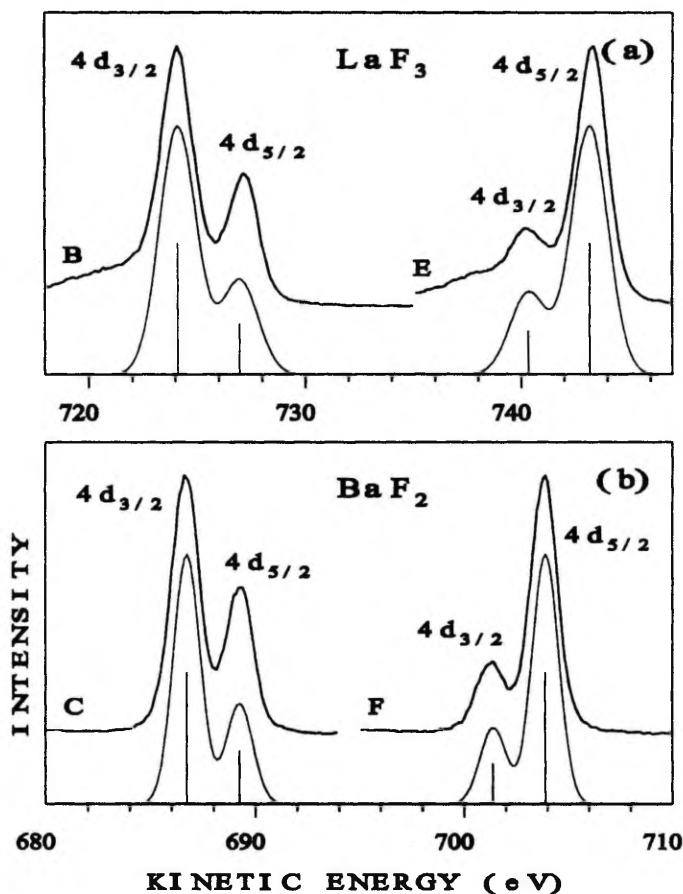


Fig. 15. The electron spectra of La in LaF_3 (a) and Ba in BaF_2 (b) in the region of 4d photolines (thick lines) as compared to the calculated Auger transitions $3d^{-1}4f(^1D_1) \rightarrow 4d^{-1}$ and $3d^{-1}4f(^1P_1) \rightarrow 4d^{-1}$ (thin lines). In (a) and (b) are shown, respectively, the spectra B and E of La in LaF_3 , and the spectra C and F of Ba in BaF_2 of Fig. 14. The computed spectra are broadened with Gaussians of 2-eV (a) and 1.5-eV (b) FWHM.

On the other hand, our calculations show that for Cs^+ in CsI the partial widths of participator decay of $3d^{-1}4f$ excited states with delocalized 4f orbital become negligible. So, we may conclude that the resonant enhancement of photolines as well as the anomaly in the branching ratios indicate that the excited 4f orbital is localized. In the case of Cs in CsI the effect seems to be due to the post-collision-induced recapture of the slow ϵf or $4, \epsilon f$ photoelectron, i.e. to the transition $3d^{-1}\epsilon f(4, \epsilon f) \rightarrow 4d^{-1}$, similarly to the spectator-like structure in the $M_{45}N_{45}N_{45}$ spectra of Cs.

THE MAIN ARGUMENTS PROPOSED

Our results demonstrate that the model of the isolated ion is suitable for the interpretation of the main singularities of the 3d absorption spectra of the xenon-like ions and 2p absorption spectra of the argon-like ions in ionic compounds. The influence of their surrounding manifests mainly itself to a crystal field splitting of 3d collapsed states for the argon-like ions. We show also that the 4f electron in the $3d^9 4f$ configuration is localized in the outer well of the effective potential in the case of the Γ ions and Xe atoms, and in the inner well in the case of the ions Ba^{2+} and La^{3+} . For the argon-like ions K^+ , Ca^{2+} , Sc^{3+} and Ti^{4+} the 3d electron in the $2p^5 3d$ configuration is localized in the inner well and in the outer well in the case of Cl^- and Ar.

We show that the collapse of the 3d or 4f orbital in the isoelectronic sequence of Ar or Xe-like ions, respectively, leads to drastic changes of the resonant Auger decay spectra. As an example, we investigate the Auger spectator transition dependence on localization of the spectator 3d and 4s electrons in the final state in the case of Cl^- and found that the collapse of the spectator electron in final states leads to a strong increase of the electrostatic interaction between the two-hole and spectator electron. The coupling scheme is now changed from the jj or Lj type, characterized the final states of "classical" spectator model, to nearly LS type which gives rise to a very complex multiplet and means that the "classical" spectator model fails for the interpretation of the decay spectra.

We show that the collapse of excited orbital in intermediate states leads to a strong enhancement the spectator and participator features in spectra. A strong term-dependence and anomalous change of the branching ratio of $4d_{3/2}$ to $4d_{5/2}$ photolines have been observed at the M_{45} resonant excitation of La in LaF_3 and Ba in BaF_2 and attributed to the multiplet dependence of the Auger transition probabilities.

Our calculations show that, in contrast to the case of Ar atoms where the shake-up processes were shown to play an important role in the formation of the Auger decay final state, in the case of K^+ and even more for Ca^{2+} where 3d orbital is completely collapsed in the $2p^5 3d$ configuration, during the Auger decay mean radius of the collapsed 3d orbital changes little and the shake probability is small.

Our measurements of various TiO_2 polymorphs demonstrate the sensitivity of x-ray absorption spectra to structural changes in the solid state. From the resonant electron spectra at the L_3 threshold of Ti is concluded a strong delocalization of the 3d electron for the excitations where the largest differences between the Ti 2p XANES of TiO_2 polymorphs are observed. These differences in absorption spectra are attributed to increasing strength of the crystal field caused by delocalization of the excited 3d electron.

CONCLUSIONS

In this work has been studied experimentally, by x-ray and photoemission spectra as well as theoretically the phenomena of the collapse of the excited 3d and 4f orbitals in ionic solids. These orbitals has been created by inner-shell excitation in two sequences, in the argon-like (Cl^- , K^+ , Ca^{2+} , Sc^{3+} , Ti^{4+} by 2p excitations) and xenon-like (I^- , Cs^+ , Ba^{2+} , La^{3+} by 3d excitations) sequences of ions, respectively. The experimental x-ray absorption and electron spectra in both sequences show the drastic intensity changes in going from the un-collapsed to collapsed excited orbital.

The interpretation of these interesting experimental results is impossible without essential theoretical calculations. As the first results indicated a dominating role of atomic effects in the collapsed electron excitations of ionic crystals, a calculation model based on the Hartree-Fock method was used. The solid-state effects were accounted using so called Watson sphere, which reduces the effect of ions surrounding the considered ion (atom) to corrections of spherical symmetry. The intensities of electron transitions (photoexcitation cross sections, Auger transition rates) were calculated in the approximation of the intermediate coupling scheme. For all these calculations was developed and used the effective FORTRAN codes.

The main results obtained may be formulated as follows:

- 1) Our results demonstrate convincingly that the model of the isolated ion is suitable for the interpretation of the main singularities of the 3d absorption and emission spectra of the xenon-like ions and 2p absorption and emission spectra of the argon-like ions in compounds with high degree of ionicity. The influence of their surrounding manifests mainly itself to a crystal field splitting of 3d collapsed states for the argon-like ions. A comparison of the measured spectra with one another and with results of the calculation shows also that the 4f electron in the $3d^9 4f$ configuration is localized in the outer well of the effective potential in the case of the I^- ions and Xe atoms, and in the inner well in the case of the ions Ba^{2+} and La^{3+} . For the argon-like ions K^+ , Ca^{2+} , Sc^{3+} and Ti^{4+} the 3d electron in the $2p^5 3d$ configuration is localized in the inner well and in the outer well in the case of Cl^- and Ar. The spatial redistribution of the charge density of the excited electron leads to a substantial redistribution of the oscillator strength from the continuous region of the 3d or 2p absorption spectrum into the region of discrete transitions.
- 2) We show that the collapse of the 3d or 4f orbital in the isoelectronic sequence of Ar or Xe-like ions, respectively, leads to drastic changes of the resonant Auger decay spectra.

While, on the one hand, the collapse of excited orbital in Auger two-hole final ionic states leads to the complete breakdown of "classical spectator" model, in which the resonant Auger spectra are the same as the normal

Auger spectra recorded above the ionization threshold except for an energy shift caused by the presence of the spectator electron. This “classical spectator” model has been used successfully to explain the Auger decay structure in free atoms, molecules and solids after resonant excitation electrons to Rydberg levels. In the case of Cl^- we investigate the Auger spectator transition dependence on localization of the spectator electron in the final ionic state and found that the collapse of the spectator electron in final states leads to a strong increase of the electrostatic interaction between the two-hole and spectator electron. The coupling scheme is now changed from the jj or L_j type, characterized the final states of “classical” spectator model, to nearly LS type which gives rise to a very complex multiplet and means that the “classical” spectator model fails completely for the interpretation of the decay spectra.

On the other hand, the collapse of excited orbital in intermediate states leads to a strong enhancement the spectator (two-hole + spectator electron) and participator (single-hole) features in spectra. So, the intensity of the participator decay channel, which are degenerate in energy with direct photoemission final states, may be in some cases much more intense than direct photoemission lines (e. g. 4d photolines of Ba and La).

- 3) A strong term-dependence and anomalous change of the branching ratio of $4d_{3/2}$ to $4d_{5/2}$ photolines have been observed at the M_{45} resonant excitation of La in LaF_3 and Ba in BaF_2 and attributed to the multiplet dependence of the Auger transition probabilities.
- 4) Our calculations show that, in contrast to the case of Ar atoms where the shake-up processes were shown to play an important role in the formation of the Auger decay final state, in the case of K^+ and even more for Ca^{2+} where 3d orbital is completely collapsed in the $2p^53d$ configuration, during the Auger decay mean radius of the collapsed 3d orbital changes little and the shake probability is small.
- 5) Our measurements of various TiO_2 polymorphs demonstrate the sensitivity of x-ray absorption spectra to structural changes in the solid state. From the resonant electron spectra at the L_3 threshold of Ti is concluded a strong delocalization of the 3d electron for the excitations where the largest differences between the Ti 2p XAS of TiO_2 polymorphs are observed. These differences in absorption spectra are attributed to increasing strength of the crystal field caused by delocalization of the excited 3d electron.
- 6) The resonant Auger spectra, for the greater part of species investigated by us, are highly atomic. Influence of the solid state environment on the resonant spectra depends strongly on the excited species, excitation and on the degree of localization of the excited electron in the intermediate and final ionic states. Main processes induced by solid state and affected to the resonant spectra may be:

- i) the tunnelling delocalization of the excited spectator electron to continuum of conduction band in the intermediate state (e. g. in the L_{23} decay spectra of potassium compounds),
- ii) a double Auger decay channels may be opened in real crystal and affect the shape of the low energy part of the spectra if the upper levels of the spectator final ionic states lie slightly above the two-hole ionization limits (e. g. in M_{45} excitation for BaF_2),
- iii) in solid state in many cases the Coster-Kronig decay becomes energetically possible (e.g. at L_2 excitation for potassium and calcium compounds and at M_4 excitation for BaF_2).
- iv) the intermediate state crystal field term-dependence is observed in spectator decay spectra (this effect is more clearly seen in decay spectra of L_{23} excited states of potassium and calcium compounds),
- v) a charge transfer from the valence band to spectator electron level in both, intermediate and final ionic state, during the excitation (e. g. in L_{23} excitation for TiO_2 and Sc_2O_3)

3d (4f) ORBITAALIDE KOLLAPS 2p (3d) ERGASTUSTEL NING SELLE MÕJU RÖNTGEN- JA ELEKTRONSPEKTRITELE

Kokkuvõte

Käesolevas töös on uuritud ergastatud 3d ja 4f radiaalse lainefunktsiooni kollapsi (lokalisatsiooni) nähtust ioonsetes ühendites nii eksperimentaalselt, kasutades röntgenspektroskoopiat ja elektronspektroskoopiat, kui ka teoreetiliselt. 3d ja 4f lainefunktsioonide kollapsit uuriti aatomite sisekihtide ergastustel kahes isoelektronses reas: argoonisarnastes uuriti ioonides Cl^- , K^+ , Ca^{2+} , Sc^{3+} ja Ti^{4+} 3d orbitaali kollapsit 2p ergastustel ja ksenoonisarnastes uuriti ioonides I^- , Cs^+ , Ba^{2+} ja La^{3+} 4f orbitaali kollapsit 3d ergastustel. Mõlemas isoelektronses reas näitab kollapseeimata ja kollapseeitud seisunditele vastavate eksperimentaalsete spektrite võrdlus väga olulisi muutusi nii röntgenneeldumis- kui ka fotoelektronspektrite intensiivsuste jaotuses.

Nende huvitavate eksperimentaalsete andmete interpretatsioon ei oleks olnud võimalik ilma oluliste teoreetiliste arvutusteta. Kuna esimesed eksperimentaalsed tulemused osutasid atomaarsete efektide domineerimisele kollapseeunud elektroni ergastustel ioonsetes kristallides, kasutati arvutusmodelit, mis baseerub Hartree-Focki meetodil. Tahkise mõju lainefunktsioonidele arvestati nn. Watsoni sfääriga, mis taandab iooni naabrite mõju sfääriliseks korrektsioonipotentsiaaliks. Elektroonsete üleminekute (fotoergastuse ristlõiked, Auger' üleminekute intensiivsused) arvutati vahepealse seose skeemi järgi. Kõikide nende arvutuste teostamiseks töötati välja efektiivsed FORTRAN-programmid.

Saadud põhitulemused võib formuleerida alljärgnevalt.

1. Meie tulemused demonstreerivad veenvalt, et vaba iooni mudel sobib põhiliste iseärasuste interpretatsiooniks 3d neeldumis- ja kiirgusspektrite puhul ksenoonisarnastes ioonides ning 2p neeldumis- ja kiirgusspektrite puhul argoonisarnastes ioonides ioonsetes ühendites. Tahkise mõju ioonidele väljendub põhiliselt 3d kollapseeinud seisundite kristallväljas lõhenemises argoonisarnastes ioonides. Erinevate eksperimentaalsete neeldumisspektrite võrdlus ja arvutused näitavad, et konfiguratsioonis $3d^9 4f$ ksenoonisarnaste ioonide isoelektronses reas on 4f elektron I^- ioonide ja Xe aatomite puhul lokaliseerunud välises Ba^{2+} ja La^{3+} puhul sisemises potentsiaaliaugus. Argoonisarnaste ioonide K^+ , Ca^{2+} , Sc^{3+} and Ti^{4+} puhul on 3d elektron $2p^5 3d$ konfiguratsioonis lokaliseerunud sisemises Cl^- ja Ar puhul välises potentsiaaliaugus. Ergastatud elektroni laengutiheduse ruumiline ümberjaotus kollapseeumisel toob kaasa väga olulise röntgenneeldumisüleminekute ostsillaatorijõudude ümberjaotuse 3d või 2p neeldumisaäre kontiinumini osast diskreetsete üleminekute regiooni.

2. Meie tulemused näitavad, et Ar- ja Xe-taoliste ioonide reas toob 3d ja 4f orbitaalide kollaps kaasa resonantsete Auger' spektrite drastilised muutused.

Siinjuures toob ergastatud orbitaalide kollaps Auger' üleminekute **kaheaugulistes lõppseisundites** ühelt poolt kaasa nn. klassikalise vaatlejamudeli (õigustas ennast täielikult aatomite, molekulide ja tahkiste Auger' spektrite interpreteerimisel resonantsel ergastamisel mittekollapseeunud seisunditesse) täieliku mitterakendatavuse. Cl^- näitel uurisime teoreetiliselt Auger' vaatleja-üleminekute sõltuvust lõppseisundi orbitaali lokaliseerumisest ja näitasime, et vaatlejaelektroni kollaps toob kaasa elektrostaatiliselt vastamõju suurenemise kaheaugulise Auger' lõppseisundi ja vaatlejaelektroni vahel, mis viib seose tüübi muutumisele jj - või Lj -tüübist, mis iseloomustab lõppseisundeid klassikalises vaatlejamudelis, LS -tüübi sarnaseks. See põhjustab keerulise Auger' lõppseisundite multipliiti tekkimise ja viib lõppkokkuvõttes selleni, et klassikalise vaatlejamudeliga ei ole Auger' lagunemisspektreid võimalik interpreteerida.

Teiselt poolt, vahepealsete, röntgenneeldumisseisundite ergastatud orbitaalide kollaps viib tugevale Auger' vaatlejastruutuuride (kaks auku + vaatlejaelektron) ja osavõtjastruutuuride (üks auk) võimendumisele spektrites. Nii võib Auger' osavõtja lagunemiskanalite intensiivsus, mille energia on sama otsese fotoemissiooni lõppseisundiga, olla mõnedel juhtudel palju suurem kui otsese fotoemissiooni üleminekute intensiivsus (nt. Ba ja La 4d fotojooned).

3. Avastasime eksperimentaalselt ja põhjendasime teoreetiliselt Auger' osavõtja-üleminekute multipliitist sõltuvuse, väga tugeva osavõtjastruutuuride sõltuvuse ergastuse energiast ning anomaalse 4d_{3/2} ja 4d_{5/2} fotojoonte suhte M_{45} resonantsetel ergastustel lantaanis (LaF_3) ning baariumis (BaF_2).

4. Meie raputus- (*shake*) protsesside arvutused näitavad, et vastupidi Ar aatomitele, kus raputusprotsessid Auger' lagunemisel on väga tugevad ja määravad Auger' lõppseisundite formeerumisel, on K^+ ja eriti Ca^{2+} ionide puhul raputusprotsesside tõenäosus väike. Näitasime, et see on põhjustatud 3d orbitaali kollapseeumisest röntgenneeldumise lõppseisundites (konfiguratsioonis $2p^5 3d$).

5. Meie mõõdetud Ti 2p neeldumisspektrid näitavad sõltuvust TiO_2 erinevate polümorfsete vormide struktuursetest erinevustest. Resonantsete fotoelektron-spektrite analüüsile tuginedes on püstitatud hüpotees erisugused 3d orbitaali lokaliseerumiseastmega seisundite ilmnemisest TiO_2 erinevate modifikatsioonide puhul Ti 2p_{3/2} neeldumisspektris.

6. Resonantsed Auger' spektrid meie mõõdetud ühendites on oluliselt atomaarsed. Tahkise mõju neile spektritele sõltub oluliselt aine, ergastusest ning ergastatud elektroni lainefunktsiooni lokaliseerumisastmest neeldumisel ja Auger' ülemineku lõppseisundis. Põhilised tahke keha põhjustatud protsessid, mis omavad mõju resonantsetele Auger' spektritele, on järgmised:

- i) ergastatud vaatleja elektroni tunnelleriv delokalisatsioon juhtivustsooni kontinuumisse röntgenneeldumisprotsessis (nt. L_{23} ergastuste lagunemisspektrites kaaliumi ühendites);
- ii) kahekordsete (*double*) Auger' kanalite avanemine mõningates kristallides, kui vaatlejaelektroni lõppseisundid on ülalpool kaheauguliste seisundite

- ioniseerimisäärt, mis mõjutab madalaenergeetilist vaatlejatüleminekute spektriosa (nt. M_{45} ergastuste lagunemisspektrites spektrid BaF_2 -s);
- iii) tahkistes on paljudel juhtudel energeetiliselt võimalik Coster-Kronigi lagunemiskanalite avanemine (nt. L_2 ergastustel kaaliumi ja kaltsiumi ühendites ja M_4 ergastustel BaF_2 -s);
- iv) resonantsete Auger' vaatlejastruktuuride sõltuvus röntgenneeldumise kristallväljaseisundist (kõige selgemini ilmneb see kaltsiumi ja kaaliumi ühendite L_{23} lagunemisspektrites);
- v) laenguülekande protsessid valentstsoonist vaatlejaelektroni tasemetele nii röntgenergastusel kui ka Auger' lagunemisel (nt. TiO_2 ja Sc_2O_3 L_{23} lagunemisspektrites).

ACKNOWLEDGMENTS

First of all, I am grateful to my supervisor Professor Mart Elango, for his continuous support, patience and interest in my work during these years when he had been among us.

I want especially thank my roommate, Anti Maiste, for the prolonged and helpful discussions, and A. Saar for his help in various practical matters.

I owe much to whole staff of the Laboratory of X-Ray Spectroscopy, A. Kikas, E. Nõmmiste, A. Ausmees, H. Käämbre, V. Bitševin, B. Sorkin as well as previous members, A. Zurakovski, J. Pruulmann.

Warmest thanks to Professor Indrek Martinson for his support and interest in our work.

The help from the staff at MAX is gratefully acknowledged.

I want to thank also to the visitor of our group, Tony Fonden.

Finally, I want to thank my mother and my brothers, as well as my friends in Tartu for encouragement and support during all these years.

REFERENCES

- ¹ E. Fermi, in "Quantentheorie und Chemie", ed. by H. Falkenhagen, S. Hinzl-Verlag, Leipzig, 1928, p. 95.
- ² M. Mayer, Phys. Rev. **60**, (1941), 184.
- ³ J. P. Connerade, Contemp. Phys. **19**, (1978), 171.
- ⁴ R. I. Karazija, Sov. Phys. Usp. **24**, (1981), 775.
- ⁵ U. Fano and J. W. Cooper, Rev. Mod. Phys. **40**, (1968), 441.
- ⁶ R. D. Cowan, J. Opt. Soc. Amer. **58**, (1968), 924.
- ⁷ D. C. Griffin K. Andrew and R. D. Phys. Rev. **A3**, (1971), 1233; Phys. Rev. **177**, (1969), 62.
- ⁸ J. P. Connerade, Contemp. Phys. **19**, (1978), 415. S. A. Kuchas, A. V. Karosene, and R. I. Karazija, Izv. Akad. Nauk SSSR Ser. Fiz. **40**, (1976), 270, R. D. Cowan, J. Opt. Soc. Amer. **58**, (1968), 924.
- ⁹ D. E. Sayers, E. A. Stern and F. W. Lytle, Phys. Rev. Lett. **27**, (1971), 1204.
- ¹⁰ R. S. Knox, Theory of Excitons (Academic Press, New York, 1963).
- ¹¹ A. B. Kunz, J. C. Boisvert, T. O. Woodruff, J. Phys. C: Solid State Phys. **15**, (1982), 5037.
- ¹² L. G. Parratt, Rev. Mod. Phys. **31**, (1959), 616.
- ¹³ R. T. Poole, J. G. Jenkin, J. Liesegang, and R. C. G. Leckey, Phys. Rev. **B11**, (1975), 5179.
- ¹⁴ L. A. Bugaev, I. I. Gegusin, V. N. Datsyuk, A. A. Novakovich and R.V. Vedrinskii, Phys. Stat. Sol. (b) **133**, (1986), 195;
V. N. Datsyuk, I. I. Gegusin and R. V. Vedrinskii, Phys. Stat. Sol. (b) **134**, (1986), 175.
- ¹⁵ J. E. Mueller, O. Jepsen, and J. W. Wilkins, Solid State Commun. **42**, (1982), 365.
- ¹⁶ T. Åberg and G. Howat, in Coruscules and Radiation in Matter I, edited by S. Flugge and W. Mehlhorn, Vol. **31** of Handbuch der Physik (Springer, Berlin, 1982), p. 469; T. Åberg, Phys. Scripta **21**, (1980), 495.
- ¹⁷ T. Åberg and B. Crasemann, in Resonant Anomalous X-ray Scattering: Theory and Applications, edited by G. Materlik, C. Sparks and K. Fisher (Elsevier, Amsterdam, 1994), p. 431.
- ¹⁸ F. Gel'mukhanov and H. Ågren, Phys. Rev. **A54**, (1996), 3960.
- ¹⁹ S. Ohtani, H. Nishimura, H. Suzuki, and K. Wakiya, Phys. Rev. Lett. **36**, (1976), 863.
- ²⁰ A. Niehaus and C. J. Zwakhals, J. Phys. **B16**, (1983), L135.
- ²¹ G. B. Armen, J. Tulkki, T. Åberg and B. Crasemann, Phys. Rev. **A36**, (1987), 5606.
- ²² G. B. Armen and J. C. Levin, Phys. Rev. **A56**, (1997), 3734.
- ²³ L. C. Davis, J. Appl. Phys. **59**, (1986), R25.
- ²⁴ A. Kay, E. Arenholz, S. Mun, F. J. Garcia de Abajo, C. S. Fadley, R. Denecke, Z. Hussain and M. A. Van Hove, Science **281**, 679, 1998.
- ²⁵ F. J. Garcia de Abajo, C. S. Fadley and M. A. Van Hove, Phys. Rev. Lett. **82**, 4126, 1999.
- ²⁶ D. Chattarji, The Theory of Auger Transitions (Academic, New York, 1976).
- ²⁷ A. Tanaka and T. Jo, J. Phys. Soc. Jpn. **62**, (1993), 1118.
- ²⁸ A. M. Cini, Solid St. Commun. **20**, (1976), 605; **24** (1977), 681; Phys. Rev. **B17**, (1978), 2788; G. A. Sawatzky Phys. Rev. Lett. **39**, (1977), 504; G. A. Sawatzky and A. Lenselink, Phys. Rev. **B21**, (1980), 1790.

- ²⁹ A. A. Nikitin and Z. B. Rudzikas, Foundations of the Theory of the Spectra of Atoms and Ions (Nauka, Moscow, 1983, in Russian).
- ³⁰ P. O. Bogdanovich, Hartree-Fock calculation program (In "Collection of the programs of software of Atomic Calculations", vol. 2, Inst. of Physics of the Lith. Acad. Sc., Vilnius, 1978, in Russian)
- ³¹ R. E. Watson, Phys. Rev. **111**, (1958), 1108.
- ³² M.I. Petrashen, A.V. Ivanova and G. Volf, Vestn. Leningrad Univ. Fiz. **10**, (1956), 29 (in Russian).
- ³³ N. N. Kristoffel, Theory of impurity centres with small radii in ionic crystals (Nauka, Moscow, 1974, in Russian).
- ³⁴ Y. M. Kanjauskas, G. V. Merkalis and Z. B. Rudzikas, Litov. Fiz. Sb. **18**, (1979), 475.
- ³⁵ T. M. Zimkina and V. A. Fomichev, Ultrasoft X-ray spectroscopy, Izdat. Leningr. Univ., Leningrad, 1971, p. 33.
- ³⁶ Aarik, J., Aidla, A., Uustare, T., and Sammelselg, V., *J. Cryst. Growth*. **148**, (1995), 268.
- ³⁷ J. E. Hansen, J. Phys. B **5**, 1083 (1972); S. A. Kuchas and A. V. Karosene, Litov. Fiz. Sb. **18**, (1978), 187.
- ³⁸ F. C. Brown, C. Gähwiller, H. Fujita, A. B. Kunz, W. Scheifley, and N. Carrera, Phys. Rev. B2, (1970), 2126.
- ³⁹ R. Haensel, G. Keitel, N. Kosuch, U. Nielsen, and P. Schreiber, J. Phys. (Parts), Colloq. **32**, (1971), C4-236.
- ⁴⁰ P. Caro, M. Faucher, M. Savy and H. Pankowska, J. Chem. Phys., **68**, (1978), 1045.
- ⁴¹ C. Satoko and S. Sugano, J. Phys. Soc. Jpn., **34**, (1973), 701.
- ⁴² F. M. F. de Groot, J. C. Fuggle, B. T. Thole and G. A. Sawatzky, Phys. Rev. B**41**, (1990), 928.
- ⁴³ R. Ruus, 2th All-Union Conference on Quantum Chemistry of the Solid State, Abstracts, Riga, 1985, p. 55 (in Russian).
- ⁴⁴ M. Yanagihara, H. Maezawa, T. Sasaki and Y. Iguchi, J. Phys. Soc. Jpn., **54**, (1985), 3628.
- ⁴⁵ C. Satoko, Solid State Comm., **13**, (1973), 1851.
- ⁴⁶ Crocombette, I. P., and Jollet, F. J. Phys. Condens. Matter. **6**, (1994), 10811.
- ⁴⁷ de Groot, F. M. F., Figueiredo, M. O., Basto, M. J., Abbate, M., Petersen, H., and Fuggle, J. C., Phys. Chem. Miner. **19**, (1992), 140.
- ⁴⁸ Brydson, R., Sauer, H., Engel, W., Thomas, J. M., Zeitler, E., Kosugi, N., and Kuroda, H., J. Phys.: Condens. Matter, **1**, (1989), 797.
- ⁴⁹ Brydson, R., Williams, B. G., Engel, W., Sauer, H., Zeitler, E., and Thornas, J. M., Solid State Commun. **64**, (1987), 609.
- ⁵⁰ van der Laan, G., Phys. Rev. B**41**, (1990), 12366.
- ⁵¹ Crocombette, I. P., and Jollet, F. J., Phys. Condens. Matter. **6**, (1994), 10811.
- ⁵² Y. Onodera and Y. Toyozawa, J. Phys. Soc. Jpn. **22**, (1967), 833.
- ⁵³ M. Watanabe, J. Phys. Soc. Jpn. **34**, (1973), 755.
- ⁵⁴ M. Meyer, E. von Raven, and B. Sonntag, Phys. Rev. A **49**, (1994), 3685; L. O. Werme, F. Bergmark, and K. Siegbahn, Physica Scripta **8**, (1973), 149.
- ⁵⁵ M. Watanabe, J. Phys. Soc. Jpn. **34**, (1973), 755.
- ⁵⁶ E. Kukk, S. Aksela, H. Aksela, E. Nömmiste, A. Kikas, A. Ausmees, and M. Elango, Phys. Rev. B **50**, 9079, (1994).

- ⁵⁷ A. Kikas, A. Ausmees, M. Elango, J. N. Andersen, R. Nyholm, and I. Martinsson, *Europhys. Letters* **15**, 683, (1991).
- ⁵⁸ T. Fondén, A. Kikas, R. Ruus, A. Saar, and M. Elango, *J. Electron Spectrosc. Relat. Phenom.* **76**, (1995), 589–594.
- ⁵⁹ R. L. Martin and D. A. Shirley, *J. Chem. Phys.* **64**, (1976), 3685.
- ⁶⁰ H. Aksela, S. Aksela, H. Pulkkinen, G. M. Bancroft and K. Tan, *Phys. Rev.* **A43**, (1991), 1798.
- ⁶¹ M. Meyer, E. v. Raven, B. Sonntag and J. E. Hansen, *Phys. Rev.* **A43**, (1991), 177.
- ⁶² M. Meyer, E. Von Raven, B. Sonntag, and J. E. Hansen, *Phys. Rev. A* **49**, (1991), 3685.
- ⁶³ F. M. F. de Groot, R. Ruus, and M. Elango, *Phys. Rev.* **B51**, (1995).
- ⁶⁴ R. D. Deslattes, *Phys. Rev. Lett.* **20**, (1968), 483.
- ⁶⁵ S. T. Manson and J. W. Cooper, *Phys. Rev.* **165**, (1968), 165.
- ⁶⁶ M. Ya. Amusia and V. K. Ivanov, *Sixth Intern. Conf. on Atomic Physics, Abstracts, Riga, 1978*, p. 446.
- ⁶⁷ C. Bonelle, R. C. Karnatak and J. Sugar, *Phys. Rev.* **A9**, (1974), 1962.
- ⁶⁸ J. Sugar, *Phys. Rev.* **A6**, (1972), 1764.
- ⁶⁹ S. J. Goroshenko, V. S. Rostovskii and N. P. Judin, *Vestn. Mosk. Univ., Ser. Fiz.* **24**, (1983), 96 (in Russian).
- ⁷⁰ M. Ya. Amusia and V. K. Ivanov, *8th All-Union Conference on physics of electron and atomic collisions, Abstracts, Leningrad, 1981*, p. 241 (in Russian).
- ⁷¹ P. Motais, E. Belin and C. Bonnelle, *Phys. Rev.* **B25**, (1982), 5492.
- ⁷² J. Tulkki, T. Åberg, S. B. Whitfield, and B. Crasemann, *Phys. Rev.* **A41**, (1990), 181; W. Eberhardt, S. Bernstorff, H. W. Jochims, S. B. Whitfield, and B. Crasemann *ibid.* **38**, (1988), 3808.
- ⁷³ K. Ichikawa, O. Aita, K. Aoki, M. Kamada, and K. Tsutsumi, *Phys. Rev.* **B45**, 3221, (1992); M. Kamada, K. Ichikawa, and O. Aita *ibid.* **47**, (1993), 3511.
- ⁷⁴ H. Ogasawara, A. Kotani, B.T. Thole, K. Ichikawa, O. Aita, and M. Kamada, *Solid State Comm.* **81**, (1992), 645.

PUBLICATIONS

A. A. Maiste, R. E. Ruus, S. A. Kuchas, R. I. Karaziya, and M. A. Elango,
Collapse of 4f-electron in the configuration $3d^9 4f$ in xenonlike ions,
Zh. Eksp. Teor. Fiz. **78**, (1980), pp. 941–951 [Sov. Phys. JETP **51**,
(1980), pp. 474–479] (in Russian).

Collapse of 4f-electron in the configuration 3d⁹4f in xenonlike ions

A. A. Maiste, R. É. Ruus, S. A. Kuchas, R. I. Karaziya, and M. A. Éiango

Physics Institute, Estonian Academy of Sciences
and Physics Institute, Lithuanian Academy of Sciences

(Submitted 21 September 1979)

Zh. Eksp. Teor. Fiz. 78, 941-951 (March 1980)

The $M_{4,5}(3d)$ absorption and emission spectra of the xenonlike ions I^- , Ca^+ , Ba^{2+} , and La^{3+} were measured in ionic compounds (spectral range 600-1100 eV). It is shown that the form of the spectrum characterizes mainly the absorbing ion and depends little on its surrounding. The absorption spectra of Ca^+ , Ba^{2+} , and La^{3+} contain an intensive doublet near the ionization threshold of the 3d shell, and their emission spectra contain bands that are at resonance with the absorption bands. It is concluded that in the Ba^{2+} and La^{3+} ions the 4f orbit in the configuration 3d⁹4f is collapsed and that its collapse takes place on going from Xe to Ca^+ . This conclusion is confirmed by a calculation of the energies and cross sections of the 3d¹⁰→3d⁹4f transitions in the Hartree-Fock-Pauli approximation.

PACS numbers: 33.20.Rm, 33.10.Ca, 33.70. - w

1. INTRODUCTION

The phenomenon of sudden compression of the radial wave function of an excited electron in a number of neutral atoms or in an isoelectronic sequence, which was named electron collapse, was predicted by Fermi in 1928.¹ Only in the last decade, however, in connection with the extensive studies of excited configurations of atoms and ions, did it attract considerable attention and made it possible to explain a number of interesting effects in atomic spectra and in the physics of atomic collisions.^{2,3}

The effective potential in the centrosymmetric field in the Hartree-Fock equation for the electron nl consists of two terms:

$$V_{eff}(nl|r) = V(nl|r) + l(l+1)/r^2,$$

where $V(nl|r)$ is the potential of the Coulomb field of the nucleus and of the other electrons, while the second term is centrifugal. In the interval $r \approx 1-5$ a. u., $V(nl|r)$ varies approximately like r^{-2} , and in the case of an electron with $l \geq 2$ these two terms compete with each other in a certain interval of r .³ This leads to a specific form of the effective potential, with two minima separated by a positive potential barrier. The localization of the electron in the field of this potential is highly sensitive to a change in the charge of the nucleus or of the states of the other electrons. Whereas in a certain configuration of the atom Z the wave function of the excited electron is localized predominantly in the region of the outer potential well, for the same configuration of

the atom $Z+1$, or even for another multielectron state of the atom Z ,⁴ it can be localized already in the region of the internal well, and this leads to a radical change—even by several orders of magnitude—in the values of the different characteristics of the excited electron and manifests itself in the spectra by a nonmonotonic change of the type of coupling and of the energy positions of the lines, as well as by a redistribution of the intensity in the spectrum.^{3,5}

The electron collapse is more clearly pronounced the larger the orbital quantum number of the electron. One can therefore expect a strong influence of the effect of the collapse of an $n'f$ electron in the configuration $nd^2n'f$ on the structure of the corresponding absorption and emission x-ray spectra. In a number of papers^{3,4,5} the collapse of the $4f$ electron in the configuration $4d^24f$ (which occurs near $Z=55$) and its influence on the $4d$ absorption spectra were considered. The intensity of the spectrum should become redistributed among the channels $4d-4f$ and $4d-cf$. In the indicated spectra, however, owing to the strong multielectron effects, a broad maximum predominates and masks the collapse effect. An interesting result of the experimental investigations is the establishment of the fact that the form of the $4d$ absorption spectra of elements that follow xenon in the periodic table is mainly of atomic origin, and the spectra of the vapors, metals, and solid-state compounds are very similar.⁷

In the present paper we present the results of experimental and theoretical investigations of the collapse of the $4f$ electron in the configuration $3d^24f$ of the xenon-like ions I^- , Cs^+ , Ba^{2+} , La^{3+} . Owing to the lesser role of the multielectron effects in this configuration, compared with the configuration $4d^24f$, one should expect the possibility of a more unambiguous interpretation of the spectra. As shown previously,⁸ collapse in an iso-electronic sequence should be more rapid than in a sequence of neutral atoms, and the fact that the ions with different values of Z are isoelectronic allows us to attribute the nonmonotonic variation of the spectra in the indicated sequence exclusively to the effect of the collapse.

We begin the article with a report of the results of experimental investigation of the $3d$ absorption and emission spectra of the ions I^- , Cs^+ , Ba^{2+} and La^{3+} in ionic compounds, followed by an analysis of the transitions $3d^{10} - 3d^94f$ in the Hartree-Fock-Pauli (HFP) approximation and calculation of the cross section for the photoionization of the $3d$ shell. In the last section we discuss the results and conclude that collapse of the $4f$ electron in the configuration $3d^24f$ takes place, at least partially, in the transition from Xe to Cs^+ .

2. $3d$ ABSORPTION AND EMISSION SPECTRA OF I^- , Cs^+ , Ba^{2+} AND La^{3+}

We have measured the absorption spectra of alkali iodides and of the halides of cesium, barium, and lanthanum in the spectral region from 600 to 1100 eV. The measurements were performed with an RSM-500 x-ray monochromator spectrometer, with a glass diffraction grating (600 lines/mm, curvature radius 6 m). An x-

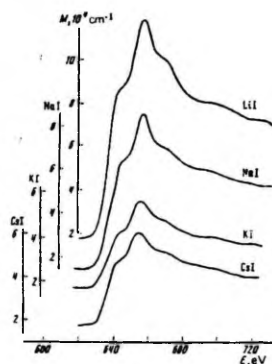


FIG. 1. $M_{4,1}$ absorption spectra of I^- in alkali iodides.

ray tube with a tungsten anode operated at 5 kV and 90 mA. The higher orders of the bremsstrahlung were suppressed by a focusing mirror. The x-rays were registered with an argon-methane flow-through proportional counter having a nitrocellulose window. Thin films of the investigated substances, whose thickness was measured with the aid of a quartz oscillator accurate to ~20%, were evaporated on the nitrocellulose films in vacuum in the measuring chamber of the spectrometer. The width of the spectrometer slits was 15 μ m, thus ensuring monochromatic radiation in the employed spectral range with intensity ~1000 quanta/sec and a spectral gap width ~2 eV.

The absorption spectra in the region of the $M_{4,1}(3d)$ edges of iodine, cesium, and barium are shown in Figs. 1, 2, and 3. In all cases there is a well pronounced albeit not very rich near-edge structure. The general form of the spectra is practically independent of the second component of the compound, and the chemical

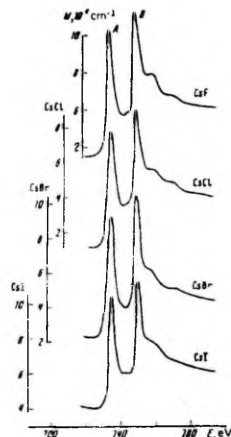


FIG. 2. $M_{4,1}$ absorption spectra of Cs^+ in cesium halides.

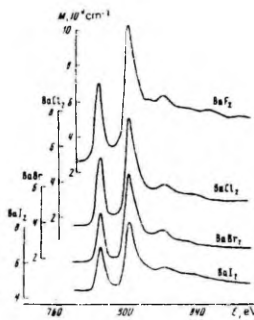


FIG. 3. $M_{4,5}$ absorption spectra of Ba^{2+} in barium halides.

shifts do not exceed 1.5 eV. This demonstrates convincingly that the main structural singularities of the spectra are of quasi-atomic character. They characterize the corresponding ion, which is possibly slightly perturbed by the crystal field. Therefore in first-order approximation we can use the presented spectra to discuss the optical transitions of the 3d electrons in the corresponding isolated ions.

For a detailed interpretation, the spectra of the isoelectronic ions I^- , Xe, Cs^+ , Ba^{2+} and La^{3+} are gathered together in Fig. 4. The Xe spectrum was borrowed from Ref. 9. The photoabsorption cross sections are marked on the ordinate scale in the same scale for all ions. The spectra have the same energy scale, the origin of which coincides with the binding energy of the

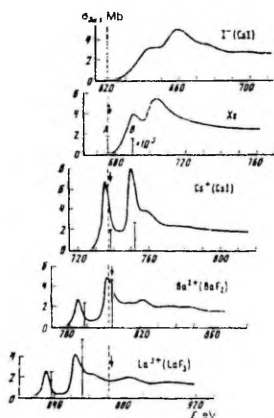


FIG. 4. Partial photoabsorption cross sections of the 3d shell of xenon-like ions. The spectra coincide in position at the ionization energies of the $3d_{5/2}$ shells of the corresponding ions (see the text), namely 620, 676, 735, 802, and 871 eV for I^- , Xe, Cs^+ , Ba^{2+} , and La^{3+} , respectively. The theoretical values (see the table) of the intensities (decreased by a factor 1.3) and of the energies of the $3d^{10} - 3d^9 4f$ lines are marked by vertical lines, while the theoretical ionization energies are marked by arrows.

$3d_{5/2}$ electrons in the corresponding free ions (the numerical values of these energies will be estimated in the next section).

In their general appearance, the considered spectra are clearly divided into two groups. In the case of I^- and Xe, the broad smooth maxima are located beyond the ionization threshold, and with further distance from the threshold the absorption decreases, but still remains appreciable. For Cs^+ , Ba^{2+} , and La^{3+} , two intense relatively narrow maxima below the ionization threshold predominate in the spectrum, and the absorption in the region of the continuous spectrum is much weaker than in the cases of I^- and Xe.

Proceeding to an interpretation of these regularities, we note first that the doublet structure separated in all the spectra is due to the spin-orbit splitting of the 3d shell. This is evidenced by the proximity of the energy intervals between the components of the doublets and the energies of the spin-orbit splitting of the 3d shells obtained by photoelectron spectroscopy (see, e.g., Ref. 10).

There are good theoretical grounds for assuming that the absorption spectrum of Xe is determined entirely by transitions of 3d electrons into a continuum of f states, i.e., by $3d-f$ transitions and that their transitions to the p state have small oscillator strengths.^{11,12} Since the f states are retained by the intra-atomic potential barrier in the region of the outer potential well, the transitions $3d-cf$ become effective only at energies sufficient for the f wave to penetrate into the inner well, and this leads to a quasisonant concentration of the oscillator strengths of the transitions in the region above the ionization threshold.

Since Z , and hence also $|V(r)|$, is smaller in the case of I^- than in the case of Xe, this interpretation can also be used with assurance for the corresponding spectra of the rare-earth atoms (see, e.g., Ref. 13). Inasmuch as in the latter case the oscillator strength stems primarily from $3d-4f$ transitions and the $3d-cf$ channel is already much less effective,¹⁴ it must be concluded that the clearly pronounced doublets in the initial regions of the spectra of Cs^+ , Ba^{2+} , and La^{3+} are due to $3d-4f$ transitions.

Thus, a qualitative analysis of the spectra presented in Fig. 4 leads to the conclusion that a collapse of the 4f orbital in the configuration $3d^9 4f$ takes place on going from Xe to Cs^+ and Ba^{2+} .

Figure 5 shows the emission $M_{4,5}$ spectra of Cs^+ (in $CsCl$), Ba^{2+} (in BaF_2), and La^{3+} (in LaF_3). They were measured, as usual, by rubbing in the objects into the surface of the anode (Cu or Al) of the x-ray tube of the spectrometer. To display the effects of self-absorption of the radiation in the objects, the spectra were measured in several regimes. Figure 5 shows the spectra measured in two regimes, of which the "weak" and the "strong" ensure respectively maximum and minimum self-absorption. The low-energy part of the spectra contains the so called diagram lines corresponding to the transitions $3d^9 5p^6 - 3d^{10} 5p^5$. The high-energy part of the spectra is at resonance with the absorption spec-

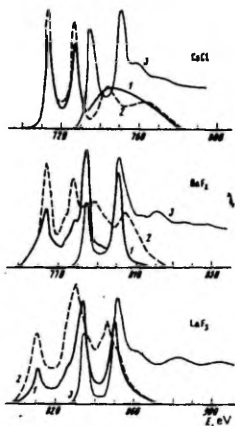


FIG. 5. $M_{4,5}$ emission spectrum of the ions Cs^+ , Ba^{2+} , and La^{3+} in ionic compounds under strong (3 kV, 20 mA) (2) and weak (1 kV, 10 mA) (1) excitation regimes; 3—absorption spectra. The ordinate scale is linear in relative units.

tra and is strongly deformed by self-absorption effects. This part of the spectrum is due to radiative decay of the bound excited states. In the case of La^{3+} and Ba^{2+} they coincide quite accurately with the corresponding absorption bands, and their intensity exceeds that of the diagram lines. This makes it undoubtedly possible to attribute them to the transitions $3d^6 4f \rightarrow 3d^{10}$ and thus confirm the conclusion drawn above that in La^{3+} and Ba^{2+} the orbital $4f$ in the configuration $3d^6 4f$ is localized in the region of the inner potential well.

In the case of Cs^+ , the high-energy part of the emission spectrum is a broad structureless band that extends over dozens of electron volts in the absorption region in the $3d$ shells. Similar bands were observed by us in the $N_{4,5}$ spectra of emission of lanthanides.¹⁵ We interpret this band as being due to radiative decay of the $3d^6 4f$ configuration of the Cs^+ ions. It is considerably broadened because of the large probability of nonradiative decay of this configuration.

3. INFLUENCE OF COLLAPSE OF $4f$ ELECTRON ON THE TRANSITIONS $3d^{10} \rightarrow 3d^6 4f$

We shall consider theoretically the transitions $3d^{10} \rightarrow 3d^6 4f$ in the Hartree-Fock-Pauli (HFP) approximation (the relativistic effects are taken into account in first order of perturbation theory with Hartree-Fock wave functions starting with Breit operators in the Pauli form). The effectiveness of this approximation in the calculation of the energy characteristics of the inner electrons was demonstrated in Ref. 16. The solution of the Hartree-Fock equations makes it possible to determine sufficiently accurately the values of Z at which collapse of the excited electron takes place (see Table II of Ref. 17). The radial wave functions were defined as the solutions of the Hartree-Fock equation for the average configuration energy (HF-ac), and also as so-

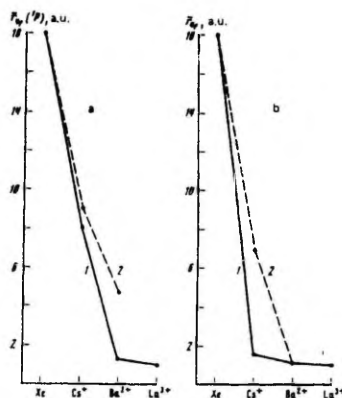


FIG. 6. Variation of the average distance of the collapsing $4f$ electrons from the nucleus in the isoelectronic Xe sequence in the configuration $3d^6 4f$ (1) and $4d^6 4f$ (2), determined by the solutions of the Hartree-Fock equations for the 1P term (a) and for the average energy (b).

lutions for individual terms (HF-t). In the latter case, however, the terms corresponding to the LS -type coupling (in the Hartree-Fock potential only the terms of the electrostatic interaction are taken into account), which is not at all similar to the real type of coupling, close to the jj coupling, in the $3d^6 4f$ configuration.

The results of the calculations are shown in Fig. 6 and in the table. The average distance of the $4f$ electron from the nucleus changes upon collapse of the orbit by approximately one order of magnitude. Its values, determined by the functions HF-av and HF-t (the 1P and 3D terms) are very close and therefore the latter are not cited separately. For Xe (non-collapsed $4f$ electron) and Ba^{2+} and La^{3+} (collapsed $4f$ electron) the results of the solution of the HF-av and HF- 1P equations are practically identical. A substantial dependence on the term is observed only for Cs^+ : according to the solutions of the equations HF-av, the collapse of the $4f$ electron has already taken place, while according to the HF- 1P solutions it has not yet occurred.

TABLE I.

	$I(4f_{7/2})$, eV			Terms	$(LS)^1P$	E , eV		$\alpha(3d^{10} \rightarrow 3d^6 4f)$, Mb
	HF	HFP	estimate			HFP	experiment	
Xe	687.6	677.1	678.4	1P	0.72	678.3	—	$2.7 \cdot 10^{-1}$
				3P	0.26	678.3	—	$4.1 \cdot 10^{-1}$
				3D	0.63	686.7	—	$2.1 \cdot 10^{-1}$
Cs^+	749.8	738.6	737.0	1P	-0.06	734.8	—	$2.3 \cdot 10^{-1}$
				3D	-0.65	738.0	735.5	2.67
				3P	0.76	751.4	750.0	3.71
Cs^{++}				1P	-0.48	734.6	—	$2.1 \cdot 10^{-1}$
				3D	0.63	735.3	—	$3.6 \cdot 10^{-1}$
				3P	0.82	749.3	—	$3.5 \cdot 10^{-1}$
Ba^{2+}	815.8	803.8	802.0	1P	-0.06	784.0	—	$3.3 \cdot 10^{-1}$
				3D	0.59	788.6	785.0	3.21
				3P	0.81	803.7	801.5	0.17
La^{3+}	863.2	872.5		1P	-0.05	833.2	—	$2.7 \cdot 10^{-1}$
				3D	0.26	838.8	835.0	3.45
				3P	0.82	853.6	852.5	7.55

A comparison of the average distance \bar{r}_{4f} for the configuration $3d^0 4f$ with the corresponding results⁴ for $4d^0 4f$ shows (Fig. 6) that collapse in the isoelectronic sequence of $3d^0 4f$ proceeds more rapidly with changing Z , and complete collapse, both in the HF-av and HF-t approximations, is completed one term of the series sooner. In the case of a collapsed electron, the localization of the electron is highly sensitive to the change of the potential, and therefore for the transition cases ($\text{Cs}^+ - 3d^0 4f$ and $\text{Cs}^+, \text{Ba}^{2+} - 4d^0 4f$) refinement of the calculation (allowance for the wave functions of the spin-orbit interaction, and for the correlation and relativistic effects in the calculation) can change the results somewhat.

Localization of the radial wave function influences strongly the integrals of the electrostatic interaction between the $3d^0$ and $4f$ shells, the spin-orbit interaction constant η_{4f} , and the integral of the dipole transition $\langle 3d | r | 4f \rangle$. They are changed by 3-5 orders of magnitude by the collapse. At the same time, the spin-orbit interaction constant η_{3d} is practically independent of the localization of $4f$ electron.

The wave functions in the intermediate type of coupling were determined in the basis of the LS -coupling functions and designated $|\tilde{L}\tilde{S}\rangle$ in accord with the leading component in the expansion. The intensity of the discrete transitions $3d^{10} 3s - 3d^0 4f$ is then proportional to the square of the coefficient of expansion of the function $|\tilde{L}\tilde{S}\rangle$ for the component $\langle P | -\langle \tilde{L}\tilde{S} |^2 P \rangle^2$. For the Cs^+ ion, a calculation of the intensity was carried out both with the wave function HF- 1P and with the function HF-av. In the remaining cases, the function HF-av was used.

The binding energies $I(3d_{3/2})$ of the $3d_{3/2}$ electrons in the energies of the dipole transitions $3d^{10} - 3d^0 4f$ were determined as the differences between the corresponding total energies

$$E(\tilde{L}\tilde{S}) = E(3d^0 4f | \tilde{L}\tilde{S}) - E(3d^{10}).$$

$$I(3d_{3/2}) = E(3d_{3/2}^1) - E(3d^{10}).$$

Experimental estimates of the binding energies were obtained in the following manner. For the Xe atoms their direct measurements by the photoelectric spectroscopy method.¹⁰ For the Cs^+ and Ba^{2+} ions we used the quality

$$I(3d_{3/2}) = +E(M_{2,3}) + I(5p).$$

The energies of the $M_{2,3}$ lines were taken from the $M_{4,5}$ emission spectra (Fig. 5), the ionization potential $I(5p)$ for Cs^+ was taken from Ref. 18, and for Ba^{2+} from the tables of Ref. 19. The calculated energies of the principal transitions $3d^{10} - 3d^0 4f$ agreed with the measured absorption peaks in Cs^+ , Ba^{2+} and La^{3+} accurate to several electron volts. The deviation is determined from the correlation effects and from the inadequacy of the model of the free ion in the ionic crystals have the same sign and approximately the same magnitude as for the binding energy.

Upon collapse of the $4f$ electron, the intensities of the ground $3d^{10} - 3d^0 4f$ lines change by six orders of magnitude. For Xe (and all the more for I⁺) these transitions take not part whatever in the formation of the

absorption spectra. For Ba^{2+} and La^{3+} , the calculation already predicts a dominant role of the discrete transitions. For the Cs^+ ion, as expected, the results with HF-av functions and with HF- 1P functions (Cs^+ in the table) differ greatly. In the former case the Cs^+ spectrum is similar to the spectra of Ba^{2+} and La^{3+} , and in the latter case to the Xe spectrum. Comparison with experiment (the results of the calculation are represented by the vertical lines in Fig. 4) shows that more adequate results are obtained with the first variant. This is attested both by the energy positions of the $M_{4,5}$ peaks and by the ratio of their intensities.

Thus, atomic calculation confirms the conclusion drawn above that for Cs^+ , Ba^{2+} , La^{3+} the and principal absorption peaks are connected with the transitions $3d^{10} - 3d^0 4f$. The experimentally observed redistribution of the oscillator strengths among the continuous and discrete spectra in the isoelectronic sequence $\text{I}^+ - \text{Xe} - \text{Cs}^+ - \text{Ba}^{2+} - \text{La}^{3+}$ is direct evidence of the collapse of the $4f$ electron in the $3d^0 4f$ configuration in the middle of the sequence.

4. CALCULATION OF THE $3d$ -SHELL PHOTOIONIZATION CROSS SECTIONS

The collapse of the $4f$ electron should be accompanied by a drastic change in the $3d$ -shell photoionization cross section. As shown by Amus'ya and co-workers,²⁰ for atoms of inert gases and of their neighboring elements (i. e., for Z values near which collapse of the excited electron as well as the associated change in the free-electron function take place), it is important to take into account multi-electron effects in the calculation of the photoionization cross sections. Therefore the results presented below on the calculation of the $3d$ photoionization in the single-electron approximation are more readily estimates.

The calculations were performed using the tabulated single-electron orbitals of Herman and Skillman.²¹

The volume potential was reduced to a local form by dividing the exchange term of the Hartree-Fock equation by the solution of the inhomogeneous equation. The free-electron functions were calculated both in the frozen field of the atomic core and with allowance for the relaxation of the core (this was approximately taken into account by using for the outer electron shells the Herman-Skillman wave functions of the next atom in the periodic system, while the orbitals of the considered atoms were used for the $3d$ and deeper shell). As noted in a number of papers (see Refs. 22, 20 and others), allowance for the relaxation of the core in the single-electron approximation at low energies of the photoelectron usually gives a better approximation.

The results using the ionization energies of the preceding section are shown in Fig. 7. It is important that the character of the photoionization spectrum in the considered isoelectronic sequence changes qualitatively. A quasisonant structure exists for I⁺, Xe, and Cs^+ appearing for Cs^+ only when the relaxation of the core is taken into account. For the succeeding elements it vanishes—this can be attributed to the vanishing of the

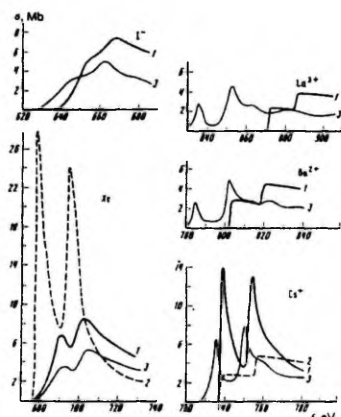


FIG. 7. Partial photoionization cross sections of the 3d shell of xenon-like ions with (1) and without (2) allowance for the relaxation of the atomic core; 3—measured absorption spectra.

effective potential barrier for the ϵf states with increasing degree of ionization.⁹ The calculated quasi-resonant structure in the $3d-\epsilon f$ spectrum of Cs^+ is similar to the experimental spectrum (see Fig. 4), but it is more probable that this is a pseudoresonance due to the inaccuracy of the model, just as in the case of calculation of the photoionization of the 4d shell in the single-electron approximation.²³ On the other hand, the results of the calculation with a nonrelaxed core can explain the additional maximum in the Cs^+ spectrum on the high-energy side of the maximum B (another additional maximum may be masked by the maximum A). This would be evidence of simultaneous manifestation of both for absorption channels in the case of a collapsing 4f electron.

5. CONCLUSIONS

The results presented above demonstrate convincingly that the model of the isolated ion is suitable for the interpretation of the main singularities of the 3d absorption and emission spectra of the xenon-like ions I^- , Cs^+ , Ba^{2+} , and La^{3+} , which are contained in compounds with high degree of ionicity. The influence of their surrounding probably manifests itself to a greater degree in the spectral region beyond the ionization threshold of the 3d shell.

A comparison of the measured spectra with one another and with results of the calculation shows also that the 4f electron in the $3d^9 4f$ configuration is localized in the outer well of the effective potential in the case of the I^- ions and Xe atoms, and in the inner well in the case of the ions Ba^{2+} and La^{3+} . This spatial redistribu-

tion of the charge density of the electron leads to a substantial redistribution of the oscillator strength from the continuous region of the 3d absorption spectrum into the region of discrete transitions.

The transition element from the point of view of the collapse of the 4f orbital in the $3d^9 4f$ configuration is cesium, whose 3d absorption spectrum and its interpretation on the basis of a calculation in the HFP approximation support the conclusion that in the case of Cs^+ the collapse has already taken place. An approximate single-electron calculation of the photoionization cross section points to the possibility of the appearance of transitions of a type $3d-\epsilon f$ in the 3d absorption spectrum of Cs^+ , but the similarity of this spectrum to the corresponding spectra of Ba^{2+} and La^{3+} indicates that the main structure in the Cs^+ spectrum is due to discrete transitions $3d^{10}-3d^9 4f$. The form of the 3d emission spectra of Cs^+ in cesium halides agrees with this conclusion if it is assumed that the nonradiative decay of the $3d^9 4f$ configuration has a high probability.

- ¹E. Fermi, in: *Quantentheorie und Chemie*, Leipzig, 1928, p. 95.
- ²U. Fano and J. W. Cooper, *Rev. Mod. Phys.* **40**, 441 (1968).
- ³J. P. Connerade, *Contemp. Phys.* **19**, 415 (1978).
- ⁴S. A. Kuchas, A. V. Karosene, and R. I. Karaziya, *Izv. Akad. Nauk SSSR Ser. Fiz.* **40**, 270 (1976).
- ⁵R. D. Cowan, *J. Opt. Soc. Amer.* **58**, 924 (1968).
- ⁶J. E. Hansen, A. W. Fillet, and H. P. Kelly, *J. Phys. B* **8**, L127 (1975).
- ⁷K. Radler and B. Sonntag, *Chem. Phys. Lett.* **39**, 371 (1976).
- ⁸E. R. Radke, *J. Phys. B* **12**, L71 (1979).
- ⁹A. V. Karosene, A. A. Kiselev, and R. I. Karaziya, *Lit. Fiz. Sb.* **13**, 363 (1973).
- ¹⁰R. D. Deslattes, *Phys. Rev. Lett.* **20**, 483 (1965).
- ¹¹*Handbook of Spectroscopy*, Vol. 1, ed. by J. W. Robinson, CRC Press, Cleveland, Ohio, 1974.
- ¹²S. T. Manson and J. W. Cooper, *Phys. Rev.* **165**, 165 (1968).
- ¹³M. Ya. Amusia and V. K. Ivanov, *Sixth Intern. Conf. on Atomic Physics, Abstracts*, Riga, 1978, p. 446.
- ¹⁴C. Bonelle, R. C. Karnatak, and J. Sugar, *Phys. Rev. A* **9**, 1962 (1974).
- ¹⁵J. Sugar, *Phys. Rev. A* **6**, 1764 (1972).
- ¹⁶V. A. Fomichev, S. A. Gribovskii, and T. M. Zimkina, *X-Ray Spectra and Electronic Structure of Matter*, München, 1973, Vol. 2, p. 197.
- ¹⁷S. A. Kuchas, A. V. Karosene, and R. I. Karaziya, *Lit. Fiz. Sb.* **18**, 593 (1978).
- ¹⁸D. C. Griffin, K. L. Andrew, and R. D. Cowan, *Phys. Rev.* **177**, 62 (1969).
- ¹⁹A. Reader, *Phys. Rev. A* **13**, 507 (1976).
- ²⁰*Svoistva elementov (Properties of Elements)*, G. V. Samsonov, ed., Part 1, M., 1976, p. 22.
- ²¹M. Ya. Amusia, *Proc. of the Fourth Intern. Conf. on Vacuum Ultraviolet Radiation Physics*, Hamburg, 1974, p. 205.
- ²²F. Herman and S. Skillman, *Atomic Structure Calculation*, Engelwood Cliffs, New Jersey, 1963.
- ²³J. W. Cooper, *Phys. Rev.* **128**, 681 (1962).
- ²⁴F. Combet-Farnaux, *Proc. Intern. Conf. on Inner Shell Ionization Phenomena*, Atlanta, 1972, Vol. 2, p. 1130.

Translated by J. G. Adashko

A. A. Maiste, R. E. Ruus, and M. A. Elango,
3d electron collapse in the $2p^53d$ configuration of argon-like ions,
Zh. Eksp. Teor. Fiz. **79**, (1980), pp. 1671–1677
[Sov. Phys. JETP **52**, (1980) pp. 844–847] (in Russian).

3d electron collapse in the $2p^5 3d$ configuration in argon-like ions

A. A. Maiste, R. É. Ruus, and M. A. Élango

Institute of Physics, Estonian Academy of Sciences
(Submitted 28 March 1980)

Zh. Éksp. Teor. Fiz. 79, 1671-1677 (November 1980)

The $L_{2,3}$ emission and absorption (or photoelectric quantum yield) spectra of K^+ in KF, KCl, KBr and KI, of Ca^{2+} in CaF_2 and $CaCl_2$, and of Sc^{3+} in Sc_2O_3 are measured (in part by using synchrotron radiation). It is shown that the onset regions of the absorption spectra are characterized by intense bands which have resonant partners in the corresponding emission spectra; these bands are associated with the $2p-3d$ transitions in the free ions K^+ , Ca^{2+} , and Sc^{3+} . Comparison of the $L_{2,3}$ spectra of the isoelectronic sequence of argon-like ions (from Cl to Sc^{3+}) shows that 3d electron collapse in the $2p^5 3d$ configuration occurs in this sequence in the transitions $Ar \rightarrow K^+ \rightarrow Ca^{2+}$.

PACS numbers: 78.55.Fv, 72.40.+w

1. INTRODUCTION

The nonmonotonic change in the energy and spatial characteristics of electrons with large orbital angular-momentum quantum numbers ($l \geq 2$) as the atomic number of effective charge increases is one of the most interesting patterns associated with the build-up of atomic electron shells. The possibility of an abrupt contraction of the radial wave function, accompanied by a sharp increase in binding energy—the so-called electron (or orbital) collapse—is explained by the characteristics of the effective potential for such electrons.¹⁻⁴

The collapse of an excited nl electron is apparent in two aspects in spectroscopic measurements. Firstly due to the increase in binding energy, the terms of the configuration with the collapsing electron sharply drop along the energy scale, crossing levels of other configurations. Secondly, due to contraction of the collapsing orbital, its overlap with subvalence orbitals located near the nucleus is increased; therefore the oscillator strengths of the corresponding transitions increase greatly.

The latter circumstance was used in the preceding work⁴ to experimentally establish 4f-electron collapse. In this work we use it to study 3d-electron collapse (in the $2p^5 3d$ configuration in the isoelectronic sequence of argon-like ions), which according to theoretical estimates^{3,5} has a number of peculiarities. We have proceeded from the premise established in recent years that the basic characteristics of the absorption spectra associated with transitions from subvalence shells of atoms or ions (especially positive ions) are preserved when they are introduced into compounds,⁶⁻⁸ and we have investigated the $L_{2,3}(2p)$ absorption and emission spectra of K^+ , Ca^{2+} , and Sc^{3+} in a number of compounds.

2. EXPERIMENTAL PART

The spectra were measured using an RSM-500 x-ray spectrometer-monochromator. Synchrotron radiation from the VEPP-2M storage ring. Institute of Nuclear Physics, Siberian Branch of the USSR Academy of Sciences, was used for measurement of the $\mu(h\nu)$ absorption spectra. In some cases instead of the $\mu(h\nu)$ spectra we measured the photoelectric quantum-yield (elec-

tron emission) spectra $\kappa(h\nu)$, using the bremsstrahlung of the tungsten target cathode. The validity of such a substitution in study of the structure of the $\mu(h\nu)$ spectrum is well known and widely used when direct measurement of $\mu(h\nu)$ is impossible or inexpedient.⁹ The $\kappa(h\nu)$ spectra were measured relative to CaI , which does not have any appreciable structure in the region under study.¹⁰ Instrument resolution for the $\mu(h\nu)$ and $\kappa(h\nu)$ spectra was 0.3-0.6 eV.

In the case of the KCl absorption spectrum, it proved to be necessary to correct for scattered radiation; taking this into account (by measuring the transmission of KCl plates of different thicknesses with various detectors) we could refine the values of μ in the region of the principal maxima.

In the measurement of the emission spectra $I(h\nu)$, the samples were attached in the form of thin sheets to copper plates serving as the target cathode of the x-ray tube, and were covered with thin aluminum sheets which provided for some deceleration of the exciting electrons (in order to reduce reabsorption) and for protection from radiolysis in the more powerful operating regimes of the tube. The resolution was on the order of 1 eV.

On Fig. 1, we present $L_{2,3}$ absorption and emission spectra of K^+ in KCl, of Ca^{2+} in CaF_2 , and of Sc^{3+} in Sc_2O_3 [in the latter case, the $\kappa(h\nu)$ spectrum is given instead of the $\mu(h\nu)$ spectrum]. All the absorption spectra start with several intense and narrow (intrinsic half-width about 0.2-0.3 eV) maxima, followed by a less intense structure. In the low-energy regions of the emission spectra, there are broad maxima associated with transitions from the valence band of the corresponding crystals, and in the high-energy region there are bands which are resonant with the primary absorption bands.

On Fig. 2 we present the $\kappa(h\nu)$ spectra of potassium halides in the $L_{2,3}$ absorption region of K^+ . It is evident that in the case of KCl, the $\kappa(h\nu)$ spectrum duplicates the shape of the $\mu(h\nu)$ spectrum in Fig. 1 quite well (taking into account the slightly lower resolution), and that the basic details of the onset region of the spectra are not very sensitive to the particular com-

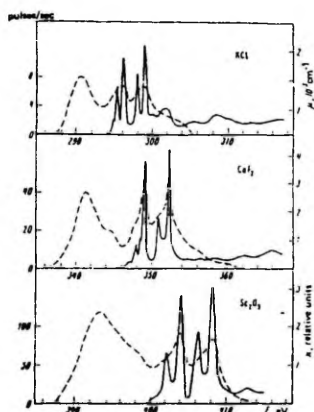


FIG. 1. $L_{2,3}$ emission spectra (dashed lines) and absorption spectra (solid lines) of potassium in KCl, calcium in CaF_2 , and scandium in Sc_2O_3 (in the latter case, the $\kappa(h\nu)$ spectrum is given instead of the $\mu(h\nu)$ spectrum—see text).

bound. Still greater similarity is observed for the absorption spectra of CaF_2 and CaCl_2 .

The general features of our spectra agree with $\kappa(h\nu)$ spectra of KCl and CaF_2 given in papers by other authors^{11,12}, but due to the substantially higher resolution (achieved primarily as a result of the use of synchrotron radiation), our spectra contain significantly more detail. The $L_{2,3}$ emission spectrum of Ca^{3+} in CaF_2 given by Nemoshkalenko *et al.*¹² does not have bands which are resonant with the absorption bands—apparently due to an insufficient decrease of the self-absorption effects.

3. DISCUSSION OF RESULTS

The high intensity of the structure in the onset region of the $\mu(h\nu)$ and $\kappa(h\nu)$ spectra presented in Figs.

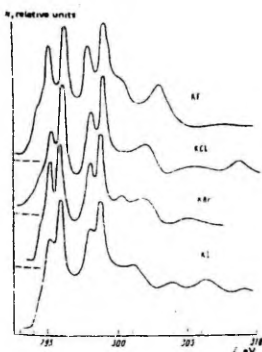


FIG. 2. Photoemission quantum yield $\kappa(h\nu)$ spectra of potassium halides in the $L_{2,3}$ -edge region of potassium.

TABLE I. Ionization energies of the $L_{2,3}$ shell, $2p-3d$, $4s$ transition energies in free argon-like ions and energies of the corresponding maxima in the $L_{2,3}$ absorption spectra of ionic crystals.

	$E(L_{2,3})$	$E(L_{2,3})$	$E(L_{2,3}-3d)$	$E(L_{2,3}-3d)$	$E(L_{2,3}-4s)$	$E(L_{2,3}-4s)$
Ar	248.6	250.7	248.9	210.0	214.2	248.3
Experiment (Ref. 14)	248.6	250.8	248.8	248.9	244.3	248.4
K^+	307.6	310.3	297.4	300.1	293.7	298.4
KCl	372.2	375.8	296.4	299.2		
Ca^{2+}			317.5	351.1	350.6	354.2
CaF_2			319.1	352.4		
Sc^{3+}	413.8	446.3	400.6	403.1	410.8	415.1
Sc_2O_3			403.8	408.0		

1 and 2, both in absolute units and relative to the structure in the higher energy region, does not leave any doubt that the intensity is due to dipole-allowed transitions—i.e., $2p-d$ and $2p-s$ transitions. In order to further interpret this structure, it is first of all necessary to establish if the wave function of the final state is primarily determined by the potential of the absorbing ion (in which the initial state is localized) or by the solid-state potential created by the environment.

It was shown above that experimental and theoretical information accumulated in recent years leads to the conclusion that both the ground and excited states of the cations in ionic crystals are determined primarily by the internal potential, and the so-called "solid-state effects" must be taken into account only in successive approximations.^{6,8}

Our work confirms the correctness of this point of view. In Table I we give a comparison of the energies of the two most intense maxima of the $L_{2,3}$ absorption spectra of K^+ in KCl, Ca^{2+} in CaF_2 , Sc^{3+} in Sc_2O_3 , and Ar with the energies of the $2p-3d$ and $2p-4s$ transitions in the free K^+ , Ca^{2+} , and Sc^{3+} ions and in the Ar atom, obtained according to the so-called " $Z+1$ scheme" (equivalent-cores approximation) as the difference between the ionization energy of the $L_{2,3}$ shell of the free ion (or atom) with the given Z [$E(L_{2,3})$] and the binding energies of the $3d$ and $4s$ levels of the $Z+1$ ion [$E(3d, 4s)$]. We may estimate $E(L_{2,3})$, using data on energies of atomic levels¹³ and ionization potentials (Ref. 14, p. 20); $E(3d, 4s)$ are tabulated.¹⁵ For Ar we also present results of direct experimental determination¹⁶ of $E(L_{2,3})$, $E(2p-3d)$, and $E(2p-4s)$. It is evident from Table I that the energy estimates found for transitions in free ions (accurate to within 1-3 eV) coincide with the energies of the most intense maxima of the corresponding solid-state absorption spectra. Consequently, the energetics of the transitions under consideration in ionic crystals are determined primarily by the energetics of the corresponding transitions in free ions. We also note that the principal maxima of the K^+ and Ca^{2+} absorption spectra presented here agree within 0.5 eV with the principal maxima of the $L_{2,3}$ absorption spectra of potassium and calcium vapors, as measured in Ref. 17.

If the final d and s states of the transitions under consideration were to be transformed into conduction-band states of the corresponding crystals, it would be extremely difficult to explain the similarity of the KCl spectrum to the KF, KBr, and KI spectra (Fig. 2) and

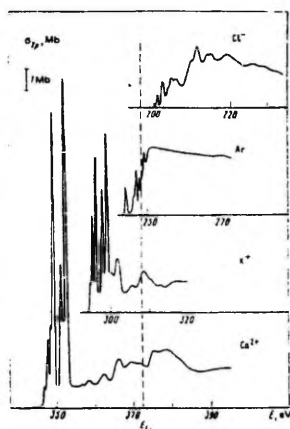


FIG. 3. Photoabsorption cross sections of the argon-like ions Cl^- , Ar, K^+ , and Ca^{2+} in the $L_{2,3}$ -edge region.

its sharp difference from the $L_{2,3}$ spectrum¹⁸ of Cl^- in KCl (Fig. 3) and the $M_{2,3}$ spectrum¹⁹ of K^+ in KCl.

Thus, the onset structure of $L_{2,3}$ absorption spectra of K^+ , Ca^{2+} , and Sc^{3+} in ionic crystals is determined primarily by the $2p-3d$ and $2p-4s$ transitions in the corresponding free ions. From Table I it follows that a fundamental role is played there by the $2p-3d$ transitions. The $2p-4s$ transitions may play some role in the K^+ case; their intensity is low, however, indicated by the Ca^{2+} and Sc^{3+} spectra (in which the energies of the $2p^33d$ and $2p^44s$ configurations differ appreciably). Furthermore, in the hydrogen model of the atom, the oscillator strength of the $p-d$ transitions exceeds the oscillator strength of the $p-s$ transitions by an order of magnitude.²⁰

A more detailed interpretation of the spectra presented is not essential from the point of view of this work. In order to carry out such an interpretation, detailed calculations are necessary, with account taken of several types of interactions having similar orders of magnitude (spin-orbit splitting of the $2p$ shell), splitting of $3d$ levels in the crystal field, electron-hole interaction, mixing of $2p^33d$ and $2p^44s$ configurations).

Let us proceed onward to a discussion of spatial localization of $3d$ orbitals in the $2p^33d$ configuration in the ions under consideration. First of all, we note that for Sc, even in the ground state, the orbital is localized within the inner electron shell region (Ref. 14, p. 28)—i.e., it is collapsed. The high intensity of the $2p-3d$ transitions and the presence of resonant bands on the $\chi(h\nu)$ and $I(h\nu)$ spectra observed in our work correspond to this. An analogous situation in the $\mu(h\nu)$ and $I(h\nu)$ spectra of K^+ and Ca^{2+} ions is evidence that $3d$ -orbital collapse has already occurred in these ions.

In order to study the dynamics of $3d$ -electron collapse in the isoelectronic sequence of argon-like ions, we pre-

sent together in Fig. 3 the $L_{2,3}$ absorption spectra of Cl^- (in KCl—Ref. 18), Ar (Ref. 16), K^+ , and Ca^{2+} , given as plots of the photoabsorption cross section σ vs. photon energy. The dashed line indicates the ionization energy $E(L_2)$ of the L_2 subshell of the corresponding free ions (see Table I). Of course, $E(L_2)$ is not the energy separation between the L_2 subshell and the bottom of the conduction band in the crystal. It is given to demonstrate the change in binding energy of $3d$ states in the ions. The fact that the first maxima of the $L_{2,3}$ spectrum of Cl^- in KCl, having an exciton character, are located above $E(L_2)$ shows that the free-ion approximation is not applicable to the interpretation of spectra of anions in ionic crystals. Nevertheless, the envelope of the $L_{2,3}$ absorption spectrum is similar for all chlorides²¹ and reflects to some degree the properties of the $\sigma(h\nu)$ function for the free Cl^- ion.

From Fig. 3 it is evident that the spectra for Cl^- and Ar are radically different from the spectra for K^+ and Ca^{2+} . These measurements are interpreted well from the point of view of $3d$ -orbital collapse in the ions of the sequence under consideration. Since these orbitals are located far from the nucleus (in the case of Cl^- and Ar), the maximum of the photoabsorption cross section is attained in the continuum region of the spectrum. As Z increases, the oscillator strength is shifted closer to the absorption threshold and increases in absolute magnitude. Ongoing to K^+ , the role of the $2p-3d$ transitions sharply increases; they completely dominate in the spectrum. In the case of Ca^{2+} , the pattern is primarily the same, but the intensity of the principal maxima increases even more. The intensity of the resonant emission bands increases in the same direction (Fig. 1). All of the data presented show that the sharp contraction of the $3d$ orbitals begins on going from Ar to K^+ and is continued on going from K^+ to Ca^{2+} .

Thus, the data presented show that, in the isoelectronic sequence of argon-like ions, $3d$ -orbital collapse in the $2p^33d$ configuration occurs in the Ar— K^+ — Ca^{2+} sequence. It occurs somewhat more slowly than the $4f$ -orbital collapse in the sequence of xenon-like ions, as was predicted by theory.^{3,4}

Application of the above discussion to experimental data of Barinskii and Kulikova²² leads to the conclusion that $4d$ -orbital collapse in the $2p^44d$ configuration occurs in the isoelectronic Kr— Rb^+ — Sr^{2+} sequence of krypton-like ions.

According to the solid-state classification of electronic excitations, the intense maxima at the threshold of all the spectra under consideration correspond to the so-called x-ray excitons. The energy separation between the L_2 subshell of the cation and the bottom of the conduction band, estimated on the basis of data from x-ray photoelectron and optical spectroscopy, is about 299 eV and 352 eV respectively in potassium and calcium halides. The fact that such excitonic states differ little from the corresponding free-ion states is well understood on the basis of the picture presented above for $3d$ -orbital collapse. The radius of such an orbital (according to the maximum of the charge density distribution) for $Z = 20$ is about 0.6 Å—i.e., about

equal to the radius of the inner $3p$ shell of the ion in the ground state (Ref. 14, p. 31). The $2p-3d$ transition occurs practically within the cation (the ionic radii of K^+ , Ca^{2+} , and Sc^{3+} are respectively 1.3, 1.0, and 0.8 Å). Therefore for such transitions, the situation on the crystal is not much different from the situation in the free ion, and the effect of the environment may be considered as a perturbation (for example, within the framework of ligand field theory). This was confirmed for the $3p$ spectra of K^+ and the $4p$ spectra of Rb^+ in alkali halide compounds.^{22,24} The situation is different in the case of $s-p$ and $p-s$ transitions; in K^+ , for example the $1s-4p$ transition leads to almost a three-fold increase in the ionic radius, and the radius of the excited free ion already exceeds the radius of the cation sphere in the crystal. Solid-state effects are already significant in the corresponding spectra.

The authors thank E. S. Gluskin and A. P. Zhurakovskii for help with the synchrotron radiation experiments, and A.M.-E. Saar for useful discussions.

¹E. Fermi Scientific Works, Part 1 (Russ. transl., Nauka, 1971, p. 298).

²M. Goeppert-Mayer, Phys. Rev. 60, 184 (1941).

³D. C. Griffin, K. L. Andrew, and R. D. Cowan, Phys. Rev. 177, 62 (1969).

⁴A. A. Maiste, R. E. Rusa, S. A. Kuchas, R. I. Karaziya, and M. A. Elango, Zh. Eksp. Teor. Fiz. 78, 941 (1980). [Sov. Phys. JETP 51, 474 (1980)].

⁵S. A. Kuchas and A. B. Karosene, Lit. Fiz. Sbornik 18, 187 (1978).

⁶V. I. Nefedov, Zh. Strukt. Khim. 11, 299 (1970).

⁷T. M. Zimkina and A. S. Vinogradov, J. Phys. (Paris), Colloq. 22, Suppl. 10, C4-278 (1971).

⁸B. Sonntage, J. Phys. (Paris) 39, Suppl. 7, C4-9 (1978).

⁹T. M. Zimkina and V. A. Pomichev, Ul'tramyagkaya rentgenovskaya spektroskopiya (Ultra-soft X-Ray Spectroscopy), Izdat. Leningrad. Univ., Leningrad, 1971, p. 33.

¹⁰A. P. Lukirskii, E. P. Savinov, I. A. Brytov, and Yu. F. Shepelev, Izv. Akad. Nauk SSSR, Ser. Fiz. 28, 866 (1964).

¹¹A. P. Lukirskii and T. M. Zimkina, Izv. Akad. Nauk SSSR, Ser. Fiz. 28, 765 (1964).

¹²V. V. Nemoshkalenko, Yu. N. Romashchenko, V. G. Aleshin, I. A. Brytov, and K. K. Sidorin, Izv. Akad. Nauk SSSR, Ser. Fiz. 38, 626 (1974).

¹³J. A. Bearden and A. F. Burr, Rev. Mod. Phys. 39, 125 (1967).

¹⁴G. V. Samsonov, ed., Svoistva elementov. Spravochnik. Chast' I. (Properties of the Elements. Handbook. Part I), Metallurgiya, 1976.

¹⁵C. E. Moore, Atomic Energy Levels, Vol. 1, U. S. National Bureau of Standards, Circular No. 467, U. S. Government Printing Office, Washington, D. C., 1949-1958.

¹⁶R. Haensel, G. Kettel, N. Kosuch, U. Nielsen, and P. Schreiber, J. Phys. (Paris), Colloq. 32, C4-236 (1971).

¹⁷M. W. Mansfield, Proc. Roy. Soc. Lond. A346, 555 (1975); *ibid.* A348, 143 (1976).

¹⁸F. C. Brown, C. Gahwiler, H. Fujita, A. B. Kunz, W. Scheffley, and N. Carrera, Phys. Rev. B3, 2126 (1970).

¹⁹U. Fano and J. W. Cooper, Spectral Distribution of Atomic Oscillator Strengths, Rev. Mod. Phys. 40, 441-507 (1968) (Russ. transl., Nauka, 1972, p. 66).

²⁰H. Saito, M. Watanabe, A. Ejiri, S. Sato, H. Yamashita, T. Shibaguchi, H. Nishida, and S. Yamaguchi, Solid State Commun. 8, 1861 (1970).

²¹A. M.-E. Saar and M. A. Elango, Fiz. Tverd. Tel. (Leningrad) 13, 3532 (1971). [Sov. Phys. Solid State 13, 2985 (1971)].

²²R. L. Barinskii and I. M. Kulikova, Izv. Akad. Nauk SSSR, Ser. Fiz. 40, 279 (1976).

²³C. Satoko, Solid State Comm. 13, 1851 (1973).

²⁴C. Satoko and S. Sugano, J. Phys. Soc. Japan 34, 701 (1973).

Translated by Cathy Flick

R. V. Vedrinskii, L. A. Bugajev, I. I. Gegusin, V. L. Kraizman, A. A. Novakovich,
S. A. Prosandeev, R. E. Ruus, A. A. Maiste and M. A. Elango,
X-ray absorption near edge structure (XANES) for KCl,
Solid St. Comm. **44**, (1982), pp. 1401–1407.



X-RAY ABSORPTION NEAR EDGE STRUCTURE (XANES) FOR KCl

R.V.Vedrinskii, L.A.Bugaev, I.I.Gegusin, V.L.Kraizman, A.A.Novakovich
and S.A.Prosandeev

Institute of Physics, Rostov State University, Prospekt Stachki 194,
344090 Rostov-on-Don, USSR

R.E.Ruus, A.A.Maiste and M.A.Elango

Institute of Physics, Academy of Sciences of the Estonian SSR, Riia 142,
202400 Tartu, USSR

(Received 15 July 1982 by V.M.Agranovich)

The cluster calculations of K and $L_{2,3}$ edge XANES of K and Cl in KCl within the multiple scattering theory formalism using nonlocal HF potentials with and without consideration of core hole field were performed. For K spectra the influence of the core hole potential is rather weak and the results are similar to those obtained with X_α potentials. For $L_{2,3}$ spectra, particularly for that of K^+ , core hole field leads to a radical redistribution of oscillator strength caused mainly by the spatial rearrangement of d like states. Calculated XANES curves show good over-all agreement with the experimental spectra (the $L_{2,3}$ absorption of K^+ in KCl was measured using the synchrotron radiation of the USSR Academy of Sciences storage ring VEPP-2M in Novosibirsk).

For a number of years X-ray absorption near edge structure (XANES) has been used for probing effective charges /1,2/ and the local environment /3/ of absorbing centres in solids and molecules. Unlike the extended X-ray absorption fine structure (EXAFS) XANES is sensitive not only to the coordination and bond lengths but through multiple scattering of the excited electron also to relative orientations and bond angles of the atoms surrounding the absorbing centre /4/. The extraction of such "local environment" information from XANES, however, seems to be more complicated than from EXAFS. So far theoretists have been mainly concerned with the

task of accurate reproduction of experimental data. In solids the calculations are complicated by the necessity of a proper treatment of band as well as core hole effects.

The crucial aspect of XANES calculations is the sensitivity of computed spectra to different approximations of the potential. In paper /5/ self-consistent- X_α -scattered wave (SC- X_α -SW) cluster calculations of the K spectra of K and Cl in KCl with local "muffin-tin" (MT) potentials were presented. Here we propose a generalization of the SW method to the case of non-local Hartree-Fock (HF) potentials, taking into account the presence of central site core hole

in the final state and using the K and $L_{2,3}$ absorption spectra of KCl for a trial. This generalization turns out to be especially important for $L_{2,3}$ spectra, where the photoabsorption cross section is mainly associated with electron transitions to d states strongly influenced by the effective potential /6/.

It has been shown for KCl /5,7/ that near the bottom of the conduction band the s, p and d partial densities of states, calculated by Xa-SW-method for 3-shell clusters $K_1Cl_6K_{12}Cl_8$ and $Cl_1K_6Cl_{12}K_8$, agree well with those obtained by the APW method. This accordance indicates a weak influence of the extracluster region and justifies the XANES calculation for clusters with central atom core holes. The calculations in /5/ resulted in a good agreement with the measured K spectra of K and Cl but revealed, however, strong discrepancies with $L_{2,3}$ spectra. Later analysis led to a conclusion that the main reason for this failure is the use of Xa approximation for the potentials. It is known /8/ that 2p and 3p electron Xa orbital energies for the third row elements in the case of $\alpha=1$ coincide with ionization energies obtained as differences of total atom-ion HF energies. This means that in the localization region of 2p and 3p orbitals electron self-interaction is effectively compensated by the exchange-correlation part of the potential. Such compensation is unnecessary for free orbitals, so the Xa potential is too strong for states with wave functions deeply penetrating into core region. The situation is illustrated in Fig.1, where Xa potential ($\alpha=1$) for d states in near-resonance energy region of K^+ ion with 2p hole is compared with the effective HF potential calculated by Slater method /8/.

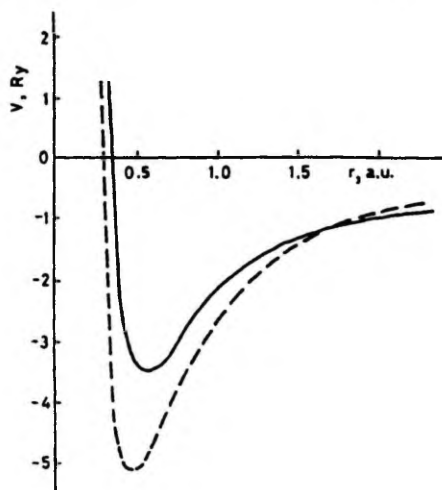


Fig.1. HF (—) and Xa (---) effective potentials for d states of K^+ ion with 2p hole.

The inclusion of HF potentials into the SW XANES calculations implies the following steps: (i) the development of a scheme for constructing the cluster potential on the basis of HF potentials of isolated atoms (ions); (ii) the reformulation of SW method for non-local HF potentials and (iii) the development of a method for including many-electron interactions, which allow the absolute photoabsorption cross-sections in the near edge region to be calculated properly. Such program can be fully realized only for ionic crystals, where the electron densities of neighbouring ions overlap rather weakly and, therefore, the non-locality of the potential can be neglected in the interatomic region. Besides, as the MT approximation applies well to the KCl crystal considered here, it is reasonable to assume the interatomic potential to be constant.

We constructed the cluster potential in the following way. The potential of an ion in an ionic crystal was

taken to differ from that in a free ion by a value of ΔE_1 , which is constant in the volume of the i -th atomic sphere. Consequently, in the MT model of a cluster the logarithmic derivatives of radial solutions for the isolated free ion (taken at the radius equal to that of the corresponding MT sphere) can be used just shifting the energy scale by the value of ΔE_1 . For the ground state cluster ΔE_1 is the corresponding Madelung energy E_M . For the cluster containing an ion with a core hole, ΔE_1 for this ion includes additional polarization term which can be shown to be equal to the twice Mott-Littleton relaxation energy /9/. For other ions of the cluster the presence of a core hole in the central ion was incorporated by adding to ΔE_1 the screened core hole Coulomb potential $-2/\epsilon_\infty r$, ϵ_∞ being the dielectric constant and r the distance from the central ion. The position of the MT zero level for the perfect cluster was chosen in such a way that the calculated energy interval between the bottom of the conduction band and 3p level of Cl should be equal to the experimental band gap (the energy of r_1 state was determined from the KKR calculation performed for the Γ point of the Brillouin zone). For the cluster with the core hole the MT zero level was shifted by the value $-\int_V 2/\epsilon_\infty r d^3r$ (here V is the volume of the interatomic region of the cluster), which approximately reflects the changes of interatomic potential in the vicinity of the absorbing centre. Now, knowing the logarithmic derivatives (found by using the HF program described in /10/) and the position of MT zero level, we were able to calculate the relevant phase shifts and the Green function (GF) of photoelectron.

To check the constructed potential we calculated the binding energies of 1s, 2p and 3p levels of K and

Cl in KCl and found them to coincide with the experimental estimates /11/ within 1 eV.

K and $L_{2,3}$ edge photoabsorption cross-sections were found by using the GF of photoelectrons calculated by the SW method /12/ according to:

$$\sigma_K^v = \frac{1}{3} \delta_{0,1}^v \text{Im} \left\{ \sum_{m=-1}^1 (1 - G_{1m1m}^v S_{11}^v) \right\}, \quad (1)$$

$$\sigma_{L_{2,3}}^v = \delta_{10}^v \text{Im} \{ 1 - G_{0000}^v S_{00}^v \} + \frac{1}{5} \delta_{12}^v \text{Im} \left\{ \sum_{m=-2}^2 (1 - G_{2m2m}^v S_{22}^v) \right\}, \quad (2)$$

where $S_l^v = \exp(2i\delta_l^v)$ is the S matrix for the v th atom of the cluster, $G_{lm lm}^v$ are the GF matrix elements in the "atomic number - orbital momentum" representation, $\delta_{ll'}^v$ is the cross-section for the v th isolated atomic sphere corresponding to the electron transition from ϕ_{nl} core state to the $\psi_{\epsilon l'}$ state of continuum.

A calculation carried out for the K and $L_{2,3}$ absorption spectra of argon atom has shown /13/ that good results

in near edge region may be obtained if the initial- and final-state wave functions are taken in Slater's single determinant approximation. According to /13/ we have computed δ_{11}^v , as follows:

$$\delta_{11}^v = \frac{4\pi^2}{3} \omega a \left| \int \phi_{n1}(r) r \psi_{\epsilon 1}(r) d^3r \right|^2. \quad (3)$$

We must underline that δ_{11}^v is not exactly the free-ion cross-section, because the MT zero level does not coincide with the vacuum level of the free ion.

As usual in the SW method, the GF matrix elements were determined from a set of algebraic equations /12/

$$G_{LL'}^{nn'} = g_{LL'}^{nn'} + \sum_{L''n''} g_{LL''}^{nn''} t_{L''}^{n''} G_{L''L'}^{n''n'} \quad (4)$$

where $g_{LL'}^{nn'}$ are free electron GF expan-

sion coefficients /12,14/ and $t_1^n = -\sin(\delta_1^n) \exp(i\delta_1^n)$ are the t matrix components corresponding to the n th atomic centre. In calculations we used 3 phase shifts ($l = 0, 1, 2$). Expression (4), initially derived for local $X\alpha$ potential, is also valid for the potential used in this paper. The change of potential reflects itself only in the value of the phase shifts.

To fit the experimental data with the theoretical ones the spectra given by expressions (1) and (2) were convoluted with the inverse lifetime of the value Γ chosen in accordance with the core level lifetimes and experimental resolution. L_2 and L_3 components were taken with a statistical ratio 1:2 and the energy shift equal to the spin-orbital splitting of the 2p level.

The values of the parameters used were: MT sphere radii 2.834 a.u. for K and 3.100 a.u. for Cl, $E_M = 8$ eV, Mott-Littleton terms - 1.9 eV for K^+ and 1.5 eV for Cl^- /9/, $\epsilon_\infty = 2.06$. For spin-orbital splittings and core level widths data were taken from /11/.

The results of calculations are presented in Fig.2 together with the experimental X-ray absorption spectra. The $L_{2,3}$ spectrum of K^+ was measured with the resolution of 0.3 eV, using the RSM-500 X-ray monochromator (6 meter radius concave grating, 600 lines per mm) and synchrotron radiation of the VEPP-2M electron-positron storage ring of the Institute of Nuclear Physics in Novosibirsk. Other experimental spectra are taken from papers /11,15/. All spectra are aligned along the energy axis according to the bottom of the conduction band energy (indicated by arrows).

As one can see, XANES, calculated with HF potentials and with the inclusion of the core hole field, agree with the experiment almost in all details. For K spectra the inclusion of

core-hole potential leads only to significant energy shifts and the results are rather close to those obtained with $X\alpha$ potentials /5/. However, for $L_{2,3}$ spectra, particularly for that of K^+ , the core-hole field induces a radical rearrangement of the spectrum leading to a transfer of oscillator strength to the immediate near edge region. General trend of the $L_{2,3}$ spectra of the crystal reflects the "atomic" cross sections σ_{12} (see Fig.2c and 2d), which are strongly modulated by the multiple scattering of electron wave in the crystal potential. The main peaks are associated with d resonances. The strong enhancement of these resonances after switching on the core-hole potential is analogous to the atomic effect of the 3d orbital collapse /6/.

Our calculation performed in one-electron approximation gives the following identification of the near-edge maxima of the spectra. Thus, the peaks A and C of the $L_{2,3}$ spectrum of K^+ correspond to the final states of t_{2g} symmetry, the peaks B and D to e_g symmetry (A and B belong to L_3 series, C and D to L_2 series).

A thorough investigation of theoretical (solid curves) and experimental spectra reveals some discrepancies in energetical positions and relative intensities of the near-edge maxima of the $L_{2,3}$ spectrum of K^+ . This is undoubtedly due to the mixing of one-electron states mainly by spin-orbital interaction and the interactions between 2p hole and d electron, which have not been represented in our scheme of calculation. Consequently, the near-edge region of $L_{2,3}$ spectra of K^+ cannot be reproduced merely by the sum of L_2 and L_3 components with final d states split in the crystal field. To consider better the multiplet near-edge structure of $L_{2,3}$ spectrum of K we computed it also in the localized excita-

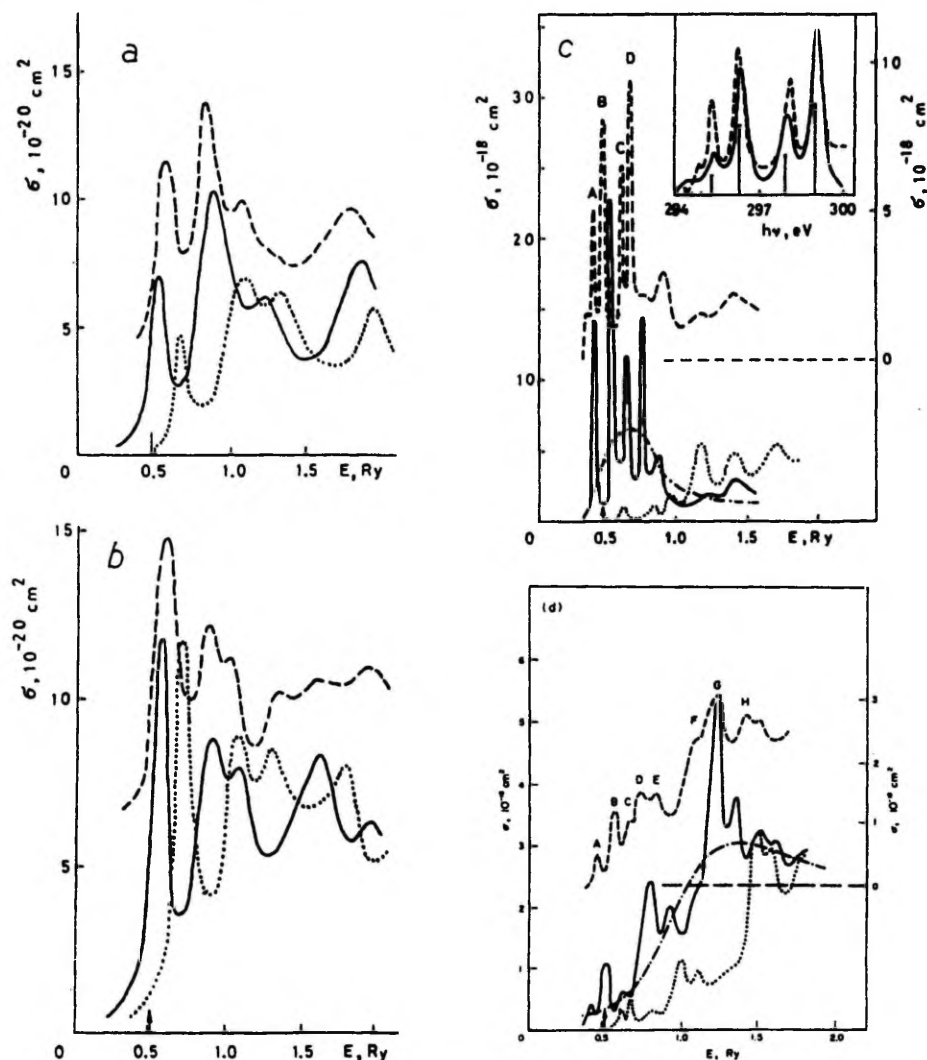


Fig.2. XANES spectra of KCl (a - K edge of potassium, b - K edge of chlorine, c - $L_{2,3}$ edge of potassium, d - $L_{2,3}$ edge of chlorine): experimental photo-absorption spectra (---), HF-SW calculation results with (—) and without (.....) taking into account the presence of core hole. Energies are given relative to MT zero level. Theoretical scales of cross sections are given on the left side, experimental ones (only for $L_{2,3}$ edges) - on the right side. In the Fig.2c and 2d "free ion" cross sections σ_{12} are also shown (----). The insert of Fig.2c gives the results of calculation of 2p-3d,4s transitions for K^+ ion in cubic crystal field ($10 Dq = 0.8$ eV).

tion model, considering the $2p^6-2p^5$ ($3d,4s$) transitions of K^+ ion in the cubic crystal field of KCl. This approach permits a proper account of spin-orbital, full Hartree-Fock exchange interaction as well as s-d mixing. As is known the crystal field approximation has turned out to be effective in explaining near-edge structure in some cation core spectra of ionic crystals, the $M_{2,3}$ spectrum of K in KCl among them /16/. The calculation method was analogous to /16/, except some differences which will be analyzed elsewhere. The results of calculation are shown in the insert of Fig.2c, where solid line shows the theoretical spectrum (convoluted by a Lorentzian of the width of 0.3 eV), the dashed line indicates the experimental one. The computed spectrum reproduces rather well the near edge structure in relative intensities as well as energy intervals between peaks. The computation reveals a large mixing of the $t_{1u}^5 e_g$ and $t_{1u}^5 t_{2g}$ configurations and a negligible role of

$t_{1u}^5 a_{1g}$ configuration in the formation of $L_{2,3}$ spectrum of K. So it is evident that a proper inclusion of many-electron interactions in the SW method is needed. Nevertheless, the mixing of states cannot change the over-all integral intensity of the spectrum. Indeed, the calculated value of $\int \sigma(E) dE$ for the $L_{2,3}$ spectrum of K in the region from 0.35 Ry to 1.25 Ry (see Fig.2c) is 2.55 Mb·Ry, which stands a comparison with the experimental value of 2.2 ± 0.9 Mb·Ry. Naturally, analogous effects of multiplet splitting influence the near edge structure of $L_{2,3}$ spectrum of Cl.

It is worth noting that our calculation confirmed the conclusion of paper /17/ that an important feature of $L_{2,3}$ spectrum of Cl - the rise of absorption at about 9 eV above the edge - is of an essentially "atomic" origin (see the curve δ_{12} on Fig.2d). So there is no need to apply for the much-discussed two-electron excitation, first suggested in /11/.

REFERENCES

1. R.L.Barinskii & V.I.Nefedov, Determination of the effective charges of atoms by the X-ray spectroscopy, Nauka, Moscow (1966).
2. P.A.Lee, P.H.Citrin, P.Eisenberger & B.M.Kincaid, Rev.Mod.Phys. **53**, 769 (1981).
3. S.P.Cramer, H.B.Gray & V.K.Rajakopalan, J.Am.Chem.Soc. **100**, 2772 (1979).
4. P.J.Durham, J.B.Pendry & H.H.Hodges, Solid State Commun. **38**, 159 (1980).
5. R.V.Vedrinskii, I.I.Gegusin, V.N.Datsyuk, A.A.Novakovich & V.L.Kraizman, phys.stat.sol. to be published.
6. A.A.Maiste, R.E.Ruus & M.A.Elango, Zh.eksper.teor.Fiz. **79**, 1671 (1980).
7. I.I.Gegusin, V.N.Datsyuk & R.V.Vedrinskii, phys.stat.sol.(b) **109**, 563 (1982).
8. J.C.Slater, The self-consistent field for molecules and solids, McGraw-Hill, N.-Y. (1974).
9. G.D.Mahan, Phys.Rev. **B21**, 4791 (1980).
10. L.V.Chernysheva & N.A.Cherepkov, Preprint FII-337, A.F.Joffe Physico-Technical Institute of Academy of Sciences of the USSR, Leningrad (1971).
11. T.Sagava, Y.Iguchi et al, Phys.Soc. Japan **21**, 2587 (1966).
12. R.V.Vedrinskii & A.A.Novakovich, Fiz. Metallov i Metallovedenie **39**, 7 (1975).
13. V.L.Sukhorukov, V.F.Demyokhin, V.V.Timoshevskaya & S.V.Lavrent'ev, Opt. i Spektrosk. **47**, 407 (1974).

14. J.M.Ziman, The calculation of Bloch functions, Solid State Phys. 26, 1 (1971).
15. F.C.Brown, C.Gähwiller, H.Fujita, A.B.Kunz, M.Scheifley & N.Carrera, Phys.Rev. B2, 2126 (1970).
16. C.Satoko & S.Sugano, J.Phys.Soc. Japan 34 701 (1973); C.Satoko, Solid State Comm. 13 1851 (1973).
17. A.M.-E.Saar & M.A.Elango, Fiz.tverd. Tela 13, 3532 (1971).

R. E. Ruus, Collapse of the 3d orbital in configurations with a 2p vacancy and its effect on the $2p^6$ - $2p^5nd,ns$ transitions, *Opt. Spektrosk.* **59**, (1985), pp. 745–750 [*Opt. Spectrosc.* **59**, (1985) pp. 450–453] (in Russian).

Collapse of the 3d orbital in configurations with a 2p vacancy and its effect on the $2p^6 \rightarrow 2p^5 nd, ns$ transitions

R. E. Ruus

(Received 6 February 1985)

Opt. Spektrosk. 59, 745-750 (October 1985)

The collapse of the 3d electron in the isoelectronic series of Ar-like ions and in argon has been studied theoretically with various populations of the 3p shell in the presence of a 2p vacancy. In the Hartree-Fock approximation in the intermediate coupling scheme, oscillator strengths in multiplets of $2p^6 \rightarrow 2p^5 nd, ns$ transitions in the argon isoelectronic series have been calculated. It has been shown that after the collapse of the 3d electron (beginning with K^+ and Ar^+), the $2p^6 \rightarrow 2p^5 nd$ transitions dominate and the intensity distribution in the multiplet changes. Multi-electron effects (configuration interaction, relaxation) exert little influence on the oscillator strengths of these transitions.

INTRODUCTION

In Reference 1 on the basis of a comparative analysis of the $L_{2,3}$ absorption and emission spectra of argon-like ions in ionic crystals, the reason for the sharp increase in intensity of near-edge maxima on transition from Ar to K^+ , i.e., collapse [step-like contraction of the radial wave function (RWF)] of the excited 3d orbital has been discovered. The present paper is devoted to a theoretical study of this phenomenon and its effect on transitions from the 2p shell in the isoelectronic series of argon and argon ions. In a series of works, for example Ref. 2, in which the collapse of the 3d electron in configurations with a 3p vacancy and its effect on $3p^6 \rightarrow 3p^5 3d$ transitions have been studied in detail, a strong dependence of the 3d RWF on the term has been discovered. For example in the K^+ ion, the 3d RWF of the singlet 1P term is localized in the external potential well (uncollapsed), and the 3d RWF of the triplet 3P and 3D terms in the internal well (collapsed). However, in calculating excited configurations with a 2p vacancy a series of properties are revealed. First, solution of the Hartree-Fock equations in LS coupling with angular coefficients dependent on the HF_{τ} term, instead of HF equations with coefficients averaged over all HF_{τ} terms, may not, in the case of a configuration with a 2p vacancy, lead to a refinement of the one-electron RWF, since a coupling close to the jj type, is realized. Second, for these configurations the internal potential well is deeper and collapse of the 3d electron occurs more rapidly than for the $3p^5 3d$ configuration. Moreover, collapse of the 3d orbital in argon may even occur in $2p^5 3d^m 3d$ ($n < 6$) con-

figurations, i.e., on decreasing the population (n) of the 3p shell, which leads to a decrease in the effective potential barrier for the 3d electron. This situation may have its principal importance for interpreting the prethreshold structure of $L_{2,3}$ absorption spectra in excimer compounds, where the 3p shell of argon participates in a chemical bond.

In contrast to Ref. 2 in the present paper, the possible role of multielectron effects on the oscillator strengths (OS) of transitions is estimated. One can expect two types of effects. First, the appearance of a vacancy in the internal shell must, in principle, lead to a significant change in the electron wave functions of this and overlying shells, therefore in the case of x-ray spectra one should expect large relaxational or retuning effects (for example, Ref. 3). Second, the closeness in energy of a series of excited s and d states in argon and argon-like ions may lead to significant configuration interaction in the final state, which can also significantly change the intensity distribution in the spectrum.

EFFECT OF COLLAPSE OF THE 3d-ELECTRON RWF ON ATOMIC CHARACTERISTICS

Calculations of configurations with a vacancy in the 2p shell were carried out in Hartree-Fock approximation using a computer program analogous to that presented in Ref. 4.

In Table I values are presented for the mean radius of the nd orbitals \bar{r}_{nd} , the radial integrals of the nonspherical portion of electrostatic interaction $F^2(2p, nd)$ and $G^1(2p, nd)$, the constant of spin-orbit interaction of the nd shell $\eta(nd)$, and of the integrals of dipole transition

TABLE I. Effect of localization of an excited nd electron on atomic values (in a.u., η in eV).

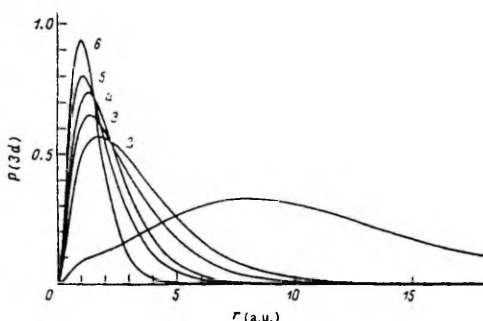
Atom (ion)	Configuration	\bar{r}_{nd}	$G^1(2p, nd)$	$F^2(2p, nd)$	$\eta(2p)$	$\eta(nd)$	$\langle 2p r nd \rangle$
Ar	$2p^5 3d$	0.24	0.00063	0.00235	1.40	0.00012	0.0228
Ar	$2p^5 4d$	18.89	0.00067	0.00152	1.40	0.00009	0.0194
Ar ⁺	$2p^5 3p^5 3d$	2.66	0.0309	0.0552	1.43	0.0044	0.132
Ar ²⁺	$2p^5 3p^5 3d$	1.75	0.0675	0.110	1.50	0.0095	0.194
Ar ³⁺	$2p^5 3d$	1.20	0.163	0.215	1.45	0.021	0.275
K ⁺	$2p^5 3d$	2.13	0.0537	0.0844	1.82	0.0070	0.147
K ⁺	$2p^5 4d$	10.08	0.0469	0.00727	1.82	0.0008	0.0421
Ca ²⁺	$2p^5 3d$	1.49	0.100	0.144	2.33	0.018	0.175
Sc ³⁺	$2p^5 3d$	1.22	0.141	0.192	2.93	0.030	0.185
Ti ⁴⁺	$2p^5 3d$	1.06	0.181	0.237	3.64	0.046	0.187

$\langle 2p|r|nd \rangle$ of a series of excited configurations in argon and argon-like ions. It is obvious that the collapse of the $3d$ electron in the isoelectronic series of argon is set in the K^+ ion, and in a series of argon ions—the Ar^+ ion; in this case r_{3d} varies in a step-like manner by many times, and the electrostatic and spin-orbit interaction of the $3d$ shell by 1 to 2 orders of magnitude.

The weak overlap of the RWF of the $2p$ and uncollapsed nd electrons dictates the small value of the integrals of electrostatic interaction and dipole transition between corresponding states, and the smallness of $\eta(nd)$ indicates the small probability of penetration of the uncollapsed nd electron into the inner region of the atom. The $\eta(2p)$ behaves otherwise, the weak increase of which in the isoelectronic series is governed primarily by the increase in the charge of the nucleus. The fact that in configurations with uncollapsed nd orbitals $\eta(2p)$ significantly exceeds $G^1(2p, nd)$ and $F^2(2p, nd)$ indicates the closeness of the coupling to the jj type. On collapse of the $3d$ electron, the electrostatic pd interaction converges in value with the spin-orbital interaction, and a significant deviation from a pure jj coupling occurs; the coupling acquires an intermediate character. One should note that in calculating the wave functions there is no basis to assume that a more accurate accounting of the electrostatic interaction over the terms in the jj coupling will provide more adequate wave functions, since on calculation, spin-orbit interaction in explicit form is not included in the self-consistent potential (accounting for this involves considerable computational difficulties).

On collapse of the $3d$ electron, significant changes in the RWF of overlying d states are also observed. In particular, on transition from Ar to K^+ , penetration of the first maximum of the $4d$ RWF to the internal potential well occurs.

In Fig. 1 the RWF are presented for the $3d$ electron in a series of excited configurations with a $2p$ vacancy. The contraction of the RWF is clearly visible on transition from Ar to Ar^+ ; this is governed by the dissipation of the positive effective potential barrier. In calculations the dependence of the RWF on the term, governed by Coulomb interaction in the $3p$ shell, was not taken into account, since the effective potential for the $3d$ electron in the $2p^3 3p^4 3d$ configuration is determined primarily by the $2p$ vacancy.



Collapse of the $3d$ orbital in Ar^+ allows us to predict the appearance of intense non-Rydberg near-edge structure in $L_{2,3}$ absorption spectra of Argon in excimer compounds, especially in compounds with halides, where ionic bonding dominates.⁵

EFFECT OF THE COLLAPSE OF THE $3d$ ORBITAL ON $2p^4 \rightarrow 2p^3 nd, n's$ TRANSITIONS

In moving to calculations of OS of electronic transitions one must keep in mind that one-electron RWFs, obtained by taking into account relaxational effects independently for various states and belonging to various series, are not orthonormal. Accounting for this situation leads to complicated expressions for the transition matrix elements, therefore we are limited to calculating $\langle nl|nl' \rangle$ type integrals, which although they differ only slightly from unity, may exert a significant effect on the matrix elements of the dipole transition of a multielectron atom, since they appear in expressions in the form of factors.

Oscillator strengths in single-configuration approximation for the electric dipole transition between the initial $k \equiv [A]nl^N(LSJ)$ and final $m \equiv [A]nl'^N-1n'l'(L'S'J')$ states ($[A]$ denotes the collection of populated shells) were calculated in intermediate type coupling according to a general formula (in the atomic system of units)

$$f(k \rightarrow m) = \frac{2}{3(2J+1)} E_{km} \left| \sum_{ij} a_{ki} a_{mj} U_{ij} Q_{ij} \right|^2, \quad (1)$$

where $E_{km} = E_m - E_k$ is the difference in the overall energies; a_{ki} and a_{mj} are the expansion coefficients of the wave function of intermediate type coupling (indices k and m) over the functions of LS coupling (i and j indices); $D_{ij} \equiv (L, S, J; L', S', J')$ are the angular coefficients of LS coupling, associated with the L, S, J and L', S', J' [Eq. (2,3) in Ref. 6]; $Q_{ij} = Q(L, S; L', S') = \pi_{ij} \langle n_i l_i n_j l_j \rangle$ is the overlap factor (multiplication of the one-electron overlap integrals is carried out over all pairs of electronic terms i and j). The matrix element of dipole transition $s_{ij} \equiv (L, S, J; L', S', J')$ is calculated according to the rate equation

$$s_{ij} = \frac{1}{E_{km}} \int P(n_i l_i) \left(\frac{d}{dr} \pm \frac{2l_i + 1}{2r} \right) P(n_j l_j) dr, \quad (2)$$

where \pm corresponds to $l_j = l_i \pm 1$.

FIG. 1. Radial wave functions of the $3d$ orbital. 1— Ar , 2— Ar^+ , 3— K^+ , 4— Ar^{2+} , 5— Ca^{2+} , 6— Ar^{3+} .

TABLE II. Oscillator strengths (f , increased by a factor of 10^3) of several $2p^6 \rightarrow 2p^5 n l (2s-1 \bar{L}_1)$ transitions, calculated in single-configuration approximation.

Atom (ion)	$n l (2s-1 \bar{L}_1)$	E^*	E_{exp}	f	f^*	f_{exp}
Ar	$4s (1P)$	244.32	244.4	1.99	2.02	3.5
	$4s' (2P)$	246.41	246.5	1.03	1.11	2.0
	$5s (1P)$	246.80	246.9	0.51	0.77	7.0
	$3d (1P)$	246.65		6.42	6.10	
	$4d (1P)$	247.33	247.7	4.71	2.55	4.2
	$6s (1P)$	247.34		0.21	2.05	
	$5s' (2P)$	248.70	249.1	0.26	0.29	5.0
	$3d' (2D)$	248.74		3.44	3.88	
	$4d' (2D)$	249.43	249.8	2.40	2.58	
	$6s' (2P)$	249.44		0.1	0.01	
	$4s (1P)$	296.46	296.4	4.2	9.5	70
	$3d (2D)$	298.21		250	249	
K ⁺	$4s' (2P)$	299.17	299.2	2.3	0.9	80
	$3d' (1P)$	300.75		320	318	
	$5s (1P)$	302.44	303.8	1.6	0.3	
	$4d (1P)$	303.35		29.8	30.1	
	$5s' (2P)$	305.15		0.8	0.4	
	$4d' (2D)$	306.08		16.4	16.3	
Ca ²⁺	$3d (2D)$	350.57	349.1	319	419	110
	$4s (1P)$	353.45	352.3	6	117	170
	$3d' (1P)$	354.05		664	550	
	$4s' (2P)$	356.96		3.3	2.4	
Sc ³⁺	$3d (2D)$	405.88		359	363	
	$3d' (1P)$	410.30		919	924	
	$4s (1P)$	415.88		7.4	7.5	
	$4s' (2P)$	420.20		4.1	1.6	
Ti ⁴⁺	$3d (2D)$	464.85		411	404	
	$3d' (1P)$	470.46		1115	1119	
	$4s (1P)$	483.20		8.9	3.0	
	$4s' (2P)$	488.57		4.7	2.4	

Note: f^* takes into account configuration interaction; E^* is the transition energy in eV (results for Ca²⁺ are in Hartree-Fock-Pauli approximation).

Equation (1) differs from the standard expression by the presence of the overlap coefficient Q_{ij} , using which, in the first approximation, the relaxation of the core can be taken into account. Use of the rate formula is associated with the fact that it is preferred when calculating transitions from deep levels. The calculation indicated that the OS, calculated according to the rate and length formulas, in the case of transitions to uncoupled states, differ by $<15\%$, and for the case of collapsed states practically coincide.

The results of the calculation are presented in Table II. For the $2p^3 3d$ configuration in the case of collapsing states (in K⁺, Ca²⁺, Sc³⁺, and Ti⁴⁺ ions), the OS are two orders of magnitude greater than in the case of noncollapsing states (Ar). The intensity of the $2p \rightarrow 4s$ transitions increase only by several times, their influence on the formation of near-edge structure of the $L_{2,3}$ absorption spectrum in argon-like ions is insignificant. Due to strongly varying values of pd interaction on collapse, the position of the levels changes and a redistribution of the transition intensities in the multiplets occurs. On transition to uncoupled states, the ratio of the OS $f(2p \rightarrow nl)/f(2p \rightarrow n'l')$ is 2 to 3, i.e., it corresponds to an approximately statistical intensity distribution under $j j$ coupling. For the collapsed $3d$ orbital, both components of the multiplet in K⁺ have approximately the same intensity. On collapse the ratio $f(2p \rightarrow nd)/f(2d \rightarrow 3d)$ also decreases for $n > 4$. The relatively high values of the OS for the $2p \rightarrow 4d$ transitions in K⁺ are explained by the penetration of the first maximum of the $4d$ RWF into the internal potential well.

Incorporating relaxation of the core decreases the oscillator strengths on the average by 10–20%. This supports the notion that one must account for relaxation effects in calculating OS for transitions from $2p$ or deeper shells. One should note that in the case of transitions from the $3p$ shells, the decrease in relaxation of the OS is only $\sim 0.1\%$, and therefore can be neglected.

The closeness in energy of the excited s and d states in argon and argon-like ions raises the question of the influence of configuration interaction (CI) on the intensity distribution in the spectrum. We studied the influence of the close $2p^3 ns$ and $2p^3 n'd$ configurations on the OS distribution by a method of superimposing the configurations (results in Table II). It turned out that in the majority of cases the effect of CI is insignificant due to the smallness of the interconfiguration integrals of Coulomb interaction. The exceptions are transitions to excited states of the $2p^3 4s$ configuration in K⁺ and Ca²⁺, where accounting for CI leads to a significant increase in OS. This is caused by the sharp increase in pd interaction on collapse of the $3d$ electron, which leads to a redistribution of the OS of transitions between states of the $2p^3 3d$ and $2p^3 4s$ configurations.

Configuration interaction exerts an especially strong influence on the OS of transitions to adjacent $2p^3 3d (1\bar{P}_1)$ and $2p^3 4s (1\bar{P}_1)$ levels in the Ca²⁺ ion. Accounting for relativistic corrections in Hartree-Fock-Pauli approximation also significantly changes the position of these levels and the distribution of OS, therefore one can assume that further

refinement in the calculation of relativistic and correlational corrections may introduce quite a large change in the OS values of transitions to these levels.

In Table II empirical estimates of OS are also presented for a series of transitions, determined using the formula $f_{exp} = 9.11 \times 10^{-3} \int \sigma(E) dE$ [where $\sigma(E)$ is the partial cross section of photoabsorption (in Mb) by electrons of the $2p$ shell in the portion of the spectrum corresponding to the transition under consideration], on the basis of experimental argon⁷ and potassium and calcium¹ spectra. For Ar the calculated and experimental values agree within the accuracy limits of the experiment. In the case of K^+ and Ca^{2+} , where in view of the absence of spectral measurements of free ions, spectra of these ions in ionic crystals were used (this is justified in the case of collapsed excited states^{1,8}), the experimental OS and transition energies differ somewhat from the calculated values, although the relative intensity distribution in the multiplet coincides. These differences may be caused by the inaccuracy in the empirical estimates as well as the approximation used to calculate the one-electron RWF of the free ions. On collapse, as was indicated above, there is a strong dependence of $3d$ RWF on the potential, and a relatively small change in the wave functions, in turn, strongly affects the calculated OS, therefore the agreement between the experimental and theoretical data can also

be considered completely acceptable for the K^+ and Ca^{2+} case. Nevertheless in view of the increased sensitivity of the calculated OS of the transitions to collapsing orbitals, it is necessary to further refine the theoretical model in particular by including spin-orbit interaction to the self-consistent potential for calculating the one-electron RWF and to account more accurately for correlational and relativistic effects.

In conclusion the author wishes to thank M. A. Elango and A. A. Maiste for their helpful comments.

¹A. A. Maiste, R. E. Ruus, and M. A. Elango, *Zh. Eksp. Teor. Fiz.* 79, 1671 (1980) [*Sov. Phys. JETP* 52, 844 (1980)].

²J. E. Hansen, *J. Phys. B* 5, 1083 (1972); S. A. Kuchas and A. V. Karosene, *Litov. Fiz. Sb.* 18, 187 (1978).

³A. D. Sukhorukov, *Opt. Spektrosk.* 47, 407 (1979) [*Opt. Spectrosc. (USSR)* 47, 228 (1979)].

⁴P. O. Bogdanovich, *Programs for Atomic Calculations* (Vilnius, 1978).

⁵B. M. Smirnov, *Usp. Fiz. Nauk* 139, 53 (1983) [*Sov. Phys. Usp.* 26, 31 (1983)].

⁶A. P. Yutsis, Ya. I. Vizbapaitė, and R. I. Karaziya, *Litov. Fiz. Sb.* 8, 551 (1968).

⁷R. Haensel, G. Keitel, D. Kosuch, U. Nielsen, and P. Schreiber, *J. Phys. (Paris)* 32, C4-236 (1971).

⁸R. V. Vedrinskii, P. A. Bugaev, I. I. Gegusin, V. L. Kraizman, A. A. Novakovich, S. A. Prosandeev, R. E. Ruus, A. A. Maiste, and M. A. Elango, *Solid State Commun.* 44, 1401 (1982).

M. Elango, A. Ausmees, A. Kikas, E. Nõmmiste, R. Ruus, A. Saar, J. F. van Acker,
J. N. Andersen, R. Nyholm and I. Martinson, Autoionization phenomena involving
the $2p^53d$ configuration of argon-like ions in ionic solids,
Phys. Rev. B, **47**, (1993), pp. 11736–11748.

Autoionization phenomena involving the $2p^5 3d$ configuration of argonlike ions in ionic solids

M. Elango, A. Ausmees, A. Kikas, E. Nõmmiste, R. Ruus, and A. Saar
Institute of Physics, Estonian Academy of Sciences, Riia 142, EE2400 Tartu, Estonia

J. F. van Acker, J. N. Andersen, and R. Nyholm
Department of Synchrotron Radiation Research, Lund University, Sölvegatan 14, S-223 62 Lund, Sweden

I. Martinson
Department of Atomic Spectroscopy, Lund University, Sölvegatan 14, S-223 62 Lund, Sweden
 (Received 4 August 1992)

The photon-induced Auger and photoelectron spectra of the argonlike ions Cl^- (in NaCl), K^+ (in KCl), Ca^{2+} (in CaCl_2 and CaF_2), and Sc^{3+} (in Sc_2O_3) have been measured in the vicinity of the L_{23} absorption edges of these ions. It is shown that at the $2p^6 \rightarrow 2p^5 3d(4s)$ resonance a spectator structure appears in the $L_{23}M_{23}M_{23}$ Auger spectra, which shifts to higher kinetic energies with increasing photon energy. This structure originates from the $3p^{-1}3d(4s)$ final configuration arising as a product of the Auger resonant-inelastic-scattering process of the incident photons. We demonstrate that the peculiarities of this process and the role of the collapsing $3d$ electron in it can be largely understood in terms of an atomic treatment. The solid-state effects, caused by the crystal field and the lattice polarization, may play an additional role.

I. INTRODUCTION

The Auger spectra, photoexcited in the regions of inner-shell ionization threshold of atoms, molecules, and solids provide sensitive probes for the dynamics of inner-shell transitions.¹ In such an excitation the creation and the decay of the inner-shell hole cannot in principle be considered as separate processes, and interesting phenomena like resonant scattering and postcollision interaction (PCI) occur (see, e.g., a recent review²).

Here we present the results of a study of these phenomena in the case of resonant photoionization of the $2p^6$ shell of the argonlike ions Cl^- , K^+ , Ca^{2+} , and Sc^{3+} in ionic solids. The photoabsorption may be described here as a transition $2p^6 \rightarrow 2p^5 3d(4s)$ in the particular ion, possibly modified by the crystal field. The important point is that the final configuration $3d$ shell collapses (i.e., its radial wave function suddenly contracts) in the sequence $\text{Cl}^- \rightarrow \text{Ar} \rightarrow \text{K}^+$, as shown by means of the absorption and emission studies of Ref. 3. We anticipated observing the results of this collapse in the relevant Auger spectra, and in this way obtaining new information on the effect of the presence of an excited $3d$ electron on the decay dynamics of the $2p$ hole.

It turned out that in all cases studied here the photo-creation of the $2p^6 \rightarrow 2p^5 3d(4s)$ resonance gives rise to new structures in the photoemission spectrum. One conspicuous structure is situated in the region of the normal $L_{23}M_{23}M_{23}$ Auger spectrum, but differs from it in two important aspects: it is excitable only at the resonance photon energies and it shifts to higher kinetic energies when the photon energy increases in the resonance region. It follows from empirical considerations and atomic calculations that this structure originates from the $3p^{-1}3d(4s)$ final configuration. In a fully consistent pic-

ture the whole process should be described as a single Auger resonant inelastic scattering event. However, we show that to a good approximation it may be treated as a two-step process: the resonant photoexcitation followed by the $3d(4s)$ spectator-affected $L_{23}M_{23}M_{23}$ Auger decay of the $2p$ hole. We also present evidence that shake processes do not contribute to the formation of the final configuration due to the collapse of the $3d$ shell in the configuration $2p^5 3d$ of K^+ , Ca^{2+} , and Sc^{3+} .

Details of the experimental procedure are presented in Sec. II. Section III deals with the theoretical background and our treatment of the two-step approach. A general interpretation of the experimental results is given in Sec. IV, while a more detailed discussion of the autoionization process and a detailed comparison with theoretical calculations in the case of KCl is given in Sec. V. We separately discuss shake probabilities in Sec. VI, and summarize our main conclusions in Sec. VII.

II. EXPERIMENTAL

The experiments were carried out using synchrotron radiation from beamline 22 at MAX-Laboratory, Lund University, Sweden.⁴ The monochromator was a modified SX-700 plane-grating monochromator, with energy resolution better than 0.3 eV in the 200- to 400-eV-photon energy region. The absorption spectra were recorded by detecting the total electron yield. For the absolute calibration of the photon energy, we have taken advantage of the radiation in second order diffraction from the monochromator. At the photon energy at which the absorption edge occurs two measurements of a photoemission core level are performed, one with the use of first-order light, and one using second-order light. The difference in kinetic energy for the photoelectron peak in these two

spectra is equal to the photon energy at the absorption edge.

The samples were films of NaCl, KCl, CaF_2 , CaCl_2 , and Sc_2O_3 , all but Sc_2O_3 prepared by thermal evaporation *in situ* from a molybdenum boat onto polished copper substrates in a vacuum of 5×10^{-7} Torr. The Sc_2O_3 film was prepared elsewhere by electron beam evaporation. The film thickness (about 200 Å and the evaporation rate (several Å/s) were controlled by a quartz crystal monitor. The vacuum in the experimental chamber was 2×10^{-10} Torr. No sample charging effects greater than 0.1 eV were observed in the experiments.

The electron energy spectra were recorded by means of a hemispherical electron energy analyzer (Scienta ESCA SES-200). A typical electron energy resolution was set to 0.15 eV. The binding energy scales for the different compounds are given so that zero binding energy corresponds to the bottom of the conduction band. This was achieved by measuring all photoemission binding energies with respect to the top of the valence band and then adding the band-gap energies [8.5 eV for NaCl,⁵ 8.4 eV for KCl,⁵ 6.9 eV for CaCl_2 ,⁶ 12.1 eV for CaF_2 ,⁷ and 6.0 eV for Sc_2O_3 (Ref. 8)] to the measured values.

III. COMPUTATIONS

In terms of a two-step approach the resonant Auger emission intensity can be given as

$$I(E, h\nu) \sim \sum_{if} A(h\nu_i - h\nu) B(E_{if} - E). \quad (1)$$

Here E is the Auger energy and $h\nu$ is the photon energy; i refers to the intermediate state and f to the final state. $A(h\nu_i - h\nu) = \sigma_i L(h\nu_i - h\nu)$ is the population of the excited $2p^3d$ ($4s$) configuration, σ_i is the photoexcitation cross section (from the ground state to the state i), and $L(h\nu_i - h\nu)$ is a line profile which includes the mono-

chromator resolution, total Auger decay width and solid-state broadening.⁹ $B(E_{if} - E) = W_{if} G(E_{if} - E)$ is the Auger energy distribution curve, where W_{if} is the Auger decay rate and $G(E_{if} - E)$ represents a line profile which in principle should include the experimental broadening, the Auger decay width, and also a phonon contribution.¹⁰ In the following we have represented this line profile by a Lorentzian. For the photoionized $2p^5$ intermediate configuration of the normal Auger process we have assumed that the intermediate levels i are uniformly populated with a statistical weight of $2J_i + 1$ (J_i is the total quantum number for the state i).

The Auger transition rate from the intermediate state i to the final ionic state f with continuum wave functions $|\epsilon l j\rangle$ normalized to represent one ejected electron per unit time is for the atomic case¹¹

$$W_{if} = \sum_j \left| \sum_{\mu} \sum_{\mu'} C_{i\mu} C_{f\mu'} \langle \gamma' L' S' J' \epsilon l j | \sum_{\alpha < \beta} 1/r_{\alpha\beta} | \gamma L S J \rangle \right|^2, \quad (2)$$

where L, S, J (or L', S', J') are the orbital, spin, and total quantum numbers of the intermediate (or final ionic) state of the ion (γ and γ' includes whatever other quantum numbers are required). $C_{i\mu}$ and $C_{f\mu'}$ are mixing coefficients for the states i and f in the intermediate coupling scheme. In intermediate coupling the spin-orbit interaction is treated as a perturbation which couples different states $|SLJ\rangle$ with the same J , constructed as zero-order wave functions in LS coupling. The total angular momenta J' and j of the final ionic states and the continuum electron, respectively, are recoupled in the final state of the system. The transition matrix elements in Eq. (2) can be evaluated by using the Jj - LS unitary transformation. Then

$$\langle \gamma' L' S' J' \epsilon l j | \sum_{\alpha < \beta} 1/r_{\alpha\beta} | \gamma L S J \rangle = [(2L+1)(2S+1)(2j+1)(2J'+1)]^{1/2} \begin{Bmatrix} L' & l & L \\ J' & j & J \end{Bmatrix} \begin{Bmatrix} L' & \frac{1}{2} & S \\ J' & \frac{1}{2} & J \end{Bmatrix} \langle \gamma' L' S' \epsilon l J S J' | \sum_{\alpha < \beta} 1/r_{\alpha\beta} | \gamma L S J \rangle, \quad (3)$$

In the configuration interaction approach we used the wave functions for each state written as a linear combination of basis wave functions, each of which represents a particular single-configuration state in the LS coupling scheme. For the determination of the Auger decay of the $2p^3d$ excited state only the most important final configurations $3s^2 3p^4 3d$, $3s^2 3p^4 4s$, and $3s 3p^6$ are included in the configuration interaction calculations. The necessary calculations for the various atomic configurations of the ions are performed using a self-consistent-field procedure within the nonrelativistic single-electron Hartree-Fock-Pauli (HFP) approximation.¹² This approximation uses the radial wave func-

tions of the zero-order Hartree-Fock (HF) Hamiltonian and takes into account the relativistic effects as corrections of the order α^2 (α is the fine structure constant). The matrix elements for the Coulomb and spin-orbit interaction are calculated using the HF radial wave functions and the matrix is diagonalized to yield eigenvalues and eigenvectors. The term-dependent effects in the energy level structures are expected to be small and therefore the configuration-average HF method is used. The continuum wave functions ϵl are generated by solving the HF equations corresponding to the final ionic states. The energy dependence and the term dependence for the continuum wave functions are found to be small and so the

averaged transition energy and the configuration-averaged coefficients of the final states are used.

The photoexcitation cross sections σ_i for the $2p^5 3d$ excited states of the argonlike ions K^+ and Ca^{2+} from the $J=0$ ground state to a state $J=1$ are computed using the dipole transition operator in the "length form." The resultant branching ratios are quite different from the statistical 2:1 ratio which indicates a quite strong deviation from the jj -coupling scheme. In the coupling conditions of the $2p^5 3d$ excited states the spin-orbit coupling of the $2p$ hole is the strongest interaction. The spin-orbit interaction of the collapsed $3d$ electron is weaker than its electrostatic interaction with the core hole. This points out that in the case of the $2p^5 3d$ excited states the coupling scheme is near to a JK coupling scheme.¹¹

To obtain the electronic wave functions for the ions in the crystals we have used the HFP approximation in conjunction with the Watson sphere model.¹³ In this model, the influence of the solid matrix on the electrons of an ion is simulated by superimposing on the potential of the free ion an additional potential due to a hollow sphere with charge $-Q=(Z-N)e$ and an appropriately chosen depth V_c or radius R of this potential well. Thus, the Hamiltonian in the crystal in this model is given by

$$H_{cr} = H_0 + \sum_{i=1}^N V(r), \quad (4)$$

where H_0 is the Hamiltonian for a free ion with nuclear charge Ze and N electrons and

$$V(r) = \begin{cases} V_c = Qe/R & \text{for } r \leq R, \\ Qe/r & \text{for } r > R. \end{cases} \quad (5)$$

We used values of V_c equal to the Madelung energies of the crystals (for KCl, for example, this is 8.00 eV and for CaF_2 19.98 eV).

When a photoelectron or an Auger electron is ejected, the medium responds by polarization, which decreases the total energy of the final state left behind by the extra-atomic relaxation energy E_p .¹⁴ We computed the binding and Auger energies in the crystals as $E_B = E_0 - E_p$ for the photoelectron binding energies, $E_A^* = E_0 + E_p$ for the Auger energies of the excited (nonionized) initial states, and $E_A = E_0 + 3E_p$ for the Auger energies of the ionized initial states (two final hole states). Here E_0 is the difference of the total energies of initial and final states of the ions in the Watson sphere. For E_p we used the values estimated for NaCl (1.58 eV) and KCl (1.97 eV) in Ref. 15 and for CaF_2 (1.73 eV) in Ref. 16. Because the ionicity of Sc_2O_3 is considerably less than for other compounds studied here, our model is not appreciable in this case.

IV. RESULTS AND GENERAL DISCUSSION

In Figs. 1(a)–1(e) we show the total electron yield spectra for NaCl, KCl, CaF_2 , $CaCl_2$, and Sc_2O_3 in the vicinity of the Cl, K, Ca, and Sc L_{23} absorption edges. They agree well with the corresponding absorption spectra^{3,9,17} and have been fully explained in previous studies, on an atomic as well as on a solid-state level.^{9,18,19} The main

maxima of these spectra are due to transitions into states related to $2p^3(3s^2 3p^6)ns$ and $2p^3(3s^2 3p^6)nd$ configurations of the ions, the latter being strongly dominant. They are accompanied by resonant emission bands, which indicates that the arising final states are well-localized atomiclike states.³ For KCl, CaF_2 , $CaCl_2$, and Sc_2O_3 the four strongest bands correspond to the collapsed $2p^3(3s^2 3p^6)3d$ configuration in the solid state and in a first approximation they reflect the spin-orbit splitting (by about 2.7 eV for K, 3.4 eV for Ca, and 4.5 eV for Sc) of the $2p^5$ shell and the $e_g - t_{2g}$ crystal field splitting

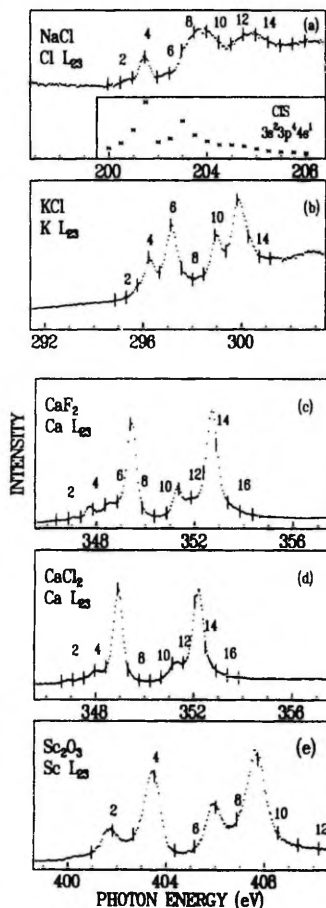


FIG. 1. L_{23} edges for NaCl (a), KCl (b), CaF_2 (c), $CaCl_2$ (d), and Sc_2O_3 (e). The numbered vertical bars show the photon energies used to induce the electron spectra in Figs. 2–6. The inset in Fig. (a) shows the CIS spectrum for the Cl $3p \rightarrow 2s$ final state.

(by about 1 eV for KCl, 1.5 eV for CaCl_2 and CaF_2 , and 2 eV for Sc_2O_3) of the $3d$ orbital. The widths of the bands have a significant phonon contribution.^{9,19} In the compounds considered here the crystal field has opposite signs for K^+ and Ca^{2+} in CaF_2 and as a consequence the lowest-energy component of the $3d$ orbital has t_{2g} symmetry in the case of K^+ and e_g symmetry in the case of Ca^{2+} .

In the $2p^5(3s^2 3p^6)3d$ configuration of the Cl^- ion the $3d$ orbital is not collapsed³ and the transitions to the d -like continuum start at photon energies around 205–210 eV.²⁰ It is generally accepted²¹ that the near-edge structure of the $\text{Cl}^- L_{23}$ absorption spectra just above 200 eV originates from the transitions $2p^6 \rightarrow 2p^5 4s$. The spin-orbit splitting of the $2p^5$ shell of Cl^- is about 1.6 eV.^{17,20}

In Figs. 2–6 the photoemission spectra of NaCl , KCl , CaCl_2 , CaF_2 , and Sc_2O_3 , induced by photons with different energies in the vicinity of the L_{23} absorption edges, are shown. For each compound the photoemission spectra were taken at fixed photon energy steps throughout the L_{23} edge (see Fig. 1) and subsequently normalized for photon flux. For CaF_2 and KCl the spectra are comparable to those obtained earlier.^{22,23}

In general, all structures in these spectra, excluding the

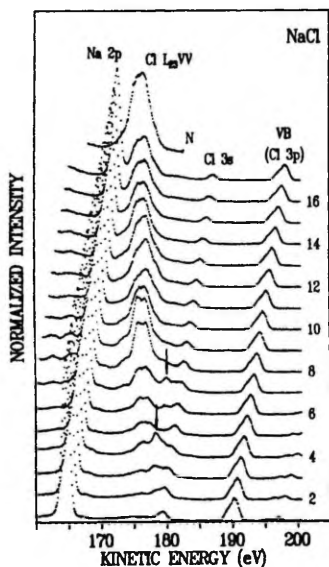


FIG. 2. Photoemission spectra for NaCl . The number at each spectrum corresponds to the vertical bar with the same number in Fig. 1 and shows the photon energy used. The spectra are normalized to equal photon flux. The energy levels and corresponding Auger transitions are indicated for most of the structures. The arrows indicate the spectator-induced structure in the Auger spectra. V stands for the valence band. N denotes the normal Auger spectrum excited by 220-eV photons.

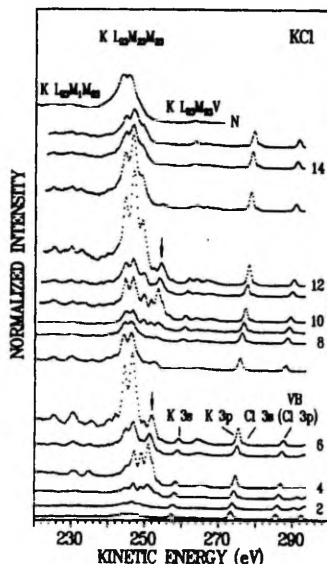


FIG. 3. The same as Fig. 2 for KCl . The normal Auger spectrum is excited by 400-eV photons.

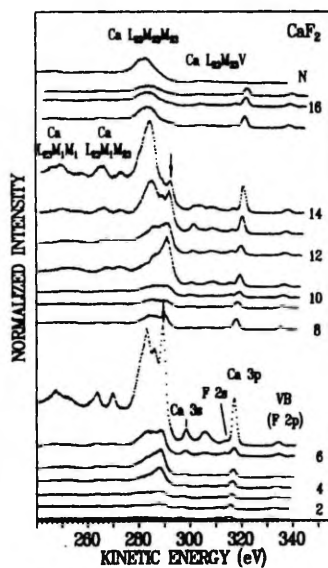


FIG. 4. The same as Fig. 2 for CaF_2 . The normal Auger spectrum is excited by 400-eV photons.

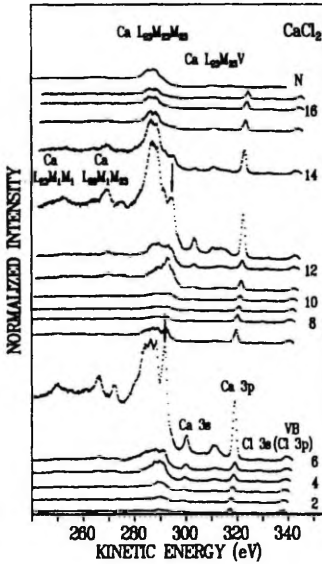


FIG. 5. The same as Fig. 2 for CaCl_2 . The normal Auger spectrum is excited by 400-eV photons.

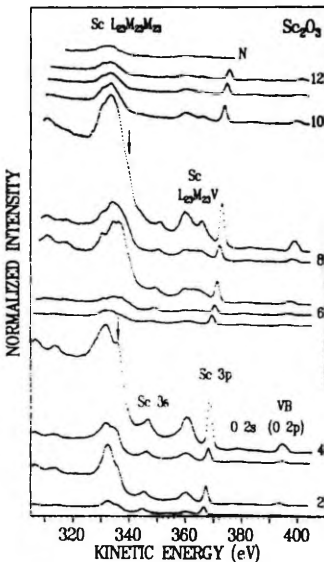


FIG. 6. The same as Fig. 2 for Sc_2O_3 . The normal Auger spectrum is excited by 450-eV photons.

weak lines with energies exceeding the energies of valence electrons and which originate from the $2p$ electrons excited by second-order photons,²⁴ may be divided into two categories.

The first category consists of photoemission peaks originating from the photoionization of different energy levels of the crystal ions. The kinetic energies of these lines E_k vary linearly with photon energy $h\nu$ so that $E_k = h\nu - E_B$, E_B being the binding energy of the electron level. If the photon energy coincides with the $2p^6 \rightarrow 2p^5 3d$ absorption edge of K^+ , Ca^{2+} , and Sc^{3+} the $3s$ and $3p$ photoemission peaks of these ions exhibit a resonant enhancement. This phenomenon is known as the participator effect of the excited ($3d$) electron and is due to its participation in the Auger decay channels $L_{23}M_{23}M_{45}$ and $L_{23}M_{11}M_{45}$ of the configuration $2p^2 3s^2 3p^6 3d$. At the resonant photon energies the final states created by either one of these Auger channels or by $3p$ and $3s$ direct photoionization become indistinguishable which leads to interference and in general a large enhancement of the $3p$ and $3s$ intensities in the electron

TABLE I. Experimental (E_B) and calculated (E_B^h) binding energies (in eV). E_B values are related to the maxima of the corresponding photoelectron lines referred to the bottom of the conduction band.

NaCl			
Ion	Level	E_B	E_B^h
Cl	3p	10.2	9.2
Cl	3s	20.8	24.8
Na	2p _{3/2}		34.2
		35.3	
	2p _{1/2}		34.3
Cl	2p _{3/2}	203.1	203.0
	2p _{1/2}	204.7	204.6
KCl			
Ion	Level	E_B	E_B^h
Cl	3p	9.6	8.7
Cl	3s	20.2	24.2
K	3p _{3/2}		20.6
		21.8	
	3p _{1/2}		20.8
K	3s	37.9	42.5
Cl	2p _{3/2}	202.9	202.5
	2p _{1/2}	204.5	204.1
K	2p _{3/2}	297.7	297.7
	2p _{1/2}	300.5	300.4
CaF ₂			
Ion	Level	E_B	E_B^h
F	2p	14.8	9.5
Ca	3p _{3/2}		28.2
		31.8	
	3p _{1/2}		28.5
F	2s	35.8	33.5
Ca	3s	50.7	53.2
Ca	2p _{3/2}	353.3	352.6
	2p _{1/2}	356.6	356.1

spectra.²⁵ The existence of such a participator enhancement is another indication of the $3d$ electron being localized in the parent ion, because such a localization is a necessity if participator Auger channels $L_{23}M_1M_{45}$ and $L_{23}M_{23}M_{45}$ are to have a significant intensity.

In Table I the experimental and computed values of E_B as explained in Sec. III are presented for NaCl, KCl, and CaF₂ crystals. The overall good agreement of the theoretical and experimental values testifies that a simple model correctly accounts for the polarization effects connected with the photoionization of atoms in ionic solids. The minor discord in the cases of the levels of s symmetry is due to strong collective effects in the ionization of these levels, not taken into account in our computational procedure.²⁶

The second category of structures in Figs. 2–6 are the Auger electron peaks. All the spectra are dominated by strong $L_{23}M_{23}M_{23}$ Auger lines situated at 170–180 eV for Cl, 240–250 eV for K, 280–295 eV for Ca, and 325–340 eV for Sc. The weaker $L_{23}M_{23}V$ (V denotes the valence band), $L_{23}M_1M_{23}$ (for K and Ca) and $L_{23}M_1M_1$ (for Ca) Auger lines are also seen. The calculated normal Auger energies, shown in Table II excellently coincide with the measured ones for the $L_{23}M_{23}M_{23}$ case. In Fig. 7 we compare the full calculated K $L_{23}M_{23}M_{23}$ Auger spectrum of KCl with the spectral data. Note that no additional alignment of theoretical and experimental results has been performed. Except for a deviation in the relative intensities of the two most intense Auger bands the agreement is quite good.

The most striking effect seen in Figs. 2–6 is that small changes of the energy of the exciting photons in the regions of the $2p^6 \rightarrow 2p^3 3d$ resonance lead to drastic changes in the $L_{23}M_{23}M_{23}$ Auger spectra both in shape and intensity. Taking the normal Auger $L_{23}M_{23}M_{23}$ spectra as references these changes may be described as new structures appearing on the high-energy side. With increasing photon energy this so-called spectator struc-

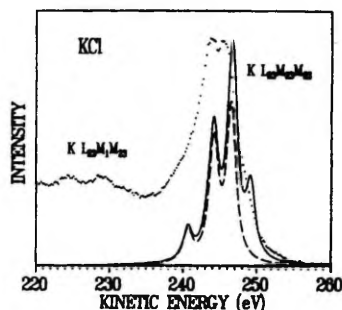


FIG. 7. The normal Auger spectrum for KCl, excited by 400-eV photons, and the calculated $K^+ L_{23}M_{23}M_{23}$ Auger spectrum (solid line), broadened with a Lorentzian of 1.5 eV FWHM. The dashed line shows the $L_{23}M_{23}M_{23}$ structure.

ture shifts to higher energies.

Generally speaking, these changes of the Auger spectra at the resonant excitation may be considered as a result of the spectator role of the excited $3d$ electron in the $L_{23}M_{23}M_{23}$ Auger transition in which it does not participate directly. Similar effects have been observed earlier for several atoms, molecules and solids (see, e.g., Ref. 1). They are due to screening by the excited (here $3d$) electron of the escaping Auger electron from the two-hole final state (here $3p^{-2}$). It turns out, however, that the spectator feature shifts with photon energy which is a comparatively novel finding. Something similar was found earlier for the $L_2M_4M_5$ (1G_4) Auger spectrum of Xe atoms^{27,28} and the $M_{23}M_{45}M_{45}$ Auger spectrum of solid Ge.²⁹ In general terms such an effect means that the Auger transition is so fast that at resonant photon ener-

TABLE II. Experimental (E_A) and calculated (E_A^h) Auger energies for the main LMM Auger transitions. Γ is the calculated partial width (in eV).

Assignment	Cl (NaCl)			K (KCl)			Ca (CaF ₂)		
	E_A	E_A^h	Γ	E_A	E_A^h	Γ	E_A	E_A^h	Γ
$L_1M_{23}M_{23}(^1D_2)$		176.4		244	244.1			281.1	
$L_1M_{23}M_{23}(^3P_2)$	176	178.2	0.12		246.6	0.18	283	283.0	0.21
				246					
$L_2M_{23}M_{23}(^1D_2)$		178.0			246.9			284.6	
$L_1M_1M_{23}(^1P_1)$					217.6			251.1	
				224			258		
$L_2M_1M_{23}(^1P_1)$					220.4			254.6	
						0.049			0.055
$L_3M_1M_{23}(^3P_2)$					226.5			260.9	
				229			265		
$L_2M_1M_{23}(^3P_1)$					229.0			264.1	
$L_3M_1M_1(^1S_0)$					199.4			230.3	
						0.0013			0.0016
$L_2M_1M_1(^1S_0)$					202.1			233.8	

gies it is not possible to separate it from the photon absorption. Both processes together should then be considered as a single Auger resonant inelastic scattering event, a transition from the "ground-state ion (atom) + resonance photon" initial state to the "excited and ionized ion (atom) + escaping electron" final state.^{2,28} The final-state ionic configuration has definite energy and long lifetime and is prepared faster than the "Auger" electron which leaves the ion carrying with it the excess photon energy. The atom remembers how it was excited and communicates this to us through the energy of the outgoing electron.

V. THE AUTOIONIZATION PROCESS

After the general points mentioned in the preceding section we will now deal with the peculiarities of each ion in a more detailed discussion of the resonant $L_{23}M_{23}M_{23}$ Auger spectra. We will compare the experimental results with theoretical calculations, and in order to follow the collapse of the $3d$ wave function we will deal successively with Cl^- in NaCl , K^+ in KCl , Ca^{2+} in CaF_2 and CaCl_2 , and Sc^{3+} in Sc_2O_3 . As will become clear, the comparison with theory proves to be particularly enlightening for K^+ in KCl . This subsection therefore carries our main discussion concerning the physical mechanism underlying the resonant Auger decay.

A. Cl^- in NaCl

In the case of Cl^- (Fig. 2) the spectator-induced structure appears at $h\nu \approx 201.5$ eV and peaks together with the first L_{23} exciton absorption maximum. This is illustrated in more detail in Fig. 1(a), which in addition to the $\text{Cl } L_{23}$ edge shows the normalized photoemission intensity of the spectator structure, or actually its constant initial-state (CIS) spectrum. The participator effect of the excited electron for the $3p$ and $3s$ photoelectron lines is very weak or absent. This is in line with the standpoint that the first maxima in the $\text{Cl}^- L_{23}$ absorption spectra of metal chlorides are due to the $2p^6 \rightarrow 2p^5 4s$ transitions, the final-state $4s$ electron being loosely bound to the parent Cl atom and having a mean radius comparable with the lattice parameter. The creation energy of the final configuration of the scattering event, the $3p^{-2}4s$ configuration, is about 23.2 eV. The appearance of the spectator-induced structure in the region of $h\nu \approx 203$ eV [see Fig. 1(a)] indicates that the $2p_{1/2}$ component of the L_{23} core exciton absorption is in the case of NaCl hidden in the wide absorption structure in the region of 203–204 eV, as proposed earlier.²⁰

Although the $3d$ wave function is not collapsed in the case of the $\text{Cl}^- 2p^3 3d$ configuration, an interesting weak high-energy feature seems to appear in the $\text{Cl}^- L_{23}M_{23}M_{23}$ Auger spectra at $204 < h\nu < 206$ eV (spectra 10–13 in Fig. 2). This feature may be interpreted as an nd -spectator-induced structure, which then means that the threshold energy for $2p^6 \rightarrow 2p^5 nd$ transitions for Cl^- in NaCl lies around 204 eV and that the $3d$ electron forms in the field of two $3p$ holes a short-living stationary state, degenerate with the s -type continuum.

B. K^+ in KCl

In order to understand the structures in the vicinity of the normal $L_{23}M_{23}M_{23}$ Auger structure of KCl (Fig. 3) in some more detail we show in Fig. 8 as function of photon energy the energy position of the two highest-energy bands of the spectator structure as well as of a peak (coinciding with the maximum of spectrum 6), which is part of a structure nearly degenerate with the normal Auger one, and which starts to be clearly observable in spectrum 5, i.e., at $h\nu \approx 296.5$ eV. The almost linear dispersion of the first two structures throughout the whole resonance region, as is clear from comparison with the dispersion of the $3s$ photoemission line in Fig. 8, indicates that the final state arising from different resonances is always the same, i.e., it does not depend on the intermediate state. The lower-energy structure, on the other hand, essentially seems to remain at constant kinetic energy. Toward higher-photon energy (spectra 14 and 15) it can be seen that this peak finally merges with the 3P peak of the normal $L_{23}M_{23}M_{23}$ Auger structure. The deviation of the dispersion from a strict linearity in the regions of the first and third absorption peaks seems systematic and could be due to an energy redistribution between escaping electrons and phonons, or to an interference (Fano) effect.

Since the final configuration for the normal $L_{23}M_{23}M_{23}$ Auger transition in K^+ is $1s^2 2s^2 2p^6 3s^2 3p^4$ (or $3p^{-2}$), the final configuration for the same transition in the presence of a $3d$ spectator electron should be $3p^{-2}3d$. This configuration has been shown to be the main product of the resonant Auger transitions in Ar atoms^{30,31} and it is also observable among the products of similar transitions in K and Ca atoms.^{32,33} The creation energies corresponding to the main maxima of the spectator-induced Auger structure, 45.6, 47.5, 49.5, and 51.5 eV, are in the same energy region as the energies of various terms of the $3p^{-2}3d$ configuration of K^+ free ions.³⁴

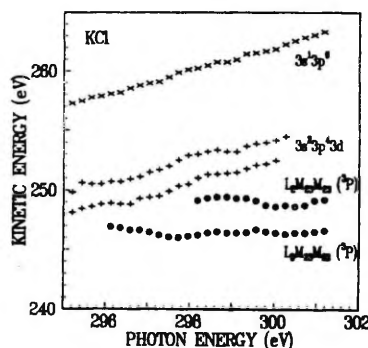


FIG. 8. The energy position of the $\text{K } 3s$ photoemission line of KCl (\times), the two high-energy spectator satellites ($+$), and the 3P peaks of the $L_{23}M_{23}M_{23}$ Auger structure (dots) as function of photon energy.

To separate the dispersive and nondispersive structures we shift spectrum 4 with respect to spectrum 6 by the difference in photon energy and renormalize its intensity so that the highest-energy spectator lines in the spectra 4 and 6 coincide. The difference of the spectra 6 and 4 obtained after this procedure is shown in Fig. 9(b). The comparison of the difference spectrum with the calculated $L_3M_{23}M_{23}$ Auger structure, also presented in Fig. 9(b), suggests that it can indeed be ascribed to a normal $L_3M_{23}M_{23}$ Auger structure presumably shifted to higher energies by about 1 eV, as can be seen by comparing spectrum 15 and the normal Auger spectrum in Fig. 3. At the position of 1S term of the Auger structure some additional weak features are seen, for which, however, we have no explanation. Similarly, we conclude that spectrum 12 in addition to the spectator structure and a normal $L_3M_{23}M_{23}$ Auger structure contains the normal $L_2M_{23}M_{23}$ Auger structure. The comparison of spectra 10–12 with each other shows that the latter starts to arise in spectrum 11, i.e., at $h\nu \approx 299.3$ eV. The energy position of the identified 3P line of this $L_2M_{23}M_{23}$ structure again proves to be essentially nondispersive, as shown in Fig. 8.

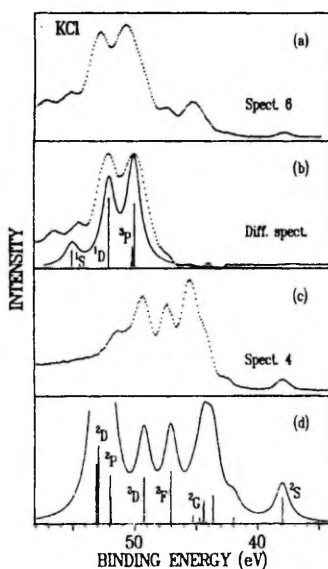


FIG. 9. Resonant $L_{23}M_{23}M_{23}$ Auger spectra for KCl as compared to the calculation of the $3s^23p^43d$ and $3s3p^6$ final states. In (a) and (c) are shown spectra 6 and 4 of Fig. 3, respectively. Their difference spectrum is shown in (b) and compared with the calculated $L_3M_{23}M_{23}$ Auger structure (solid line). Our calculation of the $3p^{-2}3d^1$ configuration of the $L_3M_{23}M_{23}$ autoionization spectrum is shown in (d). The theoretical multiplets are broadened with a Lorentzian of 1.5 eV FWHM. Further explanation in text.

This decomposition procedure leads to the conclusion that at resonant $2p^6 \rightarrow 2p^53d$ excitation the photoemission spectra of K^+ in the vicinity of the $L_{23}M_{23}M_{23}$ Auger structure contains three components, the spectator-induced structure, which shifts to higher-kinetic energy with increasing photon energy, and the normal $L_3M_{23}M_{23}$ and $L_2M_{23}M_{23}$ Auger structures. The small high-energy shift of this Auger structure at photon energies close to the ionization threshold may be understood as the PCI of the slow photoelectron and the fast Auger electron.²

Although in a straightforward treatment the development of the $3p^{-2}3d$ final configuration at resonant photon energies should be considered as the result of a single scattering event $2p^6 + h\nu \rightarrow 3p^{-2}3d + e$, we treat it here as a two-step process, the first step being the creation of the $2p^{-1}3d$ excited configuration and the second one the spectator decay $2p^{-1}3d \rightarrow 3p^{-2}3d + e$ of this configuration. On these grounds we use the model explained in Sec. III to compute the spectator structure in the electron spectra as the structure which corresponds to this second step. In Fig. 9(a) this result is shown. The 3D_1 state was chosen as the atomic intermediate state. For this state the probability of a $2p_{3/2}$ hole is largest. It should, however, be noted that the Auger intensity distribution does not critically depend on the choice of the intermediate state. Note, also, that for this more detailed comparison we have aligned and compressed the energy scale of the calculated spectrum. The compression (here 85%) is a common practice to correct for the configuration interaction and the solid state effects not considered in our calculations. This many-body correction can, for instance, also be achieved by a renormalization of the Slater integrals involved.³⁵ Either method yields in essence the same result.

After this correction we find for the spectrum in Fig. 9(c) a good agreement in position and relative intensity of the indicated $(^1D)3d^2D$, $(^1D)3d^2F$ terms and the 2S term, which coincides with the $3s$ photoemission line. The $3p^4$ parent terms are given in parentheses. Note that the intensity of the $3s$ photoemission line is determined by interference effects with the direct photoemission process. This effect is neglected in a two-step approach. The position of the most intense spectator peak differs by about 1.5 eV from the theoretical result, but this discrepancy can be understood from the multitude of terms (15 in total) which contribute to its intensity. The relative balance of the Auger intensities is in a rather subtle way dependent on the final-state potential, which determines the shape of the continuum wave function and the value of the radial integrals. The Auger intensities are therefore easily affected by the approximations in our scheme, and we believe that the cause of the discrepancy here is the intensity of the 2G term which seems strongly underestimated in the calculation. There is, however, a much stronger discrepancy between calculation and experimental result, because intensity in the $(^1D)3d^2D$ and $(^1D)3d^2P$ terms at higher-binding energy seems completely lacking. We suggest, that this is caused by the fact that at these energies the $3p^43d$ multiplet states are degenerate with the final state of the $3p^4$ normal Auger

processes. The underlying physics is that the excited $3d$ electron in the intermediate $2p^{-1}3d$ state has a certain probability to be delocalized. This probability depends on the particular resonance, or more specifically on the wave function of the $3d$ electron in the crystal field and the coupling of the $3d$ state with the conduction band continuum. This should also affect the fate of the $3d$ wave function in the final two-hole configuration, where it may or may not collapse progressively to form the $3p^4 3d^1$ multiplet state. In Fig. 9(b) it can be seen that the 1D term of the experimentally determined $L_3 M_{23} M_{23}$ structure, which is the parent structure of the lacking spectator terms, can be considered to mark the energy boundary between both possible decay processes.

For higher-photon energies exactly the same process takes place in relation to the $2p^{-1}_{1/2} 3d$ configuration and the observed $L_2 M_{23} M_{23}$ structure (starting at spectrum 10). But here also a relatively strong $L_3 M_{23} M_{23}$ structure is observed. The latter is a consequence of the generally very fast $L_2 L_3 M_{45}$ Coster-Kronig (CK) process involving the $3d$ electron, which escapes into the continuum leaving the $2p^{-1}_{1/2}$ configuration. The additional Lorentzian broadening found in the " L_2 " part of the absorption spectrum is a signature of this additional decay channel.⁹

It is important to note that the same final configuration $3p^{-2} 3d$ arises as the cause of satellite structures in the L_{23} emission spectra of K^+ in potassium halides (the $2p^3 3s^2 3p^6 \rightarrow 2p^6 3s^2 3p^4 3d$ satellites of the $2p^3 3s^2 3p^6 \rightarrow 2p^6 3s^1 1^3 p^6$ diagram lines^{36,37}) and in the $3s$ photoelectron spectra.³⁸ The spectator as well as participator structures can therefore actually be considered as photoemission structures that resonate at the $2p$ core level threshold. The energy of the center of gravity of the satellite emission band is about 249 eV for KCl,³⁶ in excellent agreement with the energy of the center of gravity of the spectator structure in spectrum 4 (Figs. 3 and 9).

In Fig. 10 the excitation spectra for the highest-energy spectator structure, the $L_3 M_{23} M_{23} (^1P)$ normal Auger structure as well as for the $3p$ and $3s$ photoemission lines are shown. They are essentially the CIS spectra for the photoelectron lines and the spectator structure and the constant final-state (CFS) spectra for the Auger line. It is clearly seen that the efficiencies to excite the spectator structure on the one hand and the Auger structure on the other compete with each other. The efficiency to excite the spectator structure is the largest in the regions of the first and third resonances, the efficiency to excite the Auger structure is the largest in the regions of the second and fourth resonances. Such a behavior of the excitation spectra can be considered as evidence for the fact that the high-energy components of the crystal-field-split $3d$ state reflected by the second and fourth resonances overlap the conduction band continuum and that the $3d$ electron excited to these states is partly delocalized, i.e., has a finite probability of leaving the region of the ion before the Auger transition occurs. The spectator structure is especially heavily suppressed in the high-energy region of the fourth resonance where it overlaps with the L_2 continuum, and where, as noted before, in addition part of the L_2 holes are transferred into L_3 holes via a CK transition before the Auger transition occurs.

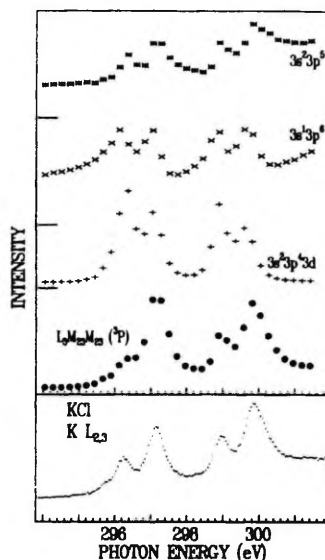


FIG. 10. The (CIS or CFS) excitation spectra for the $3p$ (*) and $3s$ (x) photoemission lines of KCl, as well as for the high-energy spectator structure (+) and the 1P $L_3 M_{23} M_{23}$ Auger line (dots), as compared with the K L_{23} edge. The excitation spectra are normalized for equal peak height; zeros are indicated by horizontal bars.

The efficiency of the participator role of the $3d$ electron (see Fig. 10) peaks at all four resonances, but the relative efficiency of the $3s$ photoelectron line is suppressed in the regions of the second and fourth resonances and seems to follow the efficiency of the spectator structure. This may be considered as an indication of the strong configuration interaction between the $3s 3p^6$ and $3s^2 3p^4 3d$ configurations. It may also explain why the resonance maxima of the $3s$ and $3p$ photoemission lines do not coincide. Note that for the detailed discussion of the fate of the excited $3d$ electron the $3s \rightarrow 2p$ and $3d \rightarrow 2p$ radiative decay channels, not studied here, should be included.

The spectator effect manifests also itself in the $L_{23} M_1 M_{23}$ and $L_{23} M_{23} V$ Auger spectra. It is observable in spectra 3–5 in Fig. 3 that both of these structures seem to have components shifted to higher energy in comparison with corresponding structures in, for example, spectra 7 and 8 or above the edge. Spectrum 6 demonstrates how the spectator-induced structures reduce to the normal spectra. In the region of the L_2 resonance (spectra 10–12) these spectator-induced structures appear again. It is, however, difficult from our data to say anything more definite about their dispersion.

To conclude, the resonant photoemission spectra of KCl at the L_{23} edge in the vicinity of the K $L_{23} M_{23} M_{23}$

Auger structure can be explained, accepting three statements.

(i) These spectra contain two major competing components, the PCI-shifted normal $L_3M_{23}M_{23}$ and $L_2M_{23}M_{23}$ structures and the spectator structure which shifts to higher energies almost linearly with increasing photon energy. The normal Auger structures are a signature of the delocalization of the $3d$ electron. As such, the presence of these structures may be considered as a solid-state effect.

(ii) The spectator structure is due to the $3p^{-1}3d$ final configuration and is always the same independently of the nature of the primary resonance; in its most pure form it can be observed only in the region of the first L_3 resonance, where its essentially atomic origin can be verified.

(iii) At the " L_2 " part of the L_{23} edge, where the probability of creating $2p_{1/2}$ holes is largest, an additional $L_2L_3M_{45}$ CK process carries a large part of the weight of the deexcitation. The presence of an intense $L_3M_{23}M_{23}$ structure is assumed to be a proof of this.

C. Ca^{2+} in CaF_2 and CaCl_2

From a general point of view the situation with the $L_{23}M_{23}M_{23}$ Auger spectra and their $3d$ -spectator-induced changes in the case of Ca^{2+} in CaF_2 and CaCl_2 (Figs. 4 and 5) should be similar to the situation for K^+ in KCl . Here also a spectator-induced structure appears for resonant photon energies at the high-energy side of the normal Auger structure and moves to higher energies as $h\nu$ increases. The creation energy of the highest-energy component of this final state configuration is about 57.3 eV. Also here we may conclude that the spectator structure is due to the final configuration $3p^{-1}3d$.

However, a more detailed analysis shows that the case of Ca^{2+} differs from the case of K^+ in some important aspects. Figure 11 illustrates some of the differences involved. We have compared similar spectra as in the case of KCl , with the atomic calculation here for CaF_2 and CaCl_2 . The energy scale of the calculation was again compressed by 85%. We observe, first, that although the spectator peak at low-binding energy reasonably aligns with the theoretical result, there are, for both CaF_2 and CaCl_2 , no further obvious agreements between spectral data and theory. Second, although components of the normal $L_3M_{23}M_{23}$ Auger structure may be present, they seem to be much weaker and also cannot be demonstrated by means of a subtracting technique as in the case of KCl , because of the intrinsic differences in these spectra. It may then, for example, be that all resonantly excited structure is spectator structure and that this structure depends on the nature of the primary photoexcitation resonance. Spectrum 11 in Fig. 4 (CaF_2) is very similar to spectra 4 and 5 showing that the replacement of the $2p_{3/2}$ hole by the $2p_{1/2}$ hole does not change the decay process of this resonance, except for the possible inclusion of an effective $L_2L_3M_{45}$ CK-like transition in the latter case. In the region of the highest-energy $2p_{1/2}^{-1}3d$ resonance (spectra 12–14 in Fig. 4 as well as in Fig. 5) the situation

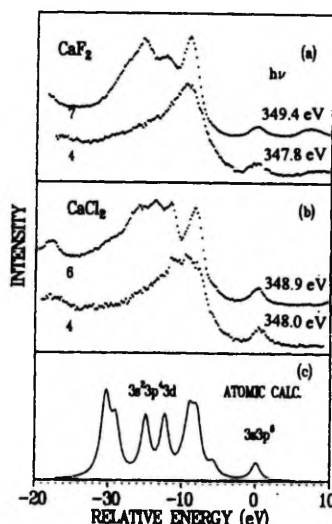


FIG. 11. (a) Resonant $L_{23}M_{23}M_{23}$ Auger spectra for CaF_2 (spectra 4 and 7 of Fig. 4). (b) Resonant $L_{23}M_{23}M_{23}$ Auger spectra for CaCl_2 (spectra 4 and 6 of Fig. 5). (c) The atomic calculation for the $3s^23p^43d$ and $3s3p^4$ final states, broadened with a Lorentzian of 1.5 eV FWHM.

differs to the extent that the spectator decay is suppressed and that a very strong $L_2L_3M_{45}$ CK transition, indicated by a large $L_3M_{23}M_{23}$ normal Auger structure, dominates. Note that the participator-induced enhancement of the $3s$ and $3p$ photoelectron lines is relatively strong as compared to the case of K^+ .

Looking for a physical difference between the cases of K^+ and Ca^{2+} it should be noted that the $2p^33d$ configuration in Ca^{2+} is more localized because of the progressed collapse of the $3d$ wave function, and that its binding energy is larger. This may explain the lack of a clear normal Auger component (except for the one caused by the CK process) in the deexcitation spectra. In the case of KCl the crystal field did not seem to prevent a comparison with the atomic calculation. But, the intrinsic differences in the autoionization spectra of CaF_2 and CaCl_2 may be indicative of a crystal-field effect that cannot be neglected.

D. Sc^{3+} in Sc_2O_3

The resonantly excited electron spectra of Sc^{3+} in Sc_2O_3 in the $L_{23}M_{23}M_{23}$ Auger region are considerably wider and less structured than those of K^+ and Ca^{2+} . The probable cause for this is that the chemical bond in Sc_2O_3 is much more covalent than in KCl , CaF_2 , or CaCl_2 . An important consequence of this circumstance is that all the $2p^33d$ resonant absorption structure is degenerate with the conduction band continuum. This may ex-

plain why in Fig. 6 structures identifiable with the normal $L_3M_{23}M_{23}$ as well as the $L_3M_{23}V$ Auger structures appear already at the first $2p^33d$ resonance. Further evidence of this covalency effect, which follows also from a detailed analysis of the L_{23} edge,⁹ is presented by the resonant enhancement of the valence band, clearly observable in spectra 4 and 9 of Fig. 6. This can only be caused by the presence of Sc d character in the occupied part of the valence band. Nevertheless, the traces of what we should identify as a spectator structure shifting to higher energies with increasing photon energy are seen in some of the spectra. The creation energy corresponding to this final-state structure is about 68 eV. As in the cases of K^+ and Ca^{2+} we assume a $3p^{-2}3d$ intermediate configuration to be responsible for this structure. Part of the normal $L_3M_{23}M_{23}$ structure at the " L_2 " resonance should, finally, be attributed to a CK-mediated decay process.⁹

VI. SHAKE PROBABILITIES

If our interpretation of the spectator-induced spectra is correct, there remains no apparent structure to be interpreted involving a shake-off or shake-up of the excited $3d$ or $4s$ electron during the Auger decay of the $2p$ hole. This is in contrast to the case of Ar atoms where the shake-up processes (mainly $3d \rightarrow 4d$ and $4s \rightarrow 5s$) were shown to play an important role in the formation of the final state.^{30,31} To solve this contradiction we have calculated the total overlap probabilities P_{nl} to verify that no ejection or excitation of $3d$ and $4s$ electrons of the configurations $2p^33s^23p^63d(4s)$ takes place during the $L_{23}M_{23}M_{23}$ -like deexcitation (Table III). This overlap is given approximately by the formula

$$P_{nl} = \left[\int R_{nl}^i R_{nl}^f r^2 dr \right]^2, \quad (6)$$

where R_{nl}^i and R_{nl}^f are the initial and final state radial wave functions of nl ($3d$ or $4s$) electrons, respectively. As seen in Table III, for $3d$ electrons $\langle r_{nl} \rangle$ decreases sharply in the sequence from Ar to Ca^{2+} . In the case of Ar the $3d$ electron collapses during the Auger decay and the shake probability is large, while for K^+ and even more

for Ca^{2+} it is completely collapsed in the $2p^33d$ configuration. During the Auger decay its mean radius changes little and the shake probability is small. Another factor which decreases the shake-up probability for the $3d$ electron is the fact that, in the configuration $2p^3nd$ ($n \geq 4$) of ions considered here, the d electron is not collapsed and contributes to the crystalline states which have low density at any particular ion state. Therefore, we cannot support the suggestion of Ref. 22 that the shake processes are important to the build up of the $3d$ spectator structure in the case of Ca^{2+} in CaF_2 .

VII. CONCLUSIONS

We have demonstrated that at incident photon energies coinciding with the $2p^6 \rightarrow 2p^33d(4s)$ resonances in the absorption spectra of argonlike ions Cl^- (in NaCl), K^+ (in KCl), Ca^{2+} (in $CaCl_2$ and CaF_2), and Sc^{3+} (in Sc_2O_3) the spectra of electrons emitted by these ions contain a spectator structure in the region of the $L_{23}M_{23}M_{23}$ normal Auger structures and that this structure shifts to higher kinetic energies with increasing photon energy. Both empirical considerations and Hartree-Fock-Pauli computations show that this structure originates from the $3p^{-2}3d(4s)$ final configuration arising as a product of the Auger resonant inelastic scattering process of incident photons. Collapse of the $3d$ electron in the $2p^33d$ configuration in the sequence $Cl^- \rightarrow Ar \rightarrow K^+$ leads to the marked increase of intensity of this process and the decrease of the role of shake processes in it. Our experimental data for Cl^- in NaCl and K^+ in KCl are clear evidence of this.

One of the main points of this study is that we propose that also the spectator structures, to the extent they are present in the resonant $L_{23}M_{23}M_{23}$ Auger structures, essentially remain at constant binding energy. Our reason for this assumption is that we consider both participator and spectator processes as decay channels to a single photoemission final state, the "main" photoemission line and its configuration interaction (CI) satellites. At resonance the intensity ratio of main line and CI satellites may, of course, completely change, because of the in-

TABLE III. The calculated probabilities P_{nl} for $3d$ and $4s$ electrons not to be ejected or excited during the Auger decay. $\langle r_{nl} \rangle$ is the mean radius of the nl excited electron wave function (in atomic units).

Initial and final configurations		Cl (NaCl)		Ar		K (KCl)		Ca (CaF ₂)	
		$\langle r_{nl} \rangle$	P_{nl}	$\langle r_{nl} \rangle$	P_{nl}	$\langle r_{nl} \rangle$	P_{nl}	$\langle r_{nl} \rangle$	P_{nl}
Initial	$2p^33s^23p^63d$			9.24		2.92		1.63	
Final	$2p^63s^23p^43d$			2.79	0.23	1.85	0.86	1.47	0.99
Initial	$2p^33s^23p^63d$			9.24		2.92		1.63	
Final	$2p^63s^03p^63d$			2.46	0.17	1.75	0.82	1.43	0.98
Initial	$2p^33s^23p^64s$	5.67		5.34					
			0.88		0.87				
Final	$2p^63s^23p^44s$	4.43		4.10					

volement of different matrix elements and selection rules. The dispersion curves of Fig. 8 could with regard to spectator structures, in principle, also be interpreted as pointing to a stepwise increase in kinetic energy, corresponding to the four (more or less relaxed) intermediate states. A fitting procedure was used to compose this figure and the data do not seem to exclude such a mechanism. However, we would want to argue in favor of the first mechanism, i.e., an altogether coherent process, because of its physical clarity and its theoretical attractiveness within the scheme of a single-step model.

In the case of Cl^- the lower resonances are due to the $2p^{-1}4s$ configuration which results in a $3p^{-2}4s$ final configuration. In the case of the metal ions, our spectra demonstrate the occurrence of a $L_2L_3M_{45}$ Coster-Kronig process which can be considered as evidence for the localization (collapse) of the $3d$ wave function. But, in spite of a general similarity, the details of the spectra of the metal ions studied here differ from each other. The main reason is the different coupling to the $2p^53d$ bound states with the conduction band continuum. In the case of Sc^{3+} all the intermediate states lie in the continuum, and the

excited $3d$ electron is substantially delocalized and the spectra are dominated by $L_3M_{23}M_{23}$ and $L_2M_{23}M_{23}$ Auger structures. In the case of K^+ only the lowest-order resonance seems completely localized and gives rise to a pure spectator structure which has an atomic origin as verified by our calculations. For Ca^{2+} the intermediate states seem nearly completely localized and give rise to a complicated "spectator" structure, indicating a possible additional role of the crystal field. However, to reach a full understanding of the latter a more detailed theoretical analysis with inclusion of crystal field effects may prove to be of importance.

ACKNOWLEDGMENTS

This work was supported by the Swedish Natural Sciences Research Council, the Crafoord Foundation, and the Royal Swedish Academy of Sciences. We wish to acknowledge stimulating discussions with Professor T. Åberg, Professor S. Aksela, Dr. J. Tulkki, Dr. H. Aksela, and Dr. A. Maiste. We thank A. Kasikov for providing the samples of Sc_2O_3 .

- ¹Several papers on this topic have recently appeared in the *Proceedings of the 2nd International Workshop on Auger Spectroscopy and Electron Structure (IWASES-II)*, Malmö, Sweden, 1991, edited by K. Wandelt, C.-O. Almblad, and R. Nyholm [Phys. Scr. T41 (1992)].
- ²T. Åberg, Phys. Scr. T41, 71 (1992).
- ³A. A. Maiste, R. E. Ruus, and M. A. Elango, Zh. Eksp. Teor. Fiz. 79, 1671 (1980) [Sov. Phys. JETP 52, 844 (1980)].
- ⁴J. N. Andersen, O. Björneholm, A. Sandell, R. Nyholm, J. Forsell, L. Thånell, A. Nilsson, and N. Mårtensson, Synchrotron Radiat. News 4, 15 (1991).
- ⁵R. T. Poole, J. G. Jenkin, J. Liesegang, and R. C. G. Leckey, Phys. Rev. B 11, 5179 (1975).
- ⁶S. Muramatsu and C. Sugiyara, Phys. Rev. B 27, 3806 (1983).
- ⁷G. W. Rubloff, Phys. Rev. B 5, 662 (1972).
- ⁸H. H. Tjippins, J. Phys. Chem. Solids 27, 1069 (1966).
- ⁹F. M. F. de Groot, J. C. Fuggle, B. T. Thole, and G. A. Sawatzky, Phys. Rev. B 41, 928 (1990).
- ¹⁰P. H. Citrin, P. Eisenberger, and D. R. Hamann, Phys. Rev. Lett. 33, 965 (1974).
- ¹¹R. Karazija, *The Theory of X-Ray and Electronic Spectra of Free Atoms. An Introduction* (Mokslas, Vilnius, 1987, in Russian); E. J. McGuire, in *Atomic Inner-Shell Processes: I. Ionization and Transition Probabilities*, edited by B. Crasemann (Academic, New York, 1975), pp. 293–330.
- ¹²Z. B. Rudzikas, in *Proceedings of the 6th International Conference on Atomic Physics*, Riga, USSR, edited by R. Damburg, (Zinatne, Riga; Plenum, New York and London, 1979), pp. 92–110.
- ¹³R. E. Watson, Phys. Rev. 111, 1108 (1958).
- ¹⁴T. Chassé, R. Franke, P. Strübel, and A. Meisel, Phys. Scr. T 41, 281 (1992).
- ¹⁵G. D. Mahan, Phys. Rev. B 22, 3102 (1980).
- ¹⁶R. T. Poole, J. Szajman, R. C. G. Leckey, J. G. Jenkin, and J. Liesegang, Phys. Rev. B 12, 5872 (1975).
- ¹⁷Y. Iguchi, T. Sagawa, S. Sato, M. Watanabe, H. Yamashita, A. Ejiri, M. Sasanuma, S. Nakai, M. Nakamura, S. Yamaguchi, Y. Nakai, and T. Oshio, Solid State Commun. 6, 575 (1968).
- ¹⁸R. E. Ruus, Opt. Spectrosc. 59, 450 (1985).
- ¹⁹F. Sette, B. Sinkovic, Y. J. Ma, and C. T. Chen, Phys. Rev. B 39, 11 125 (1989).
- ²⁰A. M.-E. Saar and M. A. Elango, Fiz. Tverd. Tela (Leningrad) 13, 3532 (1971) [Sov. Phys. Solid State 13, 2985 (1971)].
- ²¹See, for example, O. Björneholm, A. Sandell, A. Nilsson, N. Mårtensson, and J. N. Andersen, Phys. Scr. T 41, 217 (1992).
- ²²T. Tiedje, K. M. Colbow, D. Rodgers, and W. Eberhardt, Phys. Rev. Lett. 65, 1243 (1990).
- ²³A. Kikas, A. Ausmees, M. Elango, J. N. Andersen, R. Nyholm, and I. Martinson, Europhys. Lett. 15, 683 (1991).
- ²⁴These lines provide a further check of the energy position of the absorption threshold relative to the $2p$ binding energy.
- ²⁵U. Fano, Phys. Rev. 124, 1866 (1961).
- ²⁶M. Ohno, J. Electron Spectrosc. Relat. Phenom. 48, 125 (1989).
- ²⁷G. S. Brown, M. H. Chen, B. Crasemann, and G. E. Ice, Phys. Rev. Lett. 45, 1937 (1980).
- ²⁸G. B. Armen, T. Åberg, J. C. Levin, B. Crasemann, M. H. Chen, G. E. Ice, and G. S. Brown, Phys. Rev. Lett. 54, 1142 (1985).
- ²⁹A. Kivimäki, H. Aksela, S. Aksela, and O.-P. Sairanen, Phys. Rev. B (to be published).
- ³⁰H. Aksela, S. Aksela, H. Pulkkinen, G. M. Bancroft, and K. H. Tan, Phys. Rev. A 37, 1798 (1988).
- ³¹M. Meyer, E. v. Raven, B. Sonntag, and J. E. Hansen, Phys. Rev. A 43, 177 (1991).
- ³²M. Meyer, E. v. Raven, M. Richter, B. Sonntag, and J. E. Hansen, J. Electron Spectrosc. Relat. Phen. 51, 407 (1990).
- ³³M. Meyer, E. v. Raven, M. Richter, B. Sonntag, R. D. Cowan, and J. E. Hansen, Phys. Rev. A 39, 4319 (1989).

- ³⁴C. E. Moore, *Atomic Energy Levels as Derived from the Analysis of Optical Spectra*, National Bureau of Standards Circular No. 467 (U.S.G.P.O., Washington, D.C., 1949).
- ³⁵R. D. Cowan, *The Theory of Atomic Structures and Spectra* (University of California Press, Berkeley, 1981).
- ³⁶B. Sorkin, A. Saar, and M. Elango, Toim, Eesti NSV Tead. Akad. Fuus. Mat. (USSR) **22**, 105 (1973).
- ³⁷J. Vajjaka, J. Phys. C **19**, 1451 (1986).
- ³⁸G. K. Wertheim and A. Rosencwaig, Phys. Rev. Lett. **26**, 1179 (1971).

R. Ruus, A. Kikas, M. Elango, A. Maiste, E. Nõmmiste, A. Saar,
Auger decay processes of resonantly excited $3d^{-1}4f$
configuration of xenon-like ions in ionic solids,
J. Electron Spectrosc. Relat. Phenom. **68**, (1994), 277–286.

Auger decay processes of resonantly excited $3d^{-1}4f$ configuration of xenon-like ions in solids

R. Ruus^a, A. Kikas^a, A. Maiste^a, E. Nõmmiste^a, A. Saar^a, and M. Elango^{a,b}

^aInstitute of Physics, Estonian Academy of Sciences, Rõia 142, EE-2400 Tartu, Estonia

^bDepartment of Experimental Physics and Technology, Tartu University, Ülikooli 18, EE-2400 Tartu, Estonia

The synchrotron-radiation-induced Auger and photoelectron spectra of xenon-like ions I^- and Cs^+ (in CsI), Ba^{2+} (in BaF_2), and La^{3+} (in LaF_3) have been measured in the vicinity of the M_{45} absorption edges of these ions. It is shown that the spectra of La and Ba excited at $3d^{10} \rightarrow 3d^9 4f$ resonances exhibit a very intense $4f$ -spectator structure which changes its energy and intensity with energy of excited photons. Calculation of the Auger decay of the $3d^{-1}4f$ configuration shows that this structure is due to transitions to the $4d^{-2}4f + 4p^{-1}$ final ionic configuration which high-energy part is overlapped with the $4d^{-2}$ continuum. In the case of Ba this structure coexist with the normal Auger structure which appears as a result of the $M_4 M_5 N_{67}$ Coster-Kronig transitions. The spectra of I^- contain only the normal $M_{45} N_{45} N_{45}$ Auger components. The spectra of Cs^+ are similar to those of I^- with a small admixture of the $4f$ -spectator-like structure. The anomalous behaviour of the intensity ratio of $4d_{3/2}$ and $4d_{5/2}$ photolines of La and Ba at the resonance excitation energies is found and attributed to the strong term-dependence of the participator Auger process.

1. INTRODUCTION

Recently it was shown that resonant Auger spectroscopy, which is known to reveal the details of the decay dynamics of excited configurations of atoms, molecules and solids, gives new interesting insight into the $2p^{-1}3d$ configuration of argon-like ions Cl^- , K^+ , Ca^{2+} , and Sc^{3+} in ionic solids [1]. A $3d$ -spectator-electron-related structure, which reflects the $3p^{-2}3d(4s)$ final configuration, appears in the $L_{23} M_{23} M_{23}$ Auger spectra of these ions at the resonant $2p^{-1}3d(4s)$ excitation energy and changes with progressing collapse of the $3d$ wave function. With increasing photon energy this structure shifts linearly to higher kinetic energies indicating that the "photon absorption - Auger decay" process should be considered here as a single

Auger-resonant inelastic scattering event [2].

Here we study another case where such phenomena could be expected, the decay of the photon-induced $3d^{-1}4f$ configuration of xenon-like ions I^- , Cs^+ , Ba^{2+} , and La^{3+} , in ionic solids CsI , BaF_2 , and LaF_3 , respectively. The near-edge structure of M_{45} absorption of these ions is due to continuous $3d^{-1}4f$ or localized $3d^{-1}4f$ states depending on collapse of the $4f$ wavefunction which occurs going from Xe to Cs^+ and Ba^{2+} [3,4].

2. EXPERIMENTAL

The measurements are carried out using synchrotron radiation from beamline 22 at MAX-laboratory, Lund University, Sweden

Table 1

Experimental (E_B) and calculated (E_{th}) binding energies (in eV). E_B values are referred to the bottom of the conduction band

Ions		Configurations				
		$3d_{3/2}^{-1}$	$3d_{5/2}^{-1}$	$4p_{3/2}^{-1}$	$4d^{-2}4f+4p^{-1}$	$4d^{-2}$
Ba free ions	E_{th}	820.0	805.0	201.0	201.0-234.8	243.4-254.8
	E_B	802.0	786.7	179.7		
Ba in BaF_2	E_{th}	800.9	785.8	181.8	181.8-215.6	204.8-216.2
	E_B	802.0	786.7	179.7		
La free ions	E_{th}	890.3	873.8	232.1	232.1-268.6	296.6-308.8
	E_B	856.8	840.0	201.5		
La in LaF_3	E_{th}	862.5	846.0	204.5	204.5-241.1	241.4-253.6
	E_B	856.8	840.0	201.5		

[5]. The electron spectra are excited by a photon beam from a modified SX-700 plane-grating monochromator with an energy resolution of 0.4 - 0.8 eV, and analyzed by a hemispherical electron spectrometer Scienta SES-200 with an energy resolution of 0.3 eV. The M_{45} absorption spectra are obtained in the electron yield mode. Other experimental details have been described earlier [1]. The thin films (~200 Å) of CsI, BaF_2 , LaF_3 are prepared by thermal evaporation from a molybdenum boat onto a polished stainless steel substrate in a preparation chamber at a pressure 10^{-7} Torr, and then transferred to the experimental chamber operated at a pressure 10^{-10} Torr.

The measured energy distribution curves (EDC) of ejected electrons are normalized to the incident photon flux. The kinetic and binding energies are given relative to the bottom of the conduction band of the sample using the band gap energies 6.2 eV for CsI [6], 11.0 eV for BaF_2 [7] and 9.4 eV for LaF_3 [8].

3. THEORETICAL CONSIDERATIONS

The theoretical analysis of the observed

spectra is based on the calculation procedure described earlier [1]. We treat the inner-shell excitation and its Auger decay as a two-step process. The calculations are essentially atomic and are based on the Hartree-Fock (HF) method to obtain the atomic wavefunctions. Relativistic effects are taken into account as corrections of the order α^2 (α is the fine structure constant) [9]. The calculations in the intermediate coupling scheme with Slater integrals found from HF treatment of the $4d^{-2}$ final state, are shown to overestimate the term separations of multiplets [10]. Therefore, for a better agreement with the observed spectra we reduce the radial Coulomb F_k ($k>0$), exchange G_k and R_k integrals for the open $4d^{-2}$ and $4d^{-2}4f$ shells by 20%.

In the case of the collapsed 4f orbital, the interaction of $4d^{-2}4f$ and $4p^{-1}$ configurations is expected to be very strong. We treat these configurations together and calculate transitions $3d^{-1}4f \rightarrow 4p^{-1} + 4d^{-2}4f$ in a configuration-superposition approximation.

The solid-state effects are accounted using the Watson sphere model [11]. The depth of potential well of the Watson sphere is taken equal to the value of the

Madelung potential on the ion site: ± 6.4 eV for I and Cs in CsI, -17.6 eV for Ba in BaF_2 and -25.8 eV for La in LaF_3 [12]. The influence of the Watson correction on the radial part of the wavefunctions is usually rather small. However, in the case of the $3d^{-1}4f$ configuration of Cs^+ the radial part of the $4f$ wavefunction crucially depends on the value of the Watson correction; if it becomes smaller than -5.2 eV the mean $4f$ radius abruptly increases from 1.5 to 17 a.u.. Another important effect of these corrections is decrease of the energy separation between configurations $4d^{-2}$ and $4d^{-2}4f + 4p^{-1}$. In the case of Ba^{2+} in BaF_2 this effect leads to overlapping of these configurations, as we can see from Table 1. In this Table the computed values of binding energies, E_{th} , of actual configurations of Ba and La ions are presented in comparison with our experimental data, E_B . We compute the binding energies in crystals as $E_0 - E_p$ for single-ionized final states and as $E_0 - 2E_p$ for double-ionized final states (e.g. for $4d^{-2}$ configuration). Here E_0 is the difference of the total energies of ground ($1S_0$) and final states of the ions in the Watson sphere. For polarization energy, E_p , we use the value 2.0 eV estimated both for Ba^{2+} in BaF_2 and La^{3+} in LaF_3 by using a classical electrostatic approach [13]. As seen, the experimental and theoretical values for absolute binding energies (and their differences) of the $3d$ and $4p$ levels of BaF_2 agree well with each other. Some mismatch (up to 6 eV) between the theoretical and experimental data for LaF_3 is probably due to the larger degree of covalency of this compound.

4. RESULTS AND DISCUSSION

Observed EDC's of LaF_3 , BaF_2 and CsI are given on Figs. 1, 3, 5, 6. The inserts demonstrate the near-edge structures of the M_{45} absorption spectra of these compounds. The upper curves of each Figure (labelled as N) show the "normal"

$M_{45}N_{45}N_{45}$ Auger spectra excited by photons with energies far above the M_{45} thresholds in the region of comparatively small absorption coefficients. Therefore, the normal Auger spectra have a considerably smaller intensities than the EDC's excited at near-edge regions. For

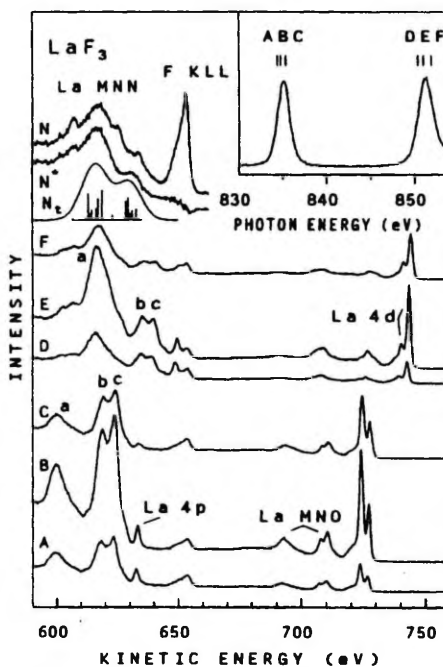


Figure 1. EDC's for LaF_3 . The resonantly excited spectra are normalized to equal photon flux. The $\text{La } M_{45}$ absorption edge is shown in the insert. The capital letters at each EDC corresponds to the vertical bar with the same capital letter in the insert and show the photon energy used. The labels a, b and c indicate the structure elements discussed in the text. N is the normal Auger spectrum excited by 900-eV photons. N' is the normal Auger spectrum after subtraction of the F KLL Auger spectrum. N_1 is the calculated $M_{45}N_{45}N_{45}$ Auger spectrum of La broadened with a Gaussian of 11-eV FWHM.

simultaneous display in the Figures the intensities of the normal spectra are strongly increased in comparison with the resonantly excited EDC's which are normalized to equal photon flux. The normal spectra are compared with calculated $3d^{-1} \rightarrow 4d^{-2}$ Auger transition intensities.

4.1. La in LaF_3

We start the examination of resonantly excited $M_{45}N_{45}N_{45}$ spectra with $\text{La}^{3+}(\text{LaF}_3)$ in which case the $4f$ orbital is collapsed both in core-excited initial and final states, and the $3d$ photoabsorption resonances represent $3d^{-1}4f$ excitations. Fig. 1 shows a set of on-resonance EDC's in a wide energy region which also contains La $4d$ and $4p$ photolines and La MNO and F KLL Auger bands. We can see a strong resonant enhancement of photolines and

significant changes in the $4d_{3/2}:4d_{5/2}$ branching ratio which indicates a high probability and strong term-dependence of the $3d^{-1}4f \rightarrow 4d^{-1}$ autoionization.

In the region of the La MNN transitions a strong and well-developed structure appears which vanishes off-resonance and drastically differs from the normal La $M_{45}N_{45}N_{45}$ bands also shown in Fig. 1. This resonant structure consists of a broad band "a" and a doublet of close-lying bands "b" and "c".

The M_4 on-resonance spectrum (curve E) turns out to be a replica of the M_5 one, shifted energetically exactly by the corresponding increase of the photon energy, with a redistribution of intensities in favor of the band "a". Comparison with the normal Auger spectrum indicates that there might be an extra intensity in the "a"-band region which might be due to normal $M_5N_{45}N_{45}$ transitions. It could be induced by the $M_4M_5N_{67}$ Coster-Kronig decay of the M_4 hole. The common observation for all resonant EDC's of La is that with increasing photon energy the whole resonant structure shifts linearly to higher kinetic energy, thus resembling the behaviour of usual photoelectron lines.

In Fig. 2(a),(b) we compare the observed on-resonance spectra with the calculated $3d^{-1}4f(J=1) \rightarrow 4d^{-2}4f + 4p^{-1}$ spectra. On the energy scale the experimental and theoretical curves are aligned by the $4p_{3/2}$ photoline. As seen, the computed curves well reproduce the major elements of the observed resonant structure. The theory confirms the composite nature of the main resonant bands and the dominance of upper $4d^{-2}4f$ final states in the M_4 decay.

The main uncertainty seems to be connected with the large widths of the measured bands, especially of band "a". Two sources of this broadening may be indicated. First, it is known that creation of single-core-hole states of La in its compounds is accompanied by relaxation processes involving electron transfer from the valence shell of neighbouring atoms to

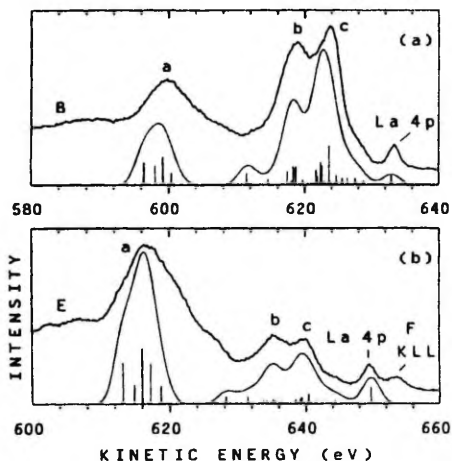


Figure 2. Resonant $M_{45}N_{45}N_{45}$ Auger spectra for LaF_3 (thick lines) as compared to the calculated Auger transitions $3d^{-1}4f(^1D_1) \rightarrow 4d^{-2}4f + 4p^{-1}$ (a) and $3d^{-1}4f(^1P_1) \rightarrow 4d^{-2}4f + 4p^{-1}$ (b) (thin lines). In (a) and (b) are shown, respectively, the spectra B and E of Fig. 1. The computed spectra are broadened with a Gaussian of 3-eV FWHM.

the La 4f level. This effect is thought to account for splitting of the $M_{4,5}$ photolines [14] and appearance of the $3d^{-1}4f \rightarrow 5p^{-1}4f$ lines in the X-ray emission [15] of LaF_3 . It is quite reasonable to suppose the possibility of such screening processes for two-core-hole ionic states, also. Then, the observed normal $M_{45}N_{45}N_{45}$ spectrum of La probably reflects a superposition of transitions between properly weighted different initial ($3d^{-1}$, $3d^{-1}4f$) and final ($4d^{-2}$, $4d^{-2}4f$, $4d^{-2}4f^2$) configurations which may lead to a strong extra broadening.

Second, we cannot exclude the possibility that in the real LaF_3 crystal the upper levels of the $4d^{-2}4f$ multiplet lie slightly above the $4d^{-2}$ ionization limit,

contrary to the predictions of Table 1. Then, a new double Auger decay route $3d^{-1}4f \rightarrow (4d^{-2}4f) \rightarrow 4d^{-2}$ may be opened and affect the shape of the spectrum in the vicinity of band "a".

Thus, the theoretical analysis allows us to attribute the resonant structures of La^{3+} $M_{45}N_{45}N_{45}$ Auger spectra to the $3d^{-1}4f(J=1) \rightarrow 4d^{-2}4f + 4p^{-1}$ transitions. Our calculations show that the width of the $3d^{-1}4f \rightarrow 4d^{-2}4f$ spectator transitions yields about 43% of the total Auger width of $3d^{-1}4f$ photoexcited state both in Ba and La. The partial width of the participator $3d^{-1}4f \rightarrow 4p^{-1}$ decay is term-dependent and has the values of 1.7% for $^3D_1(M_5)$ and 2.3% for $^1P_1(M_4)$ excitations. So, strictly speaking, the resonant structure should be considered as a result of the mixed "spectator-participator" decay of the $3d^{-1}4f$ configuration. However, the relatively small contribution of the participator component justifies the pure spectator approach.

4.2. Barium in BaF_2

The major features of the resonant spectra of Ba^{2+} (BaF_2) presented in Fig. 3 are quite similar to those of La. The $4p_{3/2}$ photoline is followed by the strong doublet "b"- "c" and the broad low-energy band "a", and even the weaker shoulder-like features seen in La spectra are present here, also. This three-band resonant structure moves linearly with exciting photon energy as a photoemission feature and is nicely repeated on the M_4 resonance. However, the latter has an additional broad strong low-energy band, absent in the La case. This band has the same width as the normal $M_5N_{45}N_{45}$ band, and nearly the same energy which does not change with changing photon energy. Therefore, it can be attributed to the normal $M_5N_{45}N_{45}$ channel opened by the $M_4M_5N_{67}$ Coster-Kronig decay. The constant high-kinetic-energy shift (about 2 eV) of this band is most probably related to post-collision interaction (PCI) of a slow Coster-Kronig and a fast Auger electrons.

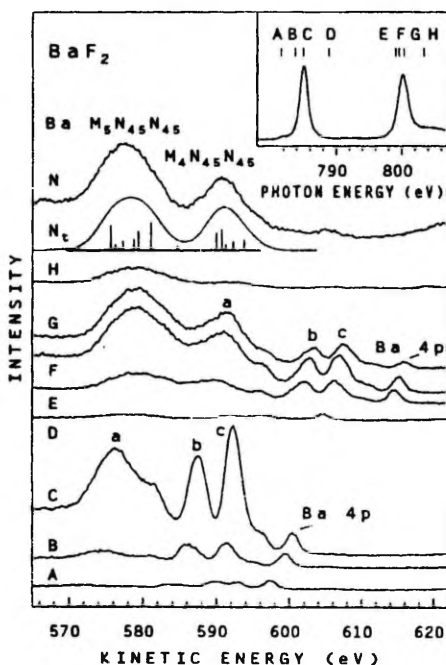


Figure 3. The same as Fig. 1 for BaF_2 . The normal Auger spectrum is excited by 880-eV photons, the calculated spectrum is broadened with a Gaussian of 5-eV FWHM.

Thus, the general similarity of resonant Auger electron spectra (RAES) of photoexcited states of Ba (BaF_2) and La (LaF_3) is evident. However, closer examination reveals some important differences. While the relative intensity and energy separation of the bands "b" and "c" are for Ba nearly the same as for La, their widths (~ 2.8 eV) are significantly smaller. Another peculiarity of band "a" is that by tuning the photon energy its intensity changes differently than that of bands "b" and "c". So, the observed MNN resonant structure seems to consist of two parts, the high-energy region of relatively narrow bands "b", "c", and the low-energy

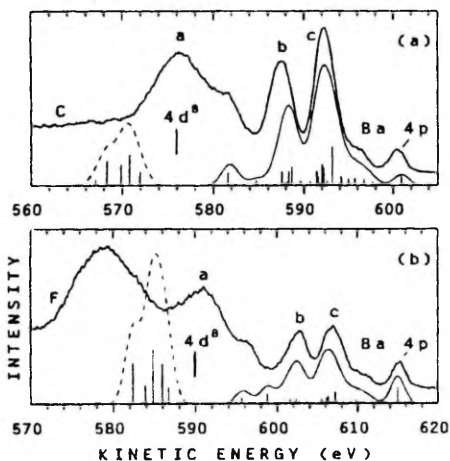


Figure 4. Resonant $M_{45}N_{45}N_{45}$ Auger spectra (thick lines) for BaF_2 as compared to the calculation (thin lines) of the Auger transitions $3d^{-1}4f(^1D_1) \rightarrow 4d^{-2}4f + 4p^{-1}$ (a) and $3d^{-1}4f(^1P_1) \rightarrow 4d^{-2}4f + 4p^{-1}$ (b). In (a) and (b) are shown, respectively, the spectra C and F of Fig. 3. The dashed part of the computed spectra corresponds to the $4d^{-2}4f$ states with energies lying above the $4d^{-2}$ threshold (labelled by the vertical bars). The computed spectra are broadened with a Gaussian of 2-eV FWHM.

region of band "a".

In Fig. 4 the observed on-resonance M_{45} spectra are compared with computed $3d^{-1}4f \rightarrow 4d^{-2}4f + 4p^{-1}$ spectra. The calculations reasonably well reproduce the high-energy region of the measured spectra, but there is a clear mismatch in the low-energy region which cannot be compensated for by the reduction of electrostatic integrals. The calculations show that band "a" lies at the energies where the $4d^{-2}$ threshold is expected to be found. In Fig. 4 these thresholds, i.e. the lowest-binding-energy states of $4d^{-2}$ ionic configuration are marked as the vertical bars on the kinetic energy scale by using the data of Table 1 and the theoretical $3d^{10} \rightarrow 3d^9 4f$ excitation energies (788.7 eV for 3D_1 and 803.8 eV for 1P_1 states). The $4d^{-2}4f$ states with energies above this threshold (dashed parts of theoretical curves) seem not to contribute to the final structure. So, theory gives a suitable explanation to the above-made empirical division: the region of resonant bands "b" and "c" corresponds to the $4d^{-2}4f$ states lying below the $4d^{-2}$ limit. Only these bands could be considered as the true $4f$ spectator features.

The interpretation of the broad low energy band "a" is, however, much more complicated. Our theoretical results allow to suggest that the band "a" is induced by the $3d^{-1}4f \rightarrow 4d^{-2}$ Auger shake-off-like transitions. These transitions are expected to produce electrons with kinetic energies slightly lower than the $3d^{-1} \rightarrow 4d^{-2}$ transitions. As seen in Fig. 3, the band "a" nearly coincides with its "normal" counterpart at on-resonance conditions. On the other hand, it has a clearly different shape than the "normal" band which is at least by 2.5 eV broader. However, the proper theoretical solution of this problem is beyond our model.

4.3. Cesium and iodine in CsI

The resonant spectra of I (Fig. 5) and Cs (Fig. 6) are completely different from those of La and Ba. They are dominated by the

"normal" photon-energy-independent M_5 and M_4 structures, shifted slightly (by ~ 1 eV for Cs and ~ 0.5 eV for I) to higher energies most probably by PCI effects (in curves G and H of Fig. 5 the $M_5N_{45}N_{45}$ band of iodine is slightly distorted by overlapping the Cs $4p_{3/2}$ photoline).

The situation is fully understandable in the light of the nature of the near-edge 3d excitations of I and Cs: as the 4f orbital is not collapsed the $3d^{-1} \rightarrow 4d^{-2}$ transitions dominate the resonantly excited MNN spectra. In this sense our RAES data once more confirm that the M_{45} near edge absorption bands of these ions are caused

by transitions to above-threshold states.

However, the resonant spectra of Cs contain two additional weaker bands pronounced most clearly on the curves B and E of Fig. 6. Their relative positions (between the $4p_{3/2}$ photoline and normal MNN bands) and widths (about 2.1 eV) as well as the photon energy dependence closely follow the behaviour of the 4f spectator bands "b" and "c" of Ba and La. It is natural to suggest that they also belong to a 4f-spectator-like structure. The calculation of $3d^{-1}4f \rightarrow 4d^{-2}4f + 4p^{-1}$ spectra for Cs^+ , using a collapsed 4f orbital, fully supports this suggestion. Thus, we conclude that the observed

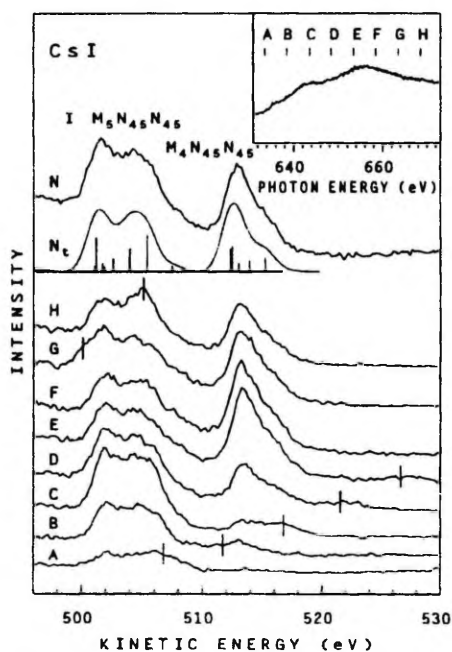


Figure 5. The same as Fig. 1 for I in CsI. The normal Auger spectrum is excited by 800-eV photons, the calculated spectrum is broadened with a Gaussian of 2-eV FWHM. The positions of the Cs $4p_{3/2}$ photoline in spectra H and G, and of the I $4p_{3/2}$ photoline in spectra A to E are indicated by vertical bars.

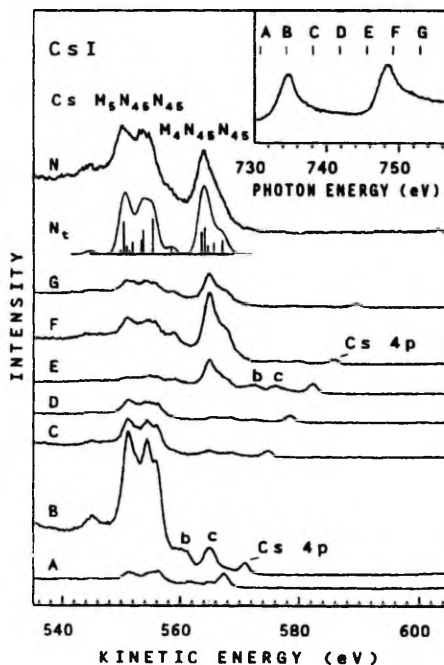


Figure 6. The same as Fig. 1 for Cs in CsI. The normal Auger spectrum is excited by 850-eV photons, the calculated spectrum is broadened with a Gaussian of 2-eV FWHM.

resonant MNN spectra of Cs contain simultaneously the $3d^{-1} \rightarrow 4d^{-2}$ and $3d^{-1}4f \rightarrow 4d^{-2}4f$ -like structures. In other words, the M_{45} near-edge photoexcitations of Cs exhibit both continuous ($3d \rightarrow \epsilon f$) and localized ($3d \rightarrow 4f$) character.

This dualistic nature of the $3d$ -excitations of Cs has earlier been observed in the M_{45} X-ray emission of Cs in CsCl [4]. Now we may add that RAES seems to be a very sensitive technique to investigate such "partially localized" excitations. In our case the apparent localization of the

excited-state electron may be considered as a result of the interaction of a low-energy ϵf photoelectron with a fast Auger electron leading to the recapture of the photoelectron by the ionized core and, subsequently, to the shake-down-like transitions $3d^{-1}\epsilon f \rightarrow 4d^{-2}4f$. A similar explanation was used to interpret the ion yield spectra of Ar near its L_{23} thresholds [16].

4.4. Branching ratios of 4d photolines.

In Fig. 7 are shown the EDC spectra of Cs^+ in CsI, Ba^{2+} in BaF_2 and La^{3+} in LaF_3 in the region of the $4d_{5/2,3/2}$ photolines excited at the M_{45} edge of cations. The resonant enhancement of 4d photolines and changes in the $4d_{3/2}:4d_{5/2}$ branching ratio are clearly seen. The effect is very strong for Ba and La, for Cs it is less expressive, but still visible. The branching ratio of the $4d_{3/2}$ and $4d_{5/2}$ photoemission bands at the $M_4(^1P_1)$ resonance excitation is about 0.24 for Ba and 0.5 for La, i.e. far from the statistical value 4:6 [as the low energy tail of the $4d_{3/2}$ photoline of La in LaF_3 introduces some uncertainty in the area below this line profile, the branching ratio after subtraction of the background may be substantially smaller). For the excitation at the $M_5(^3D_1)$ resonance the $4d_{3/2}$ photoline becomes more intense than the $4d_{5/2}$ photoline, the branching ratio being about 1.9 for Ba and 3.6 for La. The branching ratio for Cs is 0.54 at the M_4 excitation and 1.0 at the M_5 excitation.

Similar strong term-dependence and anomalous change of the branching ratio of $5p_{1/2}$ to $5p_{3/2}$ photolines have been observed at the $4d \rightarrow 4f$ resonant excitation of La in LaF_3 and Ba in BaF_2 [17] and attributed to the multiplet dependence of the Auger transition probabilities [18].

Our theoretical analysis of the Auger decay channels of the $3d^{-1}4f(J=1)$ excited states with collapsed 4f orbital show that the participator $3d^{-1}4f \rightarrow 4d^{-1}$ decay channel has a significant probability. Its partial widths are term-dependent,

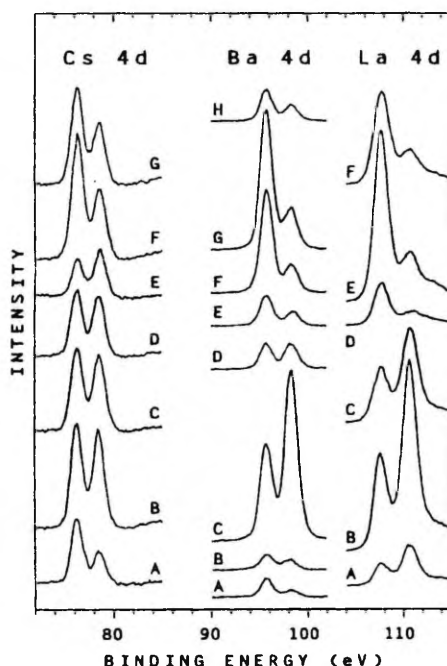


Figure 7. EDC's of Cs^+ in CsI, Ba^{2+} in BaF_2 and La^{3+} in LaF_3 in the region of the $4d_{5/2,3/2}$ photolines excited at the M_{45} absorption edge of cations. The spectra are normalized to equal photon flux. The capital letter at each EDC correspond to the vertical bar with the same capital letter in the inserts of Figs. 1, 3, 6 and show the photon energy used.

similarly to the $3d^{-1}4f \rightarrow 4p^{-1}$ channel discussed in Sect. 4.1, but are considerably larger: 8.7%(7.4%) for 3D_1 and 15.0%(11.5%) for 1P_1 excitations in $La^{3+}(Ba^{2+})$. In Fig. 8 we compare the experimental EDC's of La in LaF_3 and Ba in BaF_2 in the region of 4d photolines with the calculated $3d^{-1}4f(J=1) \rightarrow 4d^{-1}$ Auger spectra. The computed curves satisfactorily reproduce the intensity variations of the observed spectra. The somewhat smaller strength of the $4d_{5/2}$ photoline relative to the $4d_{3/2}$ photoline in the observed spectra as compared to the theoretical spectra is mainly due to

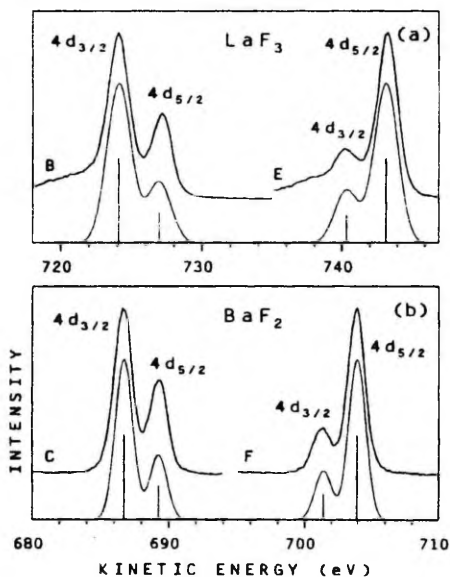


Figure 8. EDC's of La in LaF_3 (a) and Ba in BaF_2 (b) in the region of 4d photolines (thick lines) as compared to the calculated Auger transitions $3d^{-1}4f(^1D_1) \rightarrow 4d^{-1}$ and $3d^{-1}4f(^1P_1) \rightarrow 4d^{-1}$ (thin lines). In (a) and (b) are shown, respectively, the spectra B and E of La in LaF_3 , and the spectra C and F of Ba in BaF_2 of Fig. 7. The computed spectra are broadened with Gaussians of 2-eV (a) and 1.5-eV (b) FWHM.

simultaneously excited direct $4d^{10} \rightarrow 4d^9$ photoemission lines. The theoretical $4d_{3/2}:4d_{5/2}$ branching ratio for Auger transitions $3d^{-1}4f \rightarrow 4d^{-1}$ of $La^{3+}(Ba^{2+})$ is 2.6(2.5) for 3D_1 resonant excitation and 0.33(0.31) for 1P_1 excitation. Therefore, our computations suggest that the change of the $4d_{3/2}:4d_{5/2}$ branching ratio in resonant photoemission originates mainly from the Auger participator transitions $3d^{-1}4f \rightarrow 4d^{-1}$.

On the other hand, our calculations show that for Cs^+ in CsI the partial widths of participator decay of $3d^{-1}4f$ excited states with delocalized 4f orbital become negligible. So, we may conclude that the resonant enhancement of photolines as well as the anomaly in the branching ratios indicate that the excited 4f orbital is localized. In the case of Cs in CsI the effect seems to be due to the PCI-induced recapture of the slow ef or 4,ef photoelectron, i.e. to the transition $3d^{-1}ef(4,ef) \rightarrow 4d^{-1}$, similarly to the spectator-like structure in the $M_{45}N_{45}N_{45}$ spectra of Cs (see Sec.4.3).

5. CONCLUSIONS

We have measured the energy distribution curves of ejected electrons of CsI , BaF_2 , and LaF_3 in the region of $M_{45}N_{45}N_{45}$ Auger transitions in xenon-like iodine, cesium, barium, and lanthanum ions, varying the energy of exciting photons stepwise through the M_{45} absorption structure of these ions. The spectra show drastic changes of the decay pattern of $3d^{-1}$ excitations in this sequence of isoelectronic ions. For I all spectra observed contain only the normal $M_{45}N_{45}N_{45}$ Auger structure which arises as a result of the $3d^{-1} \rightarrow 4d^{-2}$ transitions. In contrast, the spectra of La and Ba excited at their $3d^{10} \rightarrow 3d^9 4f$ resonances, exhibit a very intensive new structure which changes its energy and intensity with the energy of the exciting photons and is induced by the spectator 4f

electron. In the case of Ba this structure coexists with the normal Auger structure, the latter appearing as a result of the $M_4M_5N_{67}$ Coster-Kronig transitions. The spectra of Cs are similar to those of I, except for a small admixture of the spectator structure visible at resonance excitation. It is caused by the Auger shake-down transitions from intermediate states with excited electron in the near-edge continuous ϵf or/and resonantly localized $4f$ orbitals. At the resonance excitation energies the intensity ratio of $4d_{3/2}$ and $4d_{5/2}$ photoelectron lines of La and Ba has an anomalous behaviour due to the strong term-dependence of the participator Auger process.

Calculation of the Auger decay of the $3d^{-1}4f$ configuration shows that the resonant structure for Ba and La is to be ascribed to transitions to the $4d^{-2}4f + 4p^{-1}$ final configuration. Its shape is influenced by the solid-state modifications of energy separation between final configurations $4d^{-2}$ and $4d^{-2}4f + 4p^{-1}$.

ACKNOWLEDGEMENTS

We wish to acknowledge the contribution of Dr. J. F. van Acker, Dr. J. N. Andersen, Dr. M. Qvarford, Dr. R. Nyholm, Dr. A. Ausmees, and Professor I. Martinson to experiments and discussions. This work was supported by the Swedish Natural Sciences Research Council, the Estonian Science Foundation, the Crafoord Foundation, and the Royal Swedish Academy of Sciences.

REFERENCES

1. M. Elango, A. Ausmees, A. Kikas, E. Nõmmiste, R. Ruus, A. Saar, J.F. van Acker, J.N. Andersen, R. Nyholm, and I. Martinson, *Phys. Rev.* **B47** (1993) 11736.
2. T. Åberg, *Physica Scripta* **T41** (1992) 71.
3. A.A. Maiste, R.E. Ruus, S.A. Kuchas, R.I. Karaziya, and M.A. Elango, *Sov. Phys.-JETP* **51** (1980) 474.
4. P. Motais, E. Belin, and C. Bonnelle, *Phys. Rev.* **B25** (1982) 5492.
5. J.N. Andersen, O. Björneholm, A. Sandell, R. Nyholm, J. Forsell, L. Thånell, A. Nilsson, and N. Mårtensson, *Synchrotron Radiation News* **4** (1991) 15.
6. T.H. DiStefano and W.E. Spicer, *Phys. Rev.* **B7** (1973) 1554.
7. G.W. Rubloff, *Phys. Rev.* **B5**, 662 (1972).
8. D.W. Lynch and G.G. Olson, *Solid State Comm.* **12** (1973) 661.
9. A.A. Nikitin and Z.B. Rudzikas, *Foundations of the Theory of the Spectra of Atoms and Ions* (Nauka, Moscow, 1983, in Russian).
10. A.C. Parry-Jones, P. Weightman, and P.T. Andrews, *J. Phys.* **C12** (1979) 1587.
11. R.E. Watson, *Phys. Rev.* **111** (1958) 1108.
12. W. van Gool and A.G. Piken, *J. of Materials Science* **4** (1969) 95.
13. N.F. Mott and R.W. Gurney, *Electronic Processes in Ionic Crystals* (Clarendon, Oxford, 1948).
14. S. Suzuki, T. Ishii, and T. Sagawa, *J. Phys. Soc. Japan* **37** (1974) 1334.
15. P. Motais, E. Belin, and C. Bonnelle, *Phys. Rev.* **B30** (1984) 4399.
16. J. Tulkki, T. Åberg, S.B. Whitfield, and B. Crasemann, *Phys. Rev.* **A41** (1990) 181; W. Eberhardt, S. Bernstorff, H.W. Jochims, S. B. Whitfield, and B. Crasemann *ibid.* **38** (1988) 3808.
17. K. Ichikawa, O. Aita, K. Aoki, M. Kamada, and K. Tsutsumi, *Phys. Rev.* **B45**, 3221 (1992); M. Kamada, K. Ichikawa, and O. Aita *ibid.* **47** (1993) 3511.
18. H. Ogasawara, A. Kotani, B.T. Thole, K. Ichikawa, O. Aita, and M. Kamada, *Solid State Comm.* **81** (1992) 645.

M. Elango, R. Ruus, A. Kikas, A. Saar, A. Ausmees, and I. Martinson,
Interplay of atomic and solid-state effects in inner-shell-resonant
photoelectron spectra, *Phys. Rev. B*, **53**, (1996), R5978–R5981.

Interplay of atomic and solid-state effects in inner-shell-resonant photoelectron spectra

M. Elango*

*Institute of Experimental Physics and Technology, Tartu University, Ülikooli 18, EE2400 Tartu, Estonia
and Institute of Physics, Estonian Academy of Sciences, Riia 142, EE2400 Tartu, Estonia*R. Ruus, A. Kikas, A. Saar, and A. Ausmees[†]*Institute of Physics, Estonian Academy of Sciences, Riia 142, EE2400 Tartu, Estonia*

I. Martinson

Department of Atomic Spectroscopy, Lund University, Sölvegatan 14, S-223 62 Lund, Sweden

(Received 22 September 1995)

We report photoelectron spectra of metal chlorides excited in the vicinity of the chlorine 2*p* absorption edge. The spectra of RbCl, which has a narrow valence band, exhibit a strong resonance behavior. Hartree-Fock calculations show that the absorption final states are the atomlike Frenkel excitons. Their decay is dominated by the Auger process where the final-state 4*s* and 3*d* electrons behave as spectators. In the sequence of chlorides with increasing width of the valence band the atomlike resonance effects are continuously replaced by the bandlike shape of the spectra.

An interesting experimental procedure, combining inner-shell resonant-photoelectron and Auger spectroscopy, and made available by the recent development of combined synchrotron radiation and electron spectroscopy techniques, has already exposed its ability to disclose complex dynamics of inner-shell excitations of atoms,¹ molecules,² and different types of solids.³⁻⁵ For nonmetallic solids, the phenomena connected with this procedure have been especially clearly emphasized in the 2*p*-resonant photoelectron spectra of elements for which the 3*p* shell is the outermost filled shell. The elements at the end of the second period, such as silicon⁶ and phosphorus,⁷ which form semiconductors with wide 3*p*-related valence bands, expose very weak (if any) resonance effects, the main feature being the appearance of the $L_{23}M_{23}M_{23}$ normal Auger spectrum at the ionization threshold of the 2*p* shell. Contrary, the argonlike ions of potassium, calcium, and scandium in ionic solids exhibit strong resonance effects,^{3,8} characteristic for the Auger-resonant inelastic scattering.¹

Here we report the results of a study for the L_{23} absorption edge of Cl^- ions, constituents of metal chlorides. This choice puts us into an intermediate situation between the two groups of atoms (ions) described above, and gives hope to build a link between them.

The experiments are performed using synchrotron radiation from beamline 22 at the MAX-laboratory, Lund University, Sweden. The monochromator is a modified SX-700 plane grating monochromator with energy resolution of 0.13 eV in the actual photon energy region. The electron spectra are recorded by a hemispherical analyzer Scienta SES-200 with energy resolution of 0.075 eV. The samples, the films of metal halides, are evaporated *in situ* from a molybdenum boat onto a stainless-steel substrate. The film thickness (about 100 Å) is controlled by a quartz monitor. Other experimental details are described in Ref. 3.

In Fig. 1 a set of electron spectra of RbCl induced by photons in the region of the $\text{Cl}^- L_{23}$ absorption edge is

shown. The absorption spectrum measured in the electron yield mode is exposed in the inset. Considering the absorption final states as the empty *s*- and *d*-like conduction-band states the comparison with the band-structure calculations⁹ leads to the scenario where the first few absorption maxima reflect the core excitons at the Γ_1 and X_3 points of the Brillouin zone (see, e.g., Ref. 10).

Three groups of lines may be distinguished in the electron spectra (Fig. 1). All spectra, starting from the bottom spectrum, the nonresonant pre-edge spectrum, show the $\text{Cl}^- 3p$ valence band, the $\text{Rb}^+ 4p$, $\text{Cl}^- 3s$, and $\text{Rb}^+ 4s$ photoelectron lines. With increasing photon energy this group keeps a constant binding energy. The intensity of the photoelectron lines does not exhibit any noticeable changes in the resonance regions, indicating a minor role of the participator Auger transitions in the decay of corresponding excitations. The second group is made up of the $L_{23}M_{23}M_{23}$ normal Auger lines composed of two sets of the 1S , 1D , and 3P terms of the final $3p^{-2}$ electron configuration shifted relative to each other by the 1.6-eV spin-orbit splitting of the 2*p* shell. This group has a constant kinetic energy. When the photon energy approaches the first absorption maximum, the third group of bands appears between the first and second groups. This group clearly exhibits a resonance behavior: it is fully developed at the maximum of the first absorption band (spectrum 5), almost disappears in the region between the first and second absorption bands, and reappears with a modified shape in the regions of the second (spectrum 9) and third (spectrum 13) absorption maxima.

For these spectra we use the theoretical model applied to analogous spectra of K^+ in Ref. 3. We treat an inner-shell excitation and its Auger decay as a two-step process. For the first step, the absorption process, the energies, and intensities of the $2p^6 \rightarrow 2p^5 4s(3d)$ transitions in the Cl^- ion are calculated in the intermediate coupling scheme and the Hartree-Fock-Pauli approximation in conjunction with the Watson sphere model. The depth of the potential well at the Cl^- site

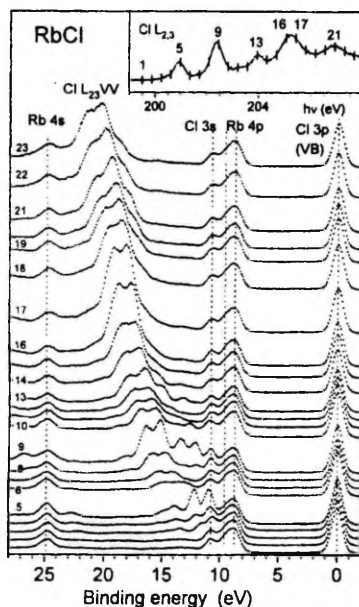


FIG. 1. Photoemission spectra for RbCl. The $\text{Cl}^- L_{23}$ absorption edge is shown in the inset. The number at each spectrum corresponds to the vertical bar with the same number in the inset and shows the photon energy used. The spectra are normalized to equal photon flux. The energy levels and corresponding Auger transitions are indicated for most of the structures. The binding energy is related to the valence-band maximum.

V_c is taken equal to 7.65 eV, the Madelung energy of the RbCl crystal, which leads to the mean radii of 5.8 (9.8) a.u. for the $4s(3d)$ orbitals. The calculated energies of the transitions $2p_{3/2}-4s$, $2p_{1/2}-4s$, $2p_{3/2}-3d$, and $2p_{1/2}-3d$ in Cl^- ions are 200.0, 201.6, 202.3, and 203.9 eV, respectively. They are reasonably close to the energies of the first three absorption maxima (200.9, 202.4, and 204.0 eV, respectively). Moreover, the calculated intensity ratio of these transitions, 33:50:17 (the second transition is here considered as a superposition of the transitions $2p_{1/2}-4s$ and $2p_{3/2}-3d$) is also very close to the observed intensity ratio 28:60:12 of these maxima. This comparison indicates that the interpretation of the absorption spectrum in terms of atomiclike Frenkel excitons may well compete with the traditional interpretation based on the calculated structure of the undisturbed conduction band.¹⁰

For the second step, the Auger process, the normal $2p^2-3p^4$ as well as the spectator $2p^3 4s(3d)-3p^4 4s(3d)$ transitions are calculated. The radial integrals (F^k, G^k) for Auger final states are reduced by comparison with their Hartree-Fock values [by 30 and 25% for the $3p^4$ and $3p^3 4s(3d)$ configurations, respectively]. As this calculation overestimates the decay rates to the 3P term of the final configuration, the term intensities in the normal and $4s$ -spectator Auger spectra of Cl^- are corrected by scaling fac-

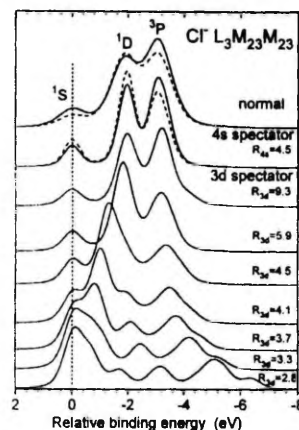


FIG. 2. Calculated $\text{Cl}^- L_3 M_{23} M_{23}$ Auger spectra for RbCl. The zero binding energy corresponds to the transition energy of the highest level of the final ionic configuration. The normal, $4s$, and $3d$ spectator spectra are broadened by the Voigt function with FWHM of 1.1, 0.7, and 0.8 eV, respectively. The depth of the Watson sphere for the $3d$ -spectator Auger spectra varies from zero (the uppermost spectrum) to 16.3 eV (the bottom spectrum). The mean radius of the spectator electron R_{3d} in the final ionic configuration is indicated at each spectrum. The dashed spectra are corrected ones using the experimental data for argon atoms (see text).

tors which lead to the correct description of analogous experimental spectra of the isoelectronic Ar atoms.¹¹ Some of the calculated Auger spectra are shown in Fig. 2.

Spectrum 5 of Fig. 1, after subtraction of the background and photoelectron lines represented by the pre-edge spectrum 1, is reproduced in Fig. 3(a). The calculated $4s$ -spectator $L_3 M_{23} M_{23}$ Auger spectrum well fits most of it. The remaining part (the broken curve) in the high-binding-energy region well fits the calculated normal $L_3 M_{23} M_{23}$ Auger spectrum. This similarity shows that the intensity of the participator process ($2p^{-1} 4s-3s^{-1}$) is negligible (this process should result in the resonant enhancement of the single-peak photoelectron line). In addition, the absence of the resonant enhancement of the valence ($\text{Cl}^- 3p$) band shows that the overlap of the wave functions of the loosely bounded excited electron and the core electron (which is included in the radial integral for participator process, but not included in the case of spectator process) is small, which is natural for the $4s$ excited state. So, the resonant structure may be unambiguously assigned to the $2p^3 4s-3p^4 4s$ pure-spectator Auger transition, shifted by 2.5 eV to the higher energy relative to the normal Auger spectrum.

Spectrum 9 of Fig. 1 is reproduced in Fig. 3(b). It may be understood as a superposition of three properly weighted components: (i) the $4s$ -spectator $L_3 M_{23} M_{23}$ Auger transition which originates from the decay of the $2p_{1/2} 4s$ state, (ii) the normal $L_3 M_{23} M_{23}$ Auger transition, which reflects ionization of the $2p_{3/2}$ subshell, and (iii) the $3d$ -spectator $L_3 M_{23} M_{23}$ Auger transition, which arises from the $2p_{3/2} 3d$ state. The calculated $2p_{3/2} 3d-3p^4 3d$ Auger spectrum is very sensitive

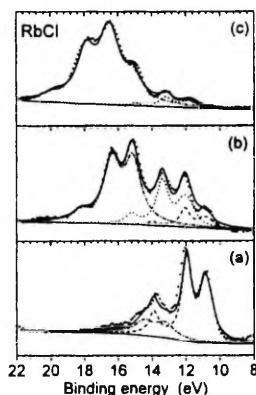


FIG. 3. The resonant photoemission spectra 5 (a), 9 (b), and 13 (c) from Fig. 1 (filled circles) and their components. The nonresonant background and photoelectron lines (spectrum 1 in Fig. 1) are subtracted. The Voigt functions which represent the calculated normal (dash-dotted line, FWHM=1.2 eV), 4s-spectator (dashed line, FWHM=0.7 eV), and 3d-spectator (dotted line, FWHM=0.8 eV) contributions to measured spectra and the resulting theoretical spectrum (solid line) are shown. The calculated spectra are shifted in the energy scale to fit the experimental spectra (by about 2–3 eV).

to the choice of V_c and, thus, to the mean radius of the 3d wave function of the final configuration R_{3d} . The small values of R_{3d} , which correspond to the collapsed 3d electron, lead to a spectrum very similar to the corresponding spectra of Ar (Ref. 11) and K^+ (Ref. 3). With increasing R_{3d} the spectrum obtains the two-band structure observable for Cl^- . If we change the fit parameter V_c systematically, the best fit for the third component of the spectrum is obtained with $V_c=4.35$ eV ($R_{3d}=5.9$ a.u.). Thus, the main effect of the spectator 3d electron is the 3.0-eV high-energy shift of the normal Auger spectrum together with some modification of its shape. Note that although in these general terms the effects of the 4s and 3d spectators on the $L_{23}M_{23}M_{23}$ Auger spectra are very similar, the careful comparison allows us to distinguish them firmly and use them as fingerprints of excitations of different nature. The underlying physics reduces mainly to the different multiplet coupling in the $3p^{-2}4s$ and $3p^{-2}3d$ configurations.

In Fig. 3(c) the Auger spectrum excited at the third absorption maximum (spectrum 13 of Fig. 1) is shown. It is dominated by the normal $L_{23}M_{23}M_{23}$ structure. In its low-energy part the resonant 3d-spectator $L_2M_{32}M_{23}$ structure is clearly visible and proves the *d* character of states responsible for this absorption band.

The normal Auger spectrum may be firmly identified in all spectra starting from spectrum 6 (Fig. 1). This means that above a photon energy of about 201.3 eV the transition electron has a noticeable probability of leaving the reaction region before or during the Auger transition. In a solid, such a threshold is naturally interpretable as the bottom of the conduction band for transitions from the $2p_{3/2}$ shell. However, the spurs of the normal $L_3M_{23}M_{23}$ structure may also be

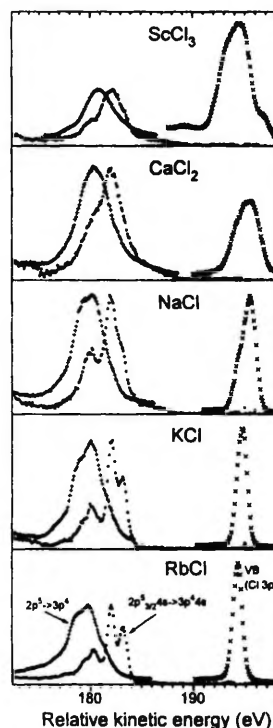


FIG. 4. The resonant (filled circles) and normal (crosses) Auger spectra and valence-band photoelectron spectra (sloping crosses) for several chlorides. The photoelectron lines are subtracted from the resonant spectra. The spectra are excited correspondingly at the first L_{23} absorption structures, far from the ionization thresholds (the photon energies used are 206 eV for $ScCl_3$, 220 eV for NaCl, KCl, and $CaCl_2$, and 212 eV for RbCl), and below absorption edges of corresponding compounds. The spectra are aligned to match the maxima of the resonant spectra. The Auger spectra of each compound are normalized to equal height.

found in the spectra excited with lower-energy photons indicating that the ionization threshold is rather smooth. This may be due to some inhomogeneous broadening of the threshold and/or to shake-up of the near-threshold excited electrons. The shape of a particular normal Auger spectrum depends on the relative weight of its L_3 and L_2 components. So, the spectra 12–14 and 18–23 clearly exhibit the 3P band of the $L_2M_{23}M_{23}$ spectrum, indicating that the absorption bands at 204.0 and 206.8 eV reflect transitions from the L_2 shell. Instead, the absorption band at 205.2 eV may be related to transitions from the L_3 shell.

Thus, the creation and decay of excitations related to the chlorine 2p shell of RbCl may be reasonably well understood in terms of atomic processes within chlorine ions. The main qualitative solid-state effect is the existence of an ionization threshold above which the transition electron is trans-

ferred into the conduction band. To disclose how much this atomiclike behavior is related to the extremely narrow valence band (VB) of RbCl we have studied the evolution of the resonant and normal $L_{23}M_{23}M_{23}$ Auger spectra in a sequence of chlorides with different VB widths. In Fig. 4 these spectra for RbCl, KCl, NaCl, CaCl_2 , and ScCl_3 are compared. The full width at half maximum (FWHM) of the VB of these compounds was estimated as 1.0, 1.1, 1.7, 2.8, and 3.0 eV, respectively, for RbCl, KCl, and NaCl in good accordance with the recent data of Ref. 12. The main effect, clearly seen in Fig. 4, is that with increasing VB width the resonant as well as normal Auger structures become wider and approach each other. The resonant spectrum loses its atomiclike nature characteristic for narrow-VB RbCl and obtains the solid-state nature characteristic for wide-VB semiconductors.^{6,7}

To conclude, we have shown, that the photoelectron and Auger spectra of RbCl exhibit a strong resonance behavior when the energy of incident photons passes through the L_{23} absorption edge of chlorine. Somewhat surprisingly, the spectra may be understood in terms of atomic transitions. In the sequence of chlorides with increasing VB width the atomiclike resonance effects are continuously replaced by the bandlike shape of the spectra. These results clarify the regularities of the structure of the $2p$ -resonant electron spectra of other solids.

The investigations were financially supported by the Estonian Science Foundation, the Swedish Natural Science Research Council, the Swedish Institute, and the International Science Foundation. The authors wish to thank Dr. E. Nõmmiste, Dr. R. Nyholm, and Dr. A. Maiste for their assistance and discussions.

*Deceased.

[†]Present address: Department of Physics, University of Uppsala, Box 530, S-75121 Uppsala, Sweden.

¹G. B. Armen *et al.*, Phys. Rev. Lett. **54**, 1142 (1985).

²W. Eberhardt, in *Applications of Synchrotron Radiation*, edited by W. Eberhardt (Springer, Berlin, 1995), p. 203.

³M. Elango *et al.*, Phys. Rev. B **47**, 11 736 (1993).

⁴H. Wang *et al.*, Phys. Rev. A **50**, 1359 (1994).

⁵W. Drube, R. Treusch, and G. Materlik, Phys. Rev. Lett. **74**, 42 (1995).

⁶K. L. I. Kobayashi, H. Daimon, and Y. Murata, Phys. Rev. Lett.

50, 1701 (1983); R. A. Riedel *et al.*, *ibid.* **52**, 1568 (1984).

⁷T. Kendelewicz *et al.*, Phys. Rev. B **30**, 2263 (1984); T. Takashi *et al.*, *ibid.* **33**, 1485 (1986).

⁸A. Saar *et al.*, Phys. Rev. B **51**, 3202 (1995).

⁹Y. Onodera and Y. Toyozawa, J. Phys. Soc. Jpn. **22**, 833 (1967).

¹⁰M. Watanabe, J. Phys. Soc. Jpn. **34**, 755 (1973).

¹¹M. Meyer, E. von Raven, and B. Sonntag, Phys. Rev. A **49**, 3685 (1994); L. O. Werme, F. Bergmark, and K. Siegbahn, Phys. Scr. **8**, 149 (1973).

¹²G. K. Wertheim *et al.*, Phys. Rev. B **51**, 13 675 (1995).

R. Ruus, A. Kikas, A. Saar, A. Ausmees, E. Nõmmiste, J. Aarik, A. Aidla, T. Uustare,
and I. Martinson, Ti 2p and O 1s X-ray absorption of TiO₂ polymorphs,
Solid State Commun. **104**, (1997), 199–203.



PII: S0038-1098(97)00300-1

Ti 2p AND O 1s X-RAY ABSORPTION OF TiO₂ POLYMORPHSR. Ruus,^a A. Kikas,^a A. Saar,^a A. Ausmees,^b E. Nõmmiste,^c J. Aarik,^d A. Aidla,^d T. Uustare^d and I. Martinson^c^aInstitute of Physics, Riia 142, EE2400 Tartu, Estonia^bDepartment of Physics, Uppsala University, Box 530, S-751 21, Uppsala, Sweden^cDepartment of Physical Sciences, University of Oulu, FIN-90570 Oulu, Finland^dInstitute of Material Science, University of Tartu, Ülikooli 18, EE2400 Tartu, Estonia^eDepartment of Atomic Spectroscopy, Lund University, Sölvegatan 14, S-223 62 Lund, Sweden

(Received 4 May 1997; accepted 25 June 1997 by B. Lundqvist)

We present and discuss the Ti 2p and O 1s X-ray absorption spectra (XAS) and resonant photoelectron emission spectra (RPES) of the various polymorphic forms (TiO₂-II, rutile and anatase) of TiO₂. The largest differences between the Ti 2p XAS of polymorphs of TiO₂ are observed in the region of the double peak structure of the L₃ edge. A strong delocalization of the excited 3d electron in this region is concluded from the RPES at the L₃ threshold of Ti. The differences in XAS are attributed to increasing strength of the crystal field caused by delocalization of the excited 3d electron.
© 1997 Elsevier Science Ltd

Keywords: A. insulators, A. thin films, C. NEXAFS, D. crystal and ligand fields.

Titanium dioxide (TiO₂) has been extensively studied in last years due to its large variety of applications. Many of these applications are based on the specific electronic properties of TiO₂. TiO₂ has several polymorphic forms which have rather different properties. Tetragonal anatase and rutile as well as orthorhombic brookite which can be synthesized at atmospheric and subatmospheric pressures are the "low-pressure" crystal modifications. Orthorhombic TiO₂-II and monoclinic baddeleyite-type TiO₂ are the high-pressure polymorphs of titanium dioxide. Baddeleyite-type TiO₂ exists only at high pressures, while TiO₂-II is most frequently synthesized at high-pressures and by shock-waves (e.g. [1]) and is metastable at atmospheric pressure and temperatures up to 600°C [1, 2]. Recently TiO₂-II has been obtained at the atmospheric and subatmospheric pressures by using ball milling of anatase [3], electron-beam irradiation of rutile [4], dissolving Ti₂O₃ in sulphuric acid [5] and the atomic layer deposition method [2, 6].

A comparative XAS and RPES study of polymorphic forms of TiO₂ enables one to elucidate the influence of the crystal structure on the electronic system of a compound. Previous experimental and theoretical studies of Ti 2p [7–11] and O 1s [9, 10, 12] XAS of low-pressure

TiO₂ phases suggest that theory provides generally an adequate interpretation of the spectra. Nevertheless, the high-energy part of the Ti L₃ XAS and its structural sensitivity remains unexplained by a ligand field multiplet model. In order to study the influence of the structure on the excited states we perform XAS and RPES studies of TiO₂-II, rutile and anatase. To our knowledge, XAS of TiO₂-II and RPES of all these compounds are presented for the first time in this paper. In this work we have concerned the behavior of the XAS of TiO₂ and the RPES has been employed to interpret the absorption spectra. A more detailed study of RPES of TiO₂ will appear elsewhere.

The XAS and RPES of TiO₂ polymorphs were measured at beamline 22 of the MAX-LAB, Lund, Sweden. The monochromator SX-700 energy resolution of 0.2 eV and the electron energy analyser Scienta SES-200 resolution of 0.3 eV were used. The absolute energy scale of XAS for the anatase was adjusted to agree with electron energy loss spectroscopy data [9]. TiO₂ films were grown *ex situ* on (111)-oriented silicon substrates using the low-pressure flow-type atomic layer deposition reactor described elsewhere [13]. The growth was accomplished by alternate leading volatilized

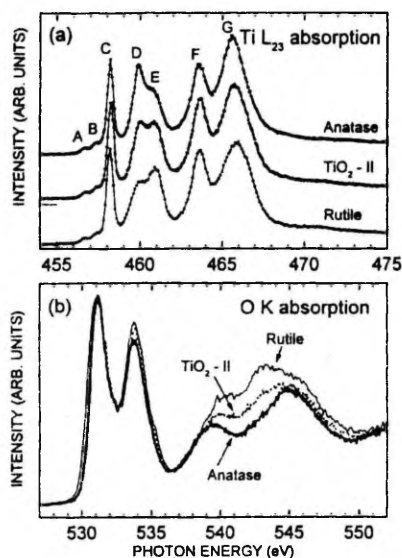


Fig. 1. The Ti 2p (a) and O 1s (b) absorption spectra of polymorphic forms of TiO₂ (anatase, TiO₂-II and rutile) measured in partial yield mode. The letters A-E indicate the incident photon energies in the RPES of Fig. 2.

TiCl₄ and H₂O onto the substrate where they subsequently reacted with the solid surface and formed the TiO₂ film. Pure nitrogen was used as the carrier of the precursors. Anatase, rutile and TiO₂-II films were grown at 300, 425 and 450°C, respectively. The thickness of the films was about 40 nm. All the films studied were polycrystalline and contained only a single TiO₂ polymorph as no reflections belonging to other crystal phases were detected by *ex situ* reflection high energy electron diffraction measurements.

The Ti 2p and O 1s absorption spectra of these anatase, rutile and TiO₂-II measured as partial yields of

Ti L₂₃M₂₃M₂₃ and O KVV Auger electrons, respectively, are presented in Fig. 1. The absorption spectra are in good accordance with earlier high resolution X-ray absorption (XAS) studies of anatase and rutile [8, 9]. As can be seen from Fig. 1(a), the main difference in Ti L₂₃ absorption spectra of different polymorphs is a change in intensities of components of a double peak (D, E) structure at 461 eV. In anatase the intensity of peak D is substantially stronger than peak E while in rutile the intensity of peak E is substantially stronger than peak D. In TiO₂-II the intensity distribution within the double peak shows an intermediate behavior while the intensities of D and E peaks are almost equal. This is similar to the case of brookite [8, 9]. Table 1 presents a detailed comparison for the Ti 2p absorption spectra of rutile, TiO₂-II and anatase. In order to make a meaningful comparison of different experimental spectra each spectrum has been fitted with a total of seven Voigt profiles by using a linear background under the line groups in question, leading to the relative energies, intensities (obtained as areas of the peaks) and full widths at half maximum (FWHM) given in Table 1. We have used two peaks to achieve an acceptable fit to double peak region of the spectra, keeping the FWHM of D and E components equal during the whole fitting process. Inspection of the data in Table 1 shows that besides a substantial change in the intensity ratio of D and E components, we can observe also a somewhat larger intensity of the high energy peak G in anatase than in rutile and TiO₂-II. All other deviations in lineshape and peak position between the various TiO₂ polymorphs are within experimental and fitting uncertainties.

The main near edge structure of the Ti 2p photoabsorption can be explained by the 2p⁶ → 2p⁵3d dipole transitions. The 2p core hole spin-orbit interaction splits the spectrum into two parts, corresponding to 2p_{3/2} and 2p_{1/2} levels with a separation of 5.4 eV which are further split by the low symmetric ligand field. Each Ti atom is surrounded by a slightly distorted octahedron of O atoms

Table 1. Positions (in eV), intensities and FWHM (in eV) of the various peaks in the Ti 2p XAS spectra of polymorphs of TiO₂, obtained by using the fitting procedure as explained in the text. All positions are relative to the first strong peak C, the absolute energy of which 458.2 eV is approximately the same for all the polymorphs

	Rutile			TiO ₂ -II			Anatase		
	Position	Intensity	FWHM	Position	Intensity	FWHM	Position	Intensity	FWHM
A	-1.55	0.01	0.3	-1.5	0.02	0.3	-1.5	0.01	0.3
B	-0.9	0.04	0.5	0.8	0.06	0.6	-0.9	0.04	0.5
C	0	1	0.5	0	1	0.6	0	1	0.45
D	1.6	1.1	1.1	1.75	1.6	1.0	1.7	1.9	1.0
E	2.7	1.5	1.1	2.7	1.5	1.0	2.7	1.1	1.0
F	5.4	2.4	1.2	5.4	2.6	1.1	5.3	2.4	1.1
G	7.7	4.4	2.2	7.6	4.6	2.1	7.5	5.5	1.9

which leads to the crystal field splitting of the excited 3d orbitals into low-energy t_{2g} and high-energy e_g orbitals. It has been shown that the main characteristic features of the experimental spectra of rutile, anatase and brookite are well reproduced by the crystal field calculations [7, 8]. The main remaining, easily recognizable, discrepancy between theory and experiment is the peculiar behavior of the component intensities in the double peak structure at 461 eV in the experimental spectra. So a thorough theoretical crystal field and charge transfer analysis of 2p X-ray absorption edge of rutile, anatase and brookite by Crocombette *et al.* [7], which explicitly took into account the exact first-neighbour surroundings of the cation, showed that the evolution of the peak splittings and intensities of the double peak structure from rutile to anatase cannot be attributed to differences in the first coordination shell of the cation. The authors [7] argued that the relatively good accordance between calculated and experimental curves in the region of double peak structure in the case of rutile [8] was achieved by using incorrect crystal field parameters. Furthermore, they stated that no improvement was obtained by including the crystal field from Ti second-neighbours because of the quick decrease of this additional crystal field as a function of distance between the central atom and the surrounding ions.

The O 1s absorption spectra of polymorphs of TiO₂ are presented in Fig. 1(b). The low-energy (530–540 eV) part of the spectra is dominated by two strong broad bands with energy splitting (about 2.6 eV) close to the energy difference of peaks C and E, i.e. to the splitting of t_{2g} and e_g states in the Ti 2p XAS. The spectra of polymorphs of TiO₂ in this region are quite similar. However, a close inspection of the spectra reveals small differences in relative intensities of bands and in values of their energy splitting. Note that the spectrum of rutile is almost identical to that of TiO₂-II, so these slight differences in the spectra are observed between the spectra of anatase and other two polymorphs. The high-energy (above 540 eV) part of the spectra shows more distinct differences between the spectra of various polymorphs while, in contrast of the low-energy part, the spectrum of TiO₂-II is more similar to that of anatase than the spectrum of rutile. Theoretical ground-state band-structure calculations by de Groot *et al.* [12] show that the O 1s absorption spectra of rutile and anatase may be successfully ascribed to the local, i.e. at the oxygen site, p -projected density of states of the conduction band. Calculations show that the double peak structure in the low-energy part of the spectra could be assigned to the Ti 3d-derived states while the high-energy part of the spectra is formed by the delocalized states derived from the antibonding O 2p and Ti 4sp band. de Groot *et al.* [12] show also that the

core-hole potential and many-electron effects have a small influence on the O 1s absorption spectra which is in sharp contrast to the case of the Ti 2p excitonic-like photoabsorption spectra. In the former case, a sudden localization or collapse of the 3d orbital [14] causes the rearrangement of atomic orbitals and, as a consequence, the self-consistent atomic states differ strongly from those for delocalized 3d orbitals of the ground state. Based on the facts described above we can conclude the similarity of the ground-state conduction band-structure of TiO₂-II and rutile in the low-energy region (up to about 8 eV above the bottom of the conduction band) and of TiO₂-II and anatase in the high-energy region (above 8 eV) of the conduction band. The position of the threshold of transitions to the conduction band in the O 1s absorption spectrum of anatase has been estimated to be about 530.6 eV by using the energy difference between the O 1s photoline and top of the valence band which has been found to be about 527.2 eV and the optical absorption band gap value of 3.4 eV [15].

In order to identify the nature of the Ti L_{23} core excitations in polymorphs of TiO₂ we have measured resonant electron spectra excited on the absorption peaks. Because the deexcitation spectra exhibit only small changes between different polymorphs, we present in Fig. 2 some selected decay spectra of anatase and the deexcitation spectra of the other polymorphs for excitations at peaks D and E, only, where the absorption spectra show a distinctly different behavior. The photoelectrons originating from valence band, O 2s, Ti 3p and Ti 3s orbitals can be well identified due to increase of their kinetic energy by increasing excitation energy. All of these photolines, except the O 2s one, show a resonant enhancement at the absorption resonances caused by participator decay processes. The resonance electron spectra show evidence of $L_{23}M_{23}M_{23}$, $L_{23}M_{23}M_{45}$ and $L_{23}M_{1}M_{23}$ Auger decay channels. The comparison with the normal Auger spectrum (labeled as N) shows that in the case of the $L_{23}M_{23}M_{23}$ channel the shape of Auger band in the spectrum C differs from other spectra, indicating the different nature of photoabsorption at this photon energy. From our spectra the value of 459.2 eV for the threshold of transitions from $2p_{3/2}$ to the bottom of the conduction band can be estimated (as a sum of the binding energy of the photoelectron line relative to the top of the valence band of 455.8 eV and the band gap of anatase 3.4 eV). This value is about 1 eV higher than the energy of peak C, showing that peak C has more excitonic character than peaks D and E. This leads to a higher probability of delocalization of the 3d electron at peaks D and E and therefore, to the similarity of resonantly excited spectra to the normal Auger spectrum. Comparison of the decay spectra show a strong decrease (about of three times by taking into

similarity of all of these curves one may conclude the same origin of D and E features in the photoabsorption spectra, i.e. the D and E components seem to be created principally by the same mechanism.

Crocombette *et al.* [7] suggested that the creation of the double peak feature in the Ti 2p photoabsorption spectra cannot be explained by local order arguments. Indeed, the long-range order structural properties vary substantially between the different TiO₂ polymorphs. The data about structure of various TiO₂ polymorphs, presented in Table 2, show significant variations in the long-range order structural properties, not only between rutile and anatase which have very different intensity ratio of D and E components in the region of double peak structure, but also between TiO₂-II and brookite which display almost the same intensity ratio. In addition, our fitting results of peaks D and E (Table 1) show nearly the same peak separation values for all TiO₂ polymorphs. These arguments clearly raise doubts as to whether the suggestion concerning the long-range order origin of the splitting of the second peak of the L₃ edge is justified. We think that the local-order crystal field model is not exhausted in the case of the Ti 2p photoabsorption spectra of TiO₂ polymorphs. Namely, it follows from our resonant electron emission data that the excited 3d electron has an increased possibility to be delocalized with increasing excitation energy. Therefore it would be justified to use substantially larger crystal field radial parameters for the high-lying e_g states than for the low-lying t_{2g} states. To avoid the distortion of the e_g - t_{2g} crystal field split by this choice of parameters, the nondiagonal matrix elements which connect different e_g - t_{2g} terms should be calculated by using an intermediate values for the radial parameters. The different screening of the e_g and t_{2g} excited states adds to the complexity of the problem and may yield a much more stronger charge transfer effect for the e_g than for the t_{2g} states in the absorption spectra. We suppose that choice of a different set of the radial crystal field and charge transfer parameters, separately for e_g and t_{2g} excited states, may improve the agreement between crystal field theory and experiment.

Summarizing, our measurements of various TiO₂ polymorphs demonstrate the sensitivity of XAS and insensitivity of RPES to structural changes in the solid state. From the RPES at the L₃ threshold of Ti is concluded a strong delocalization of the 3d electron for the excitations where the largest differences between the Ti 2p XAS of TiO₂ polymorphs are observed. These differences in XAS are attributed to increasing strength of the crystal field caused by delocalization of the excited 3d electron.

Acknowledgements—This work was supported by the Estonian Science Foundation, the Swedish Natural Sciences Research Council, the Crafoord Foundation and the Royal Swedish Academy of Sciences. We wish to acknowledge stimulating discussions with Dr. A. Maiste and the help of staff of MAX-laboratory in the experimental work.

REFERENCES

1. Simons, P.Y. and Dacheille, F., *Acta Cryst.*, **23**, 1967, 334.
2. Aarik, J., Aidla, A. and Uustare, T., *Phil. Mag. Lett.*, **73**, 1996, 115.
3. Begin-Colin, S., Caer, G.L., Mocellin, A. and Zandona, M., *Phil. Mag. Lett.*, **69**, 1994, 1.
4. McCartney, M.R. and Smith, D.J., *Surf. Sci.*, **250**, 1991, 169.
5. Grey, I.E., Li, C. and Madsen, I.C., *Mat. Res. Bull.*, **23**, 1988, 743.
6. Aarik, J., Aidla, A., Sammelselg, V., Siimon, H. and Uustare, T., *J. Cryst. Growth*, **169**, 1996, 496.
7. Crocombette, I.P. and Jollet, F.J., *Phys. Condens. Matter*, **6**, 1994, 10811.
8. de Groot, F.M.F., Figueiredo, M.O., Basto, M.J., Abbate, M., Petersen, H. and Fuggle, J.C., *Phys. Chem. Miner.*, **19**, 1992, 140.
9. Brydson, R., Sauer, H., Engel, W., Thomas, J.M., Zeitler, E., Kosugi, N. and Kuroda, H., *J. Phys.: Condens. Matter*, **1**, 1989, 797.
10. Brydson, R., Williams, B.G., Engel, W., Sauer, H., Zeitler, E. and Thomas, J.M., *Solid State Commun.*, **64**, 1987, 609.
11. van der Laan, G., *Phys. Rev.*, **B41**, 1990, 12366.
12. de Groot, F.M.F., Faber, J., Michiels, J.J.M., Czyzyk, M.T., Abbate, M. and Fuggle, J.C., *Phys. Rev.*, **B48**, 1993, 2074.
13. Aarik, J., Aidla, A., Uustare, T. and Sammelselg, V., *J. Cryst. Growth*, **148**, 1995, 268.
14. Maiste, A.A., Ruus, R.E. and Elango, M.A., *Zh. Eksp. Teor. Fiz.*, **79**, 1980, 1671 [*Sov. Phys. JETP*, **52**, 1980, 844]; Elango, M., Ausmees, A., Kikas, A., Nõmmiste, E., Ruus, R., Saar, A., van Acker, J.F., Andersen, J.N., Nyholm, R. and Martinson, I., *Phys. Rev.*, **B47**, 1993, 11736.
15. Tang, H., Lévy, F., Berger, H. and Schmid, P.E., *Phys. Rev.*, **B52**, 1995, 7771.
16. de Groot, F.M.F., Fuggle, J.C., Thole, B.T. and Sawatzky, G.A., *Phys. Rev.*, **B41**, 1990, 928.
17. Uozumi, T., Okada, K., Kotani, A., Tezuka, Y. and Shin, S., *J. Phys. Soc. Jpn.*, **65**, 1996, 1150.
18. Woning, J. and van Santen, R.A., *Chem. Phys. Lett.*, **101**, 1983, 541.
19. Freeman, C.M., Newsam, J.M., Levine, S.M. and Catlow, C.R.A., *J. Mater. Chem.*, **3**, 1993, 531.

CURRICULUM VITAE

REIN RUUS

Date and place of birth: 16 August 1948, Põltsamaa, Estonia

Citizenship: Estonian

Address: University of Tartu, Institute of Physics
142 Riia Street, Tartu, 51014, Estonia

Phone: +372 7 383 009

Fax: +372 7 383 033

E-mail: rein@fi.tartu.ee

Education

1956–1964 Tartu Secondary School No. 8

1964–1967 Tartu Secondary School No. 1

1967–1972 Tartu University, Faculty of Physics and Chemistry

Employment

1975–1980, 1990–1996 Estonian Academy of Sciences, Institute of Physics,
engineer

1980–1986 Estonian Academy of Sciences, Institute of Physics, junior
research associate

1986–1990, 1996– Estonian Academy of Sciences, Institute of Physics, research
associate

Scientific work

Main topics of research: x-ray spectroscopy, electron spectroscopy

CURRICULUM VITAE

REIN RUUS

Sünniaeg ja koht: 16. august 1948, Põltsamaa
Kodakondsus: Eesti
Aadress: Tartu Ülikool, Füüsika Instituut
Riia 142, Tartu 51014
Telefon: (27) 383 009
Faks: (27) 383 033
E-post: rein@fi.tartu.ee

Hariduskäik

1956–1964 Tartu 8. Keskkool
1964–1967 Tartu 1. Keskkool
1967–1972 Tartu Ülikooli füüsika-keemiaosakond, füüsika eriala,

Teenistuskäik

1972–1975 Eesti Põllumajanduse Akadeemia füüsika kateedri vanem-laborant
1975–1980, 1990–1996 Füüsika Instituudi röntgenspektroskoopia labori insener
1980–1986 Füüsika Instituudi röntgenspektroskoopia labori noorem-teadur
1986–1990, alates 1996 Füüsika Instituudi röntgenspektroskoopia labori teadur

Teadustegevus

Põhisuunad: Tahkiste röntgenspektroskoopia ja viimastel aastatel rönt-genergastusega elektronspektroskoopia

DISSERTATIONES PHYSICAE UNIVERSITATIS TARTUENSIS

1. Andrus Ausmees. XUV-induced electron emission and electron-phonon interaction in alkali halides. Tartu, 1991.
2. Heiki Sõnajalg. Shaping and recalling of light pulses by optical elements based on spectral hole burning. Tartu, 1991.
3. Sergei Savihhin. Ultrafast dynamics of F-centers and bound excitons from picosecond spectroscopy data. Tartu, 1991.
4. Ergo Nõmmiste. Leelishalogeniidide röntgenelektronemissioon kiiritamisel footonitega energiaga 70–140 eV. Tartu, 1991.
5. Margus Rätsep. Spectral gratings and their relaxation in some low-temperature impurity-doped glasses and crystals. Tartu, 1991.
6. Tõnu Pullerits. Primary energy transfer in photosynthesis. Model calculations. Tartu, 1991.
7. Olev Saks. Attoampri diapsoonis voolude mõõtmise füüsikalised alused. Tartu, 1991.
8. Andres Virro. AlGaAsSb/GaSb heterostructure injection lasers. Tartu, 1991.
9. Hans Korge. Investigation of negative point discharge in pure nitrogen at atmospheric pressure. Tartu, 1992.
10. Jüri Maksimov. Nonlinear generation of laser VUV radiation for high-resolution spectroscopy. Tartu, 1992.
11. Mark Aizengendler. Photostimulated transformation of aggregate defects and spectral hole burning in a neutron-irradiated sapphire. Tartu, 1992.
12. Hele Siimon. Atomic layer molecular beam epitaxy of A^2B^6 compounds described on the basis of kinetic equations model. Tartu, 1992.
13. Tõnu Reinot. The kinetics of polariton luminescence, energy transfer and relaxation in anthracene. Tartu, 1992.
14. Toomas Rõõm. Paramagnetic H^{2-} and F^+ centers in CaO crystals: spectra, relaxation and recombination luminescence. Tallinn, 1993.
15. Erko Jalviste. Laser spectroscopy of some jet-cooled organic molecules. Tartu, 1993.
16. Alvo Aabloo. Studies of crystalline celluloses using potential energy calculations. Tartu, 1994.
17. Peeter Paris. Initiation of corona pulses. Tartu, 1994.
18. Павел Рубин. Локальные дефектные состояния в CuO_2 плоскостях высокотемпературных сверхпроводников. Тарту, 1994.
19. Olavi Ollikainen. Applications of persistent spectral hole burning in ultrafast optical neural networks, time-resolved spectroscopy and holographic interferometry. Tartu, 1996.

20. Ülo Mets. Methodological aspects of fluorescence correlation spectroscopy. Tartu, 1996.
21. Mikhail Danilkin. Interaction of intrinsic and impurity defects in CaS:Eu luminophors. Tartu, 1997.
22. Ирина Кудрявцева. Создание и стабилизация дефектов в кристаллах KBr, KCl, RbCl при облучении ВУФ-радиацией. Тарту, 1997.
23. Andres Osvet. Photochromic properties of radiation-induced defects in diamond. Tartu, 1998.
24. Jüri Örd. Classical and quantum aspects of geodesic multiplication. Tartu, 1998.
25. Priit Sarv. High resolution solid-state NMR studies of zeolites. Tartu, 1998.
26. Сергей Долгов. Электронные возбуждения и дефектообразование в некоторых оксидах металлов. Тарту, 1998.
27. Каupo Kukli. Atomic layer deposition of artificially structured dielectric materials. Tartu, 1999.
28. Ivo Heinmaa. Nuclear resonance studies of local structure in $\text{RBa}_2\text{Cu}_3\text{O}_{6+x}$ compounds. Tartu, 1999.
29. Aleksander Shelkan. Hole states in CuO_2 planes of high temperature superconducting materials. Tartu, 1999.
30. Dmitri Nevedrov. Nonlinear effects in quantum lattices. Tartu, 1999.



ISSN 1406-0647
ISBN 9985-56-439-1